HOMOGENIZATION AND DEHOMOGENIZATION SCHEMES FOR BWR ASSEMBLIES

by

PHILIPPE JEAN FINCK
Ingénieur Civil des Mines
Ecole Nationale Supérieure des Mines de Paris
(1980)

SUBMITTED IN PARTIAL FULFILLMENT
OF THE REQUIREMENTS FOR THE
DEGREE OF
DOCTOR OF PHILOSOPHY
at the
MASSACHUSETTS INSTITUTE OF TECHNOLOGY
January 1983 (289)

Signature of Author: .....
Department of Nuclear Engineering
November 22, 1982

Certified by: .....
Allan F. Henry
Thesis Supervisor

Accepted by: .....
Allan F. Henry
Chairman, Department Graduate Committee

HOMOGENIZATION AND DEHOMOGENIZATION SCHEMES FOR BWR ASSEMBLIES

by

Philippe Jean Finck

Submitted to the Department of Nuclear Engineering on November 22, 1982 in partial fulfillment of the requirements for the Degree of Doctor of Philosophy in the field of Nuclear Engineering.

ABSTRACT

The objective of this research is to apply nodal equivalence theory and the analytic nodal method to the analysis of Boiling Water Reactors. This includes developing accurate homogenization schemes for estimating equivalence theory parameters, and devising accurate methods for inferring local fuel pin power densities from the nodal results.

The use of surface flux response matrices for estimating equivalence theory parameters is first investigated. Analysis of several realistic two-dimensional BWR benchmark problems shows that the use of surface flux response matrices leads to maximum errors in assembly powers of less than 3%. This scheme is shown to improve consistently the nodal results predicted by conventional homogenization methods. The computational efficiency of this scheme is shown to be one order of magnitude larger than that of conventional finite-differences methods.

Two-dimensional homogenization schemes are then extended for three-dimensional calculations. Analysis of a three-dimensional benchmark problem shows that axial discontinuity factors are well approximated by unity.

Reconstruction methods are developed for various nodal solutions. They result in maximum errors in pin powers of less than 6%.

Homogenization and reconstruction methods are then applied to depletion calculations. A simple approximation allows these methods to yield consistent results throughout life.

Thesis Supervisor: Allan F. Henry

Title: Professor of Nuclear Engineering

TABLE OF CONTENTS

		Page
ABSTRACT		ii
TABLE OF CONTENTS		iii
ACKNOWLEDGEMENTS		ix
LIST OF FIGURES		x
LIST OF TABLES		xiii
CHAPTER 1	INTRODUCTION	1-1
	1.1 Introduction	1-1
	1.2 Solution Methods	1-1
	1.3 The Development of Nodal Methods	1-3
	1.4 The Determination of Spatially Homogenized Parameters for Diffusion Theory	1-3
	1.5 The Reconstruction of Heterogeneous Fluxes	1-7
	1.6 The Application of Nodal Methods to Depletion Calculations	1-8
	1.7 Objectives and Summary	1-8
CHAPTER 2	THE NODAL EQUIVALENCE THEORY AND THE ANALYTIC NODAL METHOD	2-1
	2.1 Introduction	2-1
	2.1.1 Notation	2-1
	2.2 Nodal Equivalence Theory	2-2
	2.3 The QUANDRY Equations	2-9
	2.3.1 Introduction	2-9
	2.3.2 Problem Description	2-9
	2.3.3 The Spatial Coupling Equations	2-10
	2.3.4 Numerical Solution to the QUANDRY Equations	2-15
	2.4 The Generation of Approximate Equivalence Theory Parameters	2-16
	2.4.1 Introduction	2-16

TABLE OF CONTENTS (continued)

		Page
2.4.2	Determination of 2-Group Heterogeneous Macroscopic Cross Sections	2-17
2.4.3	The Determination of Approximate Equivalence Theory Parameters .	2-18
2.4.3.1	Problem Definition . .	2-18
2.4.3.2	Non-Iterative Scheme for the Approximation of Equivalence Theory Parameters: "Assembly" Homogenized Parameters	2-20
2.4.3.3	Iterative Scheme for the Approximation of Equivalence Theory Parameters Based on Partial or Net Surface Currents .	2-24
2.5	Summary	2-26
CHAPTER 3	HOMOGENIZATION TECHNIQUES BASED ON SURFACE FLUX RESPONSE MATRICES . .	3-1
3.1	Introduction	3-1
3.1.1	Two-Dimensional BWR Benchmarks	3-2
3.1.1.1	The CISE BWR Benchmark Problem . . .	3-2
3.1.1.2	The LSH BWR Benchmark Problem . . .	3-2
3.1.1.3	The MVY BWR Benchmark Problem . . .	3-3
3.2	Polynomial Approximations for Assembly Boundary Conditions	3-4
3.3	The Interpolation of Cornerpoint Fluxes	3-7
3.3.1	Problem Description	3-7
3.3.2	The Source-Free Condition . .	3-8
3.4	An Iterative Scheme Based on Surface Response Matrices	3-10
3.4.1	Definition of Surface Flux Response Matrices	3-10

TABLE OF CONTENTS (continued)

		Page
	3.4.2 The Generation of Surface Flux Response Matrices	3-12
	3.4.3 The Interpolation of Surface Flux Response Matrices	3-13
	3.4.4 The Implementation of Surface Flux Response Matrices in an Iterative Scheme	3-14
	3.4.4.1 The Non-Selective Use of Response Matrices	3-14
	3.4.4.2 The Selective Use of Response Matrices	3-17
3.5	Numerical Testing of the Surface Flux Response Matrix Iterative Scheme	3-18
	3.5.1 A Preliminary Test Problem	3-18
	3.5.2 The CISE BWR Benchmark Problem	3-23
	3.5.3 The LSH BWR Benchmark Problem	3-26
	3.5.3.1 The CLSH BWR Benchmark Problem	3-26
	3.5.3.2 The NLSH BWR Benchmark Problem	3-30
	3.5.4 The MVY BWR Benchmark Problem	3-33
	3.5.5 Physical Interpretation of the Converged Solution	3-34
	3.5.6 Execution Time Comparison	3-34
3.6	Extension of Homogenization Methods to Three-Dimensional Calculations	3-36
	3.6.1 The Estimation of Three-Dimensional Equivalence Theory Parameters	3-36
	3.6.2 Numerical Testing of Three-Dimensional Homogenization Schemes	3-36
3.7	Summary	3-39

TABLE OF CONTENTS (continued)

		Page
CHAPTER 4	FLUX RECONSTRUCTION TECHNIQUES BASED ON COARSE MESH NODAL METHODS	4-1
	4.1 Introduction	4-1
	4.2 The Relation Between Homogenization and Reconstruction Schemes	4-2
	4.3 Flux Reconstruction Techniques Based on the Converged Solution of the Iterative Scheme	4-4
	4.3.1 The "One-Assembly" Flux Reconstruction Technique	4-4
	4.3.2 Numerical Testing	4-5
	4.3.2.1 The CLSH Benchmark .	4-5
	4.3.2.2 The NLSH Benchmark .	4-5
	4.4 Flux Reconstruction Techniques Based on the ADF-AXS Nodal Solution	4-12
	4.4.1 The "Four-" and "Nine-Assemblies" Reconstruction Techniques	4-12
	4.4.2 Numerical Testing	4-14
	4.5 The Extension of Reconstruction Schemes to Three-Dimensional Calculations . .	4-16
	4.6 Summary	4-16
CHAPTER 5	THE APPLICATION OF NODAL METHODS TO DEPLETION CALCULATIONS	5-1
	5.1 Introduction	5-1
	5.2 The Assembly Depletion Approximation	5-1
	5.3 Numerical Testing	5-3
	5.3.1 Description of Benchmark Problems	5-3
	5.3.1.1 The DEP1 BWR Benchmark Problem .	5-3
	5.3.1.2 The DEP1 BWR Benchmark Problem .	5-4

TABLE OF CONTENTS (continued)

		Page
	5.3.2 Numerical Testing of Homogenization Methods	5-5
	5.3.2.1 The DEP1 Benchmark	5-5
	5.3.2.2 The DEP2 Benchmark	5-6
	5.3.3 Numerical Testing of Reconstruction Schemes	5-10
	5.3.3.1 The DEP1 Benchmark	5-12
	5.3.3.2 The DEP2 Benchmark	5-14
	5.4 Summary	5-18
CHAPTER 6	SUMMARY	6-1
	6.1 Overview of the Investigation . . .	6-1
	6.2 Recommendation for Future Research	6-3
	6.2.1 Improved Cornerpoint Flux Interpolation Schemes . . .	6-3
	6.2.2 Tabulation and Interpolation of Response Matrices	6-4
	6.2.3 Three-Dimensional Flux Reconstructions	6-4
	6.2.4 The Analytic Generation of Response Matrices	6-4
	6.2.5 Improved Depletion Studies .	6-5
REFERENCES	. . . . .	7-1
APPENDIX 1	DESCRIPTION OF BWR BENCHMARK PROBLEMS	A1-1
	A1.1 The CISE BWR Benchmark Problem .	A1-2
	A1.2 The LSH BWR Benchmark Problem .	A1-5
	A1.3 The MVY BWR Benchmark Problem .	A1-12
	A1.4 The TRD BWR Benchmark Problem .	A1-13
	A1.5 The Preliminary Test Problem . .	A1-17
APPENDIX 2	DESCRIPTION OF DEPLETABLE BWR BENCHMARKS	A2-1
	A2.1 The DEP1 BWR Benchmark Problem	A2-2

TABLE OF CONTENTS (continued)

			Page
	A2.2	The DEP2 BWR Benchmark Problem .	A2-19
APPENDIX 3		CURRENTS AND FLUX SHAPES IN THE LSH BWR AND MVY BWR	A3-1
APPENDIX 4		EQUATIONS FOR CORNERPOINT FLUXES INTERPOLATION	A4-1
	A4.1	Introduction	A4-1
	A4.2	Problem Description	A4-1
	A4.3	Problem Solution	A4-1
APPENDIX 5		THE GENERATION OF SURFACE FLUX RESPONSE MATRICES	A5-1
	A5.1	Introduction	A5-1
	A5.2	Definition of Surface Flux Response Matrices	A5-1
	A5.3	The Generation of Surface Flux Response Matrices using CITATION .	A5-2
	A5.4	The Generation of Surface Flux Response Matrices in the PDQ7 Formalism	A5-3
APPENDIX 6		DETAILED NODAL RESULTS	A6-1
	A6.1	Nodal Results for the Preliminary Test Problem	A6-2
	A6.2	Nodal Results for the CISE Benchmark Problem	A6-3
	A6.3	Nodal Results for the CLSH Benchmark Problem	A6-5
	A6.4	Nodal Results for the NLSH Benchmark Problem	A6-7
	A6.5	Nodal Results for the MVY Benchmark Problem	A6-11
	A6.6	Nodal Results for the TRD-BWR Benchmark Problem	A6-14
	A6.7	Nodal Results for the DEP2 Benchmark Problem	A6-17

ACKNOWLEDGEMENTS

My stay at M.I.T. has been a most rewarding and enjoyable experience. This rare, and surprising, combination is a consequence of my having had Professor Allan F. Henry as my thesis supervisor. His willingness to teach, argue, and learn, along with his commitment to scientific quality, have created an ideal environment for the completion of this research.

Thanks are also due to Professor David D. Lanning, who served as reader for this thesis.

I am also indebted to my office-mates, Bruce Hægemeier, Chris Hoxie, Kent Parsons, and especially Hussein Khalil, for having provided extensive arguments and suggestions.

I also wish to thank Ms. Delphine Radcliffe for her skill and infinite patience in typing the final manuscript.

LIST OF FIGURES

Figure No.		Page
2.1	Three adjacent QUANDRY nodes.	2-13
3.1	The source-free condition.	3-9
3.2	Description of the iterative scheme.	3-15
3.3	Eigenvalue convergence for the Preliminary Test Problem.	3-21
3.4	Eigenvalue convergence for the CLSH BWR Benchmark Problem.	3-27
4.1	Extended assemblies for the LSH benchmark. .	4-7
4.2	Different Reconstruction Methods.	4-13
5.1	Extended assemblies for the DEP2 benchmark. .	5-16
A1.1.1	Core layout for the CISE Benchmark Problem. .	A1-2
A1.1.2	Assembly description for the CISE Benchmark Problem.	A1-3
A1.2.1	Core layout for the LSH BWR Benchmark Problem.	A1-5
A1.2.2	Assembly description for the LSH BWR Benchmark.	A1-6
A1.3.1	Core layout for the MVY BWR Benchmark Problem.	A1-12
A1.4.1	Radial core layout for the TRD BWR Benchmark Problem.	A1-13
A1.4.2	Axial core layout for the TRD BWR Benchmark Problem.	A1-13
A1.4.3	Void fractions for the TRD BWR Benchmark	A1-14
A1.4.4	Assembly description for the TRD BWR Benchmark.	A1-15

LIST OF FIGURES (continued)

Figure No.		Page
A1.5.1	Core layout for the Preliminary Test Problem.	A1-17
A1.5.2	Assembly description for the Preliminary Test Problem.	A1-17
A2.1.1	Core layout for the DEP1 BWR Benchmark Problem.	A2-2
A2.2.1	Core layout for the first cycle of the DEP2 BWR Benchmark.	A2-19
A2.2.2	Core layout for the second cycle of the DEP2 BWR Benchmark.	A2-20
A2.2.3	Core layout for the third cycle of the DEP2 BWR Benchmark.	A2-21
A2.2.4	Assembly description for the DEP2 Benchmark.	A2-22
A3.1	Location of Figures A3.2 to A3.9 in the LSH BWR Benchmark.	A3-2
A3.2	Partial currents along Segment 1.	A3-3
A3.3	Partial currents along Segment 2.	A3-3
A3.4	Net transverse currents along Segment 1.	A3-4
A3.5	Net transverse currents along Segment 2.	A3-4
A3.6	Albedo along Segment 1.	A3-5
A3.7	Albedo along Segment 2.	A3-5
A3.8	Flux and form function along Segment 1.	A3-6
A3.9	Flux and form function along Segment 2.	A3-6
A3.10	Location of Figures A3.11 to A3.22 in the MVY BWR Benchmark.	A3-7
A3.11	Flux and form function along Segment 1.	A3-8

LIST OF FIGURES (continued)

Figure No.		Page
A3.12	Flux and form function along Segment 2. . . .	A3-8
A3.13	Flux and form function along Segment 3. . . .	A3-9
A3.14	Flux and form function along Segment 4. . . .	A3-9
A3.15	Flux and form function along Segment 5. . . .	A3-10
A3.16	Flux and form function along Segment 6. . . .	A3-10
A3.17	Flux and form function along Segment 7. . . .	A3-11
A3.18	Flux and form function along Segment 8. . . .	A3-11
A3.19	Flux and form function along Segment 9. . . .	A3-12
A3.20	Flux and form function along Segment 10. . . .	A3-12
A3.21	Flux and form function along Segment 11. . . .	A3-13
A3.22	Flux and form function along Segment 12. . . .	A3-13
A4.1	Definition of quantities used in cornerpoint flux interpolation.	A4-2

LIST OF TABLES

Table No.		Page
2.1	LSH-BWR Nodal Results	2-21
2.2	CISE Nodal Results	2-22
3.1	Nodal Results for the Preliminary Test Benchmark	3-22
3.2	Nodal Results for the CISE BWR Benchmark . .	3-25
3.3	The Oscillatory-Exponential Convergence for the CLSH Benchmark	3-29
3.4	Nodal Results for the CLSH BWR Benchmark . .	3-29
3.5	Nodal Results for the NLSH Benchmark . . .	3-32
3.6	Nodal Results for the MVY Benchmark . . .	3-32
3.7	The Oscillatory-Exponential Convergence for the MVY Benchmark	3-35
3.8	Comparison of Costs for Non-Iterative and Iterative Schemes	3-35
3.9	Nodal Results for the TRD-BWR Benchmark . .	3-38
3.10	Radially Averaged Nodal Powers for the TRD-BWR Benchmark	3-38
3.11	Nodal Results for Two-Dimensional Cuts of the TRD-BWR Benchmark	3-40
4.1	Errors in Reconstructed Fluxes for the CLSH Benchmark	4-6
4.2	Maximum Error for Pin-Wise Flux Reconstruction in the NLSH Benchmark when "Normal" Assemblies are Used	4-9
4.3	Nodal Results for the NLSH Benchmark when Extended Assemblies are Used	4-10

LIST OF TABLES (continued)

Table No.		Page
4.4	Maximum Errors for Pin-Wise Flux Reconstruction in the NLSH Benchmark, when Extended Assemblies are Used	4-11
4.5	Maximum Errors for Pin-Wise Flux Reconstruction in the Central Assemblies of the NLSH Benchmark when the ADF-AXS Solution and the "One-Assembly" Reconstruction Scheme are Used	4-15
4.6	Maximum Errors in Flux Reconstruction . . .	4-17
4.7	Maximum Errors in Hottest Pin	4-17
5.1	B.O.L. Nodal Powers for the DEP1 BWR Benchmark	5-7
5.2	E.O.L. Nodal Powers for the DEP1 BWR Benchmark	5-8
5.3	Nodal Results at B.O.L. for the DEP1 Benchmark	5-9
5.4	Nodal Results at E.O.L. for the DEP1 Benchmark	5-9
5.5	Errors in Nodal Quantities at Each Time Step of the DEP2 Benchmark	5-11
5.6	Errors in Reconstruction for the DEP1 Benchmark Using Nodal Quantities from Response Matrices .	5-13
5.7	Maximum Errors in Reconstruction of Heterogeneous Quantities for the DEP2 Benchmark	5-15
5.8	Errors in Nodal Quantities when using "Extended Assemblies" in the DEP2 Benchmark	5-17
5.9	Errors in Reconstruction of Heterogeneous Quantities when using "Extended Assemblies" in the DEP2 Benchmark	5-17

LIST OF TABLES (continued)

Table No.		Page
A1.1.1	Material Positions for Assemblies of the CISE Benchmark	A1-3
A1.1.2	Heterogeneous Cross Sections for the CISE Benchmark	A1-4
A1.2.1	Material Positions for Assemblies of the LSH BWR Benchmark	A1-6
A1.2.2	Heterogeneous Cross Sections for the LSH-BWR Benchmark	A1-7
A1.2.3	Material Description for the LSH-BWR Benchmark	A1-11
A1.4.1	Material Positions for Assemblies of the TRD BWR Benchmark	A1-15
A1.4.2	Heterogeneous Cross Sections for the TRD BWR Benchmark	A1-16
A1.5.1	Material Positions for Assemblies of the Preliminary Test Problem	A1-18
A1.5.2	Heterogeneous Cross Sections for the Preliminary Test Problem	A1-19
A.2.1.1	Heterogeneous Cross Sections for the DEP1 BWR Benchmark	A2-4
A2.2.1	Material Positions for Assemblies of the DEP2 BWR Benchmark	A2-22
A2.2.2	Heterogeneous Cross Sections for the DEP2 BWR Benchmark at Burnup = 0 MWD/MT	A2-23
A2.2.3	Heterogeneous Cross Sections for the DEP2 BWR Benchmark at Burnup = 10,000 MWD/MT . . .	A2-27
A2.2.4	Heterogeneous Cross Sections for the DEP2 BWR Benchmark at Burnup = 20,000 MWD/MT . . .	A2-31

LIST OF TABLES (continued)

Table No.		Page
A6.1.1	Nodal Powers for the Preliminary Test Problem .	A6-2
A6.2.1	Nodal Powers for the CISE Benchmark Problem .	A6-4
A6.3.1	Nodal Powers for the CLSH Benchmark Problem .	A6-6
A6.4.1	Interpolated Cornerpoint Fluxes in the Fast Group for the Fueled Region of the NLSH Benchmark . .	A6-8
A6.4.2	Interpolated Cornerpoint Fluxes in the Thermal Group for the Fueled Region of the NLSH Benchmark	A6-9
A6.4.3	Nodal Powers for the NLSH Benchmark	A6-10
A6.5.1	Nodal Powers for the MVY Benchmark	A6-12
A6.6.1	Nodal Powers for the TRD BWR Benchmark . .	A6-15
A6.6.2	Nodal Powers for Two-Dimensional Slices of the TRD BWR Benchmark	A6-16
A6.7.1	Nodal Powers for the DEP2 Benchmark	A6-18

CHAPTER 1

INTRODUCTION

1.1 Introduction

The safe and economical operation of a modern nuclear reactor requires the precise knowledge of the spatial power distribution. The early developments in the field of nuclear reactors relied on a large quantity of experimental information. Unfortunately, with the increasing complexity and extreme operating conditions of modern reactors, any major use of experimental facilities to guide design becomes prohibitively expensive. Thus in the last forty years complex theoretical and computational tools have been developed to calculate the space and energy distributions of the free neutron population. These methods have now reached a high degree of reliability, and are very accurate provided the necessary basic nuclear data can be accurately measured.

These reactor physics calculations serve, from an engineering viewpoint, to determine the state variables (temperature, power, void fraction, xenon concentration, $\cdots$) which describe the condition of the core. Thus, the operating limits of a reactor can be determined in order to insure the safety of the reactor and its environment. These calculations allow for better fuel management capabilities, and reduce the safety margins included in the design of the core. Thus, important financial savings can be achieved if reliable methods of analyzing reactor behavior are available.

1.2 Solution Methods

The Boltzmann transport equation [1] accurately describes the behavior of the neutron population in phase space (position, energy, and

direction of travel). Unfortunately, for realistic problems the solution of that equation is beyond the reach of even the most sophisticated computational tools available today.

Therefore, different levels of approximations to the transport equation have been devised. Numerical schemes to solve this equation, such as Monte Carlo or discrete ordinate methods [1], yield very accurate results, but are still prohibitively expensive for large problems. The most commonly employed approximation for industrial purposes is the group diffusion equation, where the angular distribution of neutrons is assumed to be at most linearly anisotropic [1]. This equation is routinely solved by finite-differences computer codes [17, 18]. Unfortunately, excessively large numbers of spatial mesh points have to be used to implement these codes for realistic three-dimensional problems. Furthermore, the information provided by these calculations is often overabundant. For example, many applications require only the determination of the global eigenvalue and the average assembly powers.

Various methods have been developed to reduce the cost of these calculations. Synthesis methods [26], finite element techniques [27], response matrix methods [28], and nodal methods [22], are the most commonly employed methods.

It is the purpose of this thesis to develop schemes based on nodal methods, aimed at replacing standard finite-differences methods for the Analysis of Boiling Water Reactors. Three distinct and successive tasks have to be carried out [14]. First it is necessary to develop a nodal procedure. Next it is necessary to determine the parameters used in the nodal equations. Finally, it is necessary to recapture the

local fuel pin power densities from the nodal results.

1.3 The Development of Nodal Methods

The general principle of Nodal Methods as applied to a BWR is to divide the reactor core into large nodes ($\sim$ 15 cm x 15 cm x 15 cm) consisting of an axial segment of a fuel assembly and its surrounding control rod and moderator material. The node-averaged fluxes and surface-averaged net currents are generally considered as the unknowns of the problem. An integration of the neutron diffusion equation over each node yields an exact balance condition relating these unknowns. Unfortunately, this equation is not sufficient for determining all the unknowns. Thus, other relations, called coupling equations, between the node-averaged fluxes and the face-averaged currents must be obtained. Numerous ways of deriving these coupling equations and solving the resulting system of coupled equations have been tested [22].

In this thesis we shall use the Analytic Nodal Method which was recently developed at M.I.T. [2, 23], and has been shown to be computationally very efficient [2, 3, 6, 7].

1.4 The Determination of Spatially Homogenized Parameters for Diffusion Theory

The Analytic Nodal Method, as implemented in the computer code QUANDRY [2], requires the knowledge of diffusion theory parameters homogenized over each node, and uses them to calculate node-averaged quantities. The solution of the nodal problem cannot reproduce the detail of the exact heterogeneous fluxes. Nevertheless, the homogenized parameters should be such that some average quantities are preserved. These quantities are the global reactor eigenvalue, the node-integrated

reaction rates in each energy group, the average net currents on all nodal faces, and the nodal powers.

The determination of "exact" homogenized parameters (i.e. they preserve all these average quantities) is not a trivial task. In order to see how they are defined, we shall assume for the moment that an exact solution to the heterogeneous problem is known. Thus, the following quantities are known:

$\varphi_g(\underline{r})$ is the scalar neutron flux in group g ($g = 1, \cdots, G$) at point $\underline{r}$;

$J_g^u(\underline{r})$ is the net neutron current in direction u, in group g, and at point $\underline{r}$;

$\Sigma_{\alpha g}(\underline{r})$ is the macroscopic cross section for event α (α = r, a, gg', f, νf) in group g, and at point $\underline{r}$;

$\chi_g(\underline{r})$ is the fission neutron spectrum contribution to group g at point $\underline{r}$;

$D_g(\underline{r})$ is the diffusion coefficient in group g, and at point $\underline{r}$;

λ is the global reactor eigenvalue.

The corresponding quantities for the homogenized problem will be denoted with a circumflex. The homogenized parameters are supposed to be spatially constant within each node.

The preservation of nodal quantities implies the following relations:

$$\int_{V_i} \Sigma_{\alpha g}(\underline{r})\, \varphi_g(\underline{r})\, dv = \int_{V_i} \hat{\Sigma}_{\alpha g}(v)\, \hat{\varphi}_g(\underline{r})\, dv$$

$$\int_{S_i^k} J_g^u(\underline{r})\, ds = - \int_{S_i^k} \hat{D}_g(v)\, \frac{\partial}{\partial u}\, \hat{\varphi}_g(\underline{r})\, ds$$

$$\lambda = \hat{\lambda}$$

$$g = 1, \cdots, G$$

$$\alpha = t, f, gg' \cdots$$

$$k = 1, \cdots, K$$

$$i = 1, \cdots, N \qquad (1.1)$$

where

v_i is the volume of the i^{th} node;

s_i^k is the k^{th} face of the i^{th} node;

K is the total number of faces per node;

G is the total number of energy groups;

N is the total number of nodes.

Consequently the exact homogenized parameters must be such that:

$$\hat{\Sigma}_{\alpha g} = \frac{\int_{v_i} \Sigma_{\alpha g}(\underline{r})\, \varphi_g(\underline{r})\, dv}{\int_{v_i} \hat{\varphi}_g(\underline{r})\, dv}$$

$$\hat{D}_g = - \frac{\int_{s_i^k} dx\, J_g^u(\underline{r})}{\int_{s_i^k} ds\, \frac{\partial}{\partial u} \hat{\varphi}_g(\underline{r})} \qquad (1.2)$$

The homogenized diffusion coefficient defined by Equation (1.2) depends on the face where it is calculated. This fact implies that there are six different diffusion constants for each group in a given node and thus that homogenized parameters giving rise to the standard mathematical formalism of diffusion theory (involving a single group-diffusion constant

for each homogeneous node) do not exist.

Two distinct approaches to overcoming this theoretical limitation have been taken. In the first approach, which is today fairly standard, "flux weighted constants" are defined. The heterogeneous flux distribution used to weight the heterogeneous cross sections in Equation (1.2) are obtained from a $\underline{J}_g \cdot \underline{n} = 0$ assembly calculation, and the volume integral of the homogeneous flux is assumed to be equal to the volume integral of that assembly flux. Thus, the flux-weighted cross sections are defined by:

$$\Sigma_{\alpha g}^{FWC} = \frac{\int_{v_i} \Sigma_{\alpha g}(\underline{r})\, \varphi_g^A(\underline{r})\, dv}{\int_{v_i} \varphi_g^A(\underline{r})\, dv} \qquad (1.3)$$

where $\varphi_g^A(\underline{r})$ is the heterogeneous assembly flux.

The homogenized diffusion coefficient is usually defined by:

$$D_g^{FWC} = \left[\frac{\int_{v_i} D_g^{-1}(\underline{r})\, \varphi_g^A(\underline{r})\, dv}{\int_{v_i} \varphi_g^A(\underline{r})\, dv} \right]^{-1} \qquad (1.4)$$

Unfortunately, the use of these parameters does not guarantee the preservation of any of the nodal quantities of interest, and errors in nodal powers as high as 20% have been reported [3].

The second approach is to define "exact" homogenized parameters by modifying the theoretical model in which they are to be used. One such method, "equivalence theory", was originally developed by Koebke [24], and later modified by Smith [3]. Instead of relaxing the

conditions imposed by Equation (1.1), it adds extra degrees of freedom to the nodal method, thus allowing for the exact preservation of all reaction rates. "Equivalence theory" will be discussed in detail in Chapter 2.

Unfortunately, "equivalence theory" does not provide a practical way of determining the exact homogenized parameters. Several schemes have been proposed [3,6,25], but, for BWR's, they yield only a marginally acceptable approximation to these parameters. It is the fundamental purpose of this thesis to study more accurate homogenization schemes applicable to BWR's.

1.5 The Reconstruction of Heterogeneous Fluxes

The fact that nodal methods do not predict detailed flux shapes throughout the core is a fundamental limitation to them since such detailed information can be of vital importance in the course of designing and operating a reactor. Thus, the necessity of reconstructing heterogeneous fluxes and pin powers was recognized early [16].

The development of accurate nodal methods brought about the creation of sophisticated reconstruction schemes. Koebke and Wagner [16] proposed two such schemes, the imbedded heterogeneous assembly calculation method and the modulation method.

In the modulation method, heterogeneous assembly calculations are multiplied by smooth shapes derived from the nodal calculations, in order to obtain reconstructed quantities. This approach was taken by Hoxie [7] and Khalil [19], who report excellent results for PWR's.

The imbedded heterogeneous assembly calculation method consists of using information obtained from the nodal calculation to determine the boundary conditions for a heterogeneous assembly calculation.

Excellent results were obtained by Koebke and Wagner [16] when incoming partial currents were used as boundary conditions. Parsons [12] also reports excellent results for PWR's, when surface fluxes are used as boundary conditions. The implementation of such schemes for BWR calculations is closely connected to the quality of the nodal solution available, and thus with the accuracy of the homogenization scheme used. In Chapter 4 of this thesis we shall develop accurate reconstruction schemes, based on imbedding methods, for various homogenization schemes.

1.6 The Application of Nodal Methods to Depletion Calculations

Depletion calculations are currently performed with great accuracy by finite differences codes such as PDQ7 [17] or CITATION [18]. These codes keep track of each nuclide concentration throughout space and time by solving the differential equations relating these nuclide concentrations to the heterogeneous fluxes [1, 9].

Heterogeneous fluxes are not obtained directly from nodal calculations, and flux reconstruction is generally a lengthy and expensive process. Thus, depletion methods based solely on nodal results must be developed. This will be the objective of Chapter 5 of this thesis.

1.7 Objectives and Summary

This thesis has three objectives. First, accurate and efficient methods to estimate equivalence theory parameters for BWR's need to be developed. Second, accurate flux reconstruction schemes need to be implemented for available nodal solutions. Third, these methods need to be applied to depletion calculations.

In Chapter 2, "equivalence theory" and the Analytic Nodal Method will be reviewed. Various homogenization schemes [3, 6, 25] will be examined. In Chapter 3 a homogenization scheme based on surface flux response matrices will be introduced. It will be shown to be very accurate and efficient . In Chapter 4, flux reconstruction methods will be described, and they will be shown to be accurate to within a few percent. These homogenization and reconstruction methods will be extended to depletion calculations in Chapter 5. Finally, Chapter 6 contains a summary of this investigation and recommendations for future research.

CHAPTER 2

THE NODAL EQUIVALENCE THEORY AND THE ANALYTIC NODAL METHOD

2.1 Introduction

In Chapter 1 it was shown that the diffusion theory model does not allow for enough degrees of freedom for exact homogenized parameters to exist: no set of homogenized parameters, including the standard flux-weighted constants, can reproduce the nodal quantities of interest (global eigenvalue, nodal reaction rates, nodal fluxes and nodal surface currents).

In this chapter we shall review the nodal equivalence theory, which by extending the hypothesis of the diffusion theory model, permits the existence of exact homogenized parameters. We shall then discuss how the resulting equations for the homogenized core are solved via the analytic nodal method, as implemented in the computer code QUANDRY.

These theories are more completely described in Smith's N.E. thesis [2] and Ph.D. thesis [3].

Section 2 presents the nodal equivalence theory. In section 3 the QUANDRY model is examined. Section 4 reviews some of the methods developed for finding close approximations to the reference parameters.

2.1.1 Notation

All reactor problems are treated in three-dimensional Cartesian geometry. The notation x, y, and z represents the coordinate directions, while u, v, w are used as generalized coordinate subscripts. Each problem is divided into a set of regular parallelepipeidal blocks (nodes) at the coordinates:

$$x_i,\ i \in [1, I]$$

$$y_j,\ j \in [1, J]$$

$$z_k, \quad k \in [1, K]$$

The node (i, j, k) is defined by

$$x \in [x_i, \; x_{i+1}]$$

$$y \in [y_j, \; y_{j+1}]$$

$$z \in [z_k, \; z_{k+1}]$$

The node widths are expressed as

$$h_\ell^u = u_{\ell+1} - u_\ell; \quad u = x, y, z$$

and the node volume is

$$v_{i,j,k} = h_i^x \, h_j^y \, h_k^z$$

2.2 Nodal Equivalence Theory

Throughout this investigation, all problems are assumed to be steady-state. The time-dependent behavior of the neutronic properties of the reactor materials, resulting from depletion effects, is significant only if integrated over very long time periods; time derivatives due to these effects are generally neglected when calculating flux distributions throughout a core.

The steady-state Boltzmann transport equation states an exact neutronic balance in the small volume dE $d\Omega$ dV around the point $(E, \underline{\Omega}, \underline{r})$ of the phase space

$$\underline{\Omega} \cdot \nabla\psi(\underline{r}, \underline{\Omega}, E) + \Sigma_t(\underline{r}, E) \, \psi(\underline{r}, \underline{\Omega}, E)$$

$$= \int_0^\infty dE' \int d\Omega' \left[\frac{1}{\lambda} \sum_j \chi^j(E)\, \nu^j\, \Sigma_f^j (\underline{r}, E') + \Sigma_s(\underline{r}, \underline{\Omega}' \rightarrow \underline{\Omega}, E' \rightarrow E) \right] \psi(\underline{r}, \underline{\Omega}', E') \tag{2.1}$$

where

$\psi(\underline{r}, \underline{\Omega}, E)$ ≡ directional flux density at point $\underline{r}$, direction $\underline{\Omega}$ and energy E

$\chi^j(E)$ ≡ fission spectrum for isotope j

λ ≡ global reactor eigenvalue

and the cross section notation is standard.

It is very common to assume that the differential scattering cross section $\Sigma_s(\underline{r}, \underline{\Omega}' \rightarrow \underline{\Omega}, E' \rightarrow E)$ is a function only of the relative angle between the in- and out-going directions of neutron travel. By integrating (2.1) over all directions of neutron travel and over an energy range ΔE_g (g = 1, ···, G), we obtain a set of G exact equations

$$\nabla \cdot \underline{J}_g(\underline{r}) + \Sigma_{tg}(\underline{r})\, \varphi_g(\underline{r}) = \sum_{g'=1}^{G} \left[\frac{1}{\lambda} \chi_g\, \nu \Sigma_{fg'}(\underline{r}) + \Sigma_{gg'}(\underline{r}) \right] \varphi_{g'}(\underline{r}) \tag{2.2}$$

where

$$\varphi_g(\underline{r}) \equiv \int d\Omega \int_{\Delta E_g} \psi(\underline{r}, \underline{\Omega}, E)\, dE$$

$$\underline{J}_g(\underline{r}) \equiv \int d\Omega \int_{\Delta E_g} \underline{\Omega}\, \psi(\underline{r}, \underline{\Omega}, E)\, dE$$

$$\Sigma\alpha_g \equiv \frac{\int_{\Delta E_{g'}} dE\, \Sigma_\alpha(\underline{r}, E)\, \varphi(\underline{r}, E)}{\varphi_g(\underline{r})} \qquad (\alpha = t, f) \tag{2.3}$$

$$\Sigma_{gg'}(\underline{r}) \equiv \frac{\int_{\Delta E_g} dE \int_{\Delta E_{g'}} dE' \, \Sigma_{so}(\underline{r}, E' \to E)\varphi(\underline{r}, E')}{\varphi_{g'}(\underline{r})}$$

$$\chi_g \equiv \int_{\Delta E_g} \chi(E)\, dE$$

where

$$\varphi(\underline{r}, E) = \int d\,\Omega\, \psi(\underline{r}, \underline{\Omega}, E)$$

$$\Sigma_{so}(\underline{r}, E' \to E) = \int_{-1}^{1} \frac{d\mu_o}{2} \Sigma_s(\underline{r}, E' \to E, \mu_o)$$

For the sake of notational simplicity, we assume there is only one fissionable isotope in the reactor.

Integrating (2.2) over node (i, j, k), and applying the divergence theorem gives:

$$h_j^y h_k^z \left(J^x_{g_{i+1,j,k}} - J^x_{g_{i,j,k}}\right) + h_i^x h_k^z \left(J^y_{g_{i,j+1,k}} - J^y_{g_{i,j,k}}\right)$$

$$+ h_i^x h_j^y \left(J^z_{g_{i,j,k+1}} - J^z_{g_{i,j,k}}\right) + V_{i,j,k}\, \overline{\Sigma}_{tg_{i,j,k}} \bar{\varphi}_{g_{i,j,k}}$$

$$= \sum_{g'=1}^{G} V_{i,j,k} \left[\frac{1}{\lambda} \chi_g \overline{\nu\Sigma}_{fg'_{i,j,k}} + \overline{\Sigma}_{gg'_{i,j,k}}\right] \bar{\varphi}_{g'_{i,j,k}} \qquad (2.4)$$

where

$$\bar{\varphi}_{g_{i,j,k}} = \frac{1}{V_{i,j,k}} \int_{V_{i,j,k}} \varphi_g(\underline{r})\, d\underline{r}$$

$$\bar{\Sigma}_{\alpha g_{i,j,k}} = \frac{\int_{V_{i,j,k}} \varphi_g(\underline{r})\ \Sigma_{\alpha g}(\underline{r})\, d\underline{r}}{\bar{\varphi}_{g_{i,j,k}} V_{i,j,k}}$$

$$\Sigma_{gg'_{i,j,k}} = \frac{\int_{V_{i,j,k}} \Sigma_{gg'}(\underline{r})\, \varphi_g(\underline{r})\, d\underline{r}}{\bar{\varphi}_{g_{i,j,k}} V_{i,j,k}}$$

$$J^u_{g_{i,j,k}} = \frac{\int_{v_m}^{v_{m+1}} dv \int_{w_n}^{w_{n+1}} dw\ J_g(u_\ell, v, w)}{h^v_m\ h^w_n} \qquad u \neq v,\ v \neq w, \text{ and } u \neq w$$

$$\{\ell, m, n\} = \{i, j, k\}$$

We now want to introduce a set of mathematical quantities called "exact homogenized parameters", denoted with a circumflex, spatially constant in each node and constant in each energy group, which, when used in the neutron balance equation

$$\nabla \cdot \hat{J}_g(\underline{r}) + \hat{\Sigma}_{tg}\ \hat{\varphi}_g(\underline{r})$$

$$= \sum_{g'=1}^{G} \left[\frac{1}{\hat{\lambda}}\, \chi_g\, \widehat{\nu\Sigma}_{fg'} + \hat{\Sigma}_{gg'} \right] \hat{\varphi}_g(\underline{r}) \qquad (2.5)$$

will yield a solution having the following properties:

1. Reference nodal surface currents are preserved in each energy range.
2. Reference nodal reaction rates are preserved in each

energy range.

3. Reference nodal fluxes are preserved in each energy range.

(2.6)

Integrating (2.5) over node (i, j, k) gives:

$$h_j^y\, h_k^z \left(\hat{J}^x_{g_{i+1,j,k}} - \hat{J}^x_{g_{i,j,k}} \right) + h_i^x\, k_k^z \left(\hat{J}^y_{g_{i,j+1,k}} - \hat{J}^y_{g_{i,j,k}} \right)$$

$$+ h_i^x\, h_j^y \left(\hat{J}^z_{g_{i,j,k+1}} - \hat{J}^z_{g_{i,j,k}} \right) + V_{i,j,k}\, \hat{\Sigma}_{tg_{i,j,k}}\, \hat{\phi}_{g_{i,j,k}}$$

$$= \sum_{g'=1}^{G} V_{i,j,k} \left[\frac{1}{\hat{\lambda}}\, \chi_g\, \widehat{\nu\Sigma}_{fg'_{i,j,k}} + \hat{\Sigma}_{gg'_{i,j,k}} \right] \hat{\phi}_{g'_{i,j,k}} \qquad (2.7)$$

where

$$\hat{\phi}_{g_{i,j,k}} = \frac{1}{V_{i,j,k}} \int_{V_{i,j,k}} \hat{\phi}_g(\underline{r})\, dv$$

Comparison of (2.7) and (2.4), along with conditions (2.6) yields

$$\hat{\lambda} = \lambda$$

$$\hat{\Sigma}_\alpha = \Sigma_\alpha \qquad \alpha = t, f, gg' \qquad (2.8)$$

All coefficients of Equation (2.7) are now known, but this equation still contains unrelated unknowns, the homogeneous fluxes and face-averaged currents. In order to find a relation between these unknowns, we shall solve Equation (2.5) within each node while assuming that Fick's law is true. Nevertheless, this assumption does not limit the equivalence

theory to the usual diffusion theory model. Any of the models used to solve the transport equation (such as Monte-Carlo, discrete ordinates, multi-group diffusion theory ...) can be implemented in the equivalence theory content.

In the diffusion theory model, adjacent nodes are coupled by imposing the continuity of surface fluxes. When heterogeneous fluxes are considered, this continuity is verified because of the physical nature of these fluxes. Homogenized fluxes have only a mathematical meaning, in the sense that they are not measurable quantities. Thus, there is no reason to expect that they are continuous at assembly interfaces. Nevertheless, a coupling relation between adjacent nodes is still needed for solving the nodal equations. If we define the heterogeneous one-dimensional fluxes by

$$\varphi^{u}_{g_{\ell,m,n}}(u) = \frac{\int_{v_m}^{v_{m+1}} dv \int_{w_n}^{w_{n+1}} dw \; \varphi_g(u,v,w)}{h^v_m \, h^w_n}$$

it is trivially true that

$$\hat{\varphi}^{u}_{g_{\ell-1,m,n}}(u_\ell) \times \frac{\varphi^{u}_{g_{\ell,m,n}}(u_\ell)}{\hat{\varphi}_{g_{\ell-1,m,n}}(u_\ell)}$$

$$= \hat{\varphi}^{u}_{g_{\ell,m,n}}(u_\ell) \times \frac{\varphi^{u}_{g_{\ell,m,n}}(u_\ell)}{\hat{\varphi}^{u}_{g_{\ell,m,n}}(u_\ell)}$$

We now define discontinuity factors as

$$f^{u^-}_{g_{\ell,m,n}} = \frac{\varphi^u_{g_{\ell,m,n}}(u_\ell)}{\hat{\varphi}^u_{g_{\ell,m,n}}(u_\ell)}$$

$$f^{u^+}_{g_{\ell-1,m,n}} = \frac{\varphi^u_{g_{\ell,m,n}}(u_\ell)}{\hat{\varphi}^u_{g_{\ell-1,m,n}}(u_\ell)}$$

and the needed boundary condition for Equation (2.5) becomes:

$$f^{u^+}_{g_{\ell-1,m,n}} \hat{\varphi}^u_{g_{\ell-1,m,n}}(u_\ell) = f^{u^-}_{g_{\ell,m,n}} \hat{\varphi}^u_{g_{\ell,m,n}} \qquad (2.9)$$

The set of homogenized parameters defined by (2.8), along with the discontinuity factors $f^{u^\pm}_{g_{\ell,m,n}}$, will reproduce, in a node and energy group averaged sense, any solution of (2.1); it is very important to note that they will do so if and only if the same relation between current and fluxes is used when determining them and when solving (2.5) (whatever this relation is!).

Throughout this investigation, we shall limit ourselves to solving the 2 group diffusion equations for the heterogeneous fluxes; although this model is far from being exact [1], especially near strong heterogeneities,our purpose will be to measure the discrepancy between our nodal schemes and "reference" finite differences methods. In that sense, we shall determine only the accuracy of the nodal scheme, not the quality of the neutronic model being used.

The next section will show how this particular model has been implemented in a computer code.

2.3 The QUANDRY Equations

2.3.1 Introduction

The purpose of the QUANDRY computer code is to solve the equations corresponding to the extension of the diffusion theory, called equivalence theory, which was described in the previous section. In the framework of this theory, a reactor is divided into an array of large homogeneous blocks whose neutronic properties are described by the homogenized cross sections defined by Equation (2.8). In this section, these parameters are assumed to be known.

In order to be able to solve the global homogeneous problem, we shall first define all variables necessary to the description of all phenomena. Then, the sufficient number of equations to determine all these variables will be derived. Finally, the numerical solution to these equations will be discussed.

2.3.2 Problem Description

Equation (2.7) states an exact neutronic balance within each node and each energy group. It can be rewritten as

$$h_j^y\, h_k^z\, \hat{L}^x_{g_{i,j,k}} + h_i^x\, h_k^z\, \hat{L}^y_{g_{i,j,k}} + h_i^x\, h_j^y\, \hat{L}^z_{g_{i,j,k}} + V_{i,j,k}\, \hat{\Sigma}_{tg_{i,j,k}}\, \hat{\varphi}_{g_{i,j,k}} = V_{i,j,k} \sum_{g'=1}^{G} \left[\hat{\Sigma}_{gg'_{i,j,k}} + \frac{1}{\hat{\lambda}}\, \chi_{g_{\ell,m,n}}\, \widehat{\nu\Sigma}_{fg'_{ijk}} \right] \hat{\varphi}_{g'_{i,j,k}} \qquad (2.10)$$

where

$$\hat{L}^u_{g_{i,j,k}} = \hat{J}^u_{g_{\ell+1,m,n}} - \hat{J}^u_{g_{\ell,m,n}}$$

is the face averaged net leakage in direction u. Equation (2.10) shows that the global problem is defined, for each node and energy group, by a set of 4 independent variables: the volume averaged flux and the three directional leakages. A set of 4 independent equations relating these quantities has to be defined for these variables to be uniquely determined. One such equation, the nodal balance Equation (2.10) is already known. Three more relations, called the spatial coupling equations, will be obtained by solving the homogeneous diffusion equation within each node.

2.3.3 The spatial coupling equations

By integrating the diffusion equation for the homogeneous flux over the two directions transverse to direction u, one obtains a second order differential equation for the one-dimensional homogeneous flux:

$$
\begin{aligned}
& - \hat{D}_{g_{\ell,m,n}} \frac{\partial^2}{\partial u^2} \hat{\varphi}^u_{g_{\ell,m,n}}(u) + \hat{\Sigma}_{tg_{\ell,m,n}} \hat{\varphi}^u_{g_{\ell,m,n}}(u) \\
& - \sum_{g'=1}^{G} \left(\hat{\Sigma}_{gg'_{\ell,m,n}} + \frac{1}{\hat{\lambda}} \chi_{g_{\ell,m,n}} \widehat{\nu \Sigma}_{fg'_{\ell,m,n}} \right) \hat{\varphi}^u_{g'_{\ell,m,n}}(u) \\
& \equiv \hat{D}_{g_{\ell,m,n}} \int_{v_m}^{v_{m+1}} dv \int_{w_n}^{w_{n+1}} dw \frac{\partial^2}{\partial v^2} \hat{\varphi}_{g_{\ell,m,n}}(u,v,w) \\
& + \hat{D}_{g_{\ell,m,n}} \int_{v_m}^{v_{m+1}} dv \int_{w_n}^{w_{n+1}} dw \frac{\partial^2}{\partial w^2} \hat{\varphi}_{g_{\ell,m,n}}(u,v,w) \\
& \equiv - \hat{S}^u_{g_{\ell,m,n}}(u) \qquad u = x,y,z; \quad g = 1,\cdots,G \qquad (2.11)
\end{aligned}
$$

In that equation, $\hat{S}^u_{g_{\ell,m,n}}(u)$ represents the net leakage rate in the directions transverse to direction u. This equation is written in matrix

form as

$$-\left[\hat{D}_{\ell,m,n}\right]\frac{\delta^2}{\delta u^2}\left[\hat{\varphi}^u_{\ell,m,n}(u)\right]+\left[\hat{\Sigma}_{\ell,m,n}\right]\left[\hat{\varphi}^u_{\ell,m,n}(u)\right]$$

$$=-\left[\hat{S}^u_{\ell,m,n}(u)\right] \qquad (2.12)$$

where

$\left[\hat{D}_{\ell,m,n}\right]$ is a G x G diagonal matrix containing homogenized diffusion coefficients;

$\left[\hat{\varphi}^u_{\ell,m,n}(u)\right]$ is a column vector of length G containing homogenized one-dimensional fluxes;

$\left[\hat{\Sigma}_{\ell,m,n}\right]$ is a full G x G matrix whose elements are:

$$a_{gg'}=\delta_{gg'}\Sigma_{tg_{\ell,m,n}}-\Sigma_{gg'_{\ell,m,n}}-\frac{1}{\hat{\lambda}}\chi_{\ell,m,n}\times\hat{\nu\Sigma}_{fg'_{\ell,m,n}}$$

where $\delta_{gg'}$ is the standard Dirac notation.

$\left[\hat{S}^u_{\ell,m,n}(u)\right]$ is a column vector of length G containing the net transverse leakages.

This inhomogeneous second order differential equation could be easily solved if the transverse leakage term $\left[\hat{S}^u_{\ell,m,n}(u)\right]$ were known. Unfortunately, only its average over u, $\left[\hat{\bar{S}}_{\ell,m,n}\right]$ is known. To overcome this difficulty, an approximation concerning the shape of the transverse leakages must be made.

Two such approximations can be made in QUANDRY: this shape can be assumed to be either flat or quadratic. For the direction u, the flat transverse leakage is equal to its average value, while the quadratic

chosen is such that the integrals of the quadratic transverse leakage approximation over the node (ℓ, m, n) and the two adjacent nodes $(\ell-1, m, n)$ and $(\ell+1, m, n)$ preserve the average transverse leakages over each node.

Once an approximation for the shape of the transverse leakage has been made, the differential Equation (2.12) can be solved for the one-dimensional homogeneous flux. This equation being of the second order, both the flux and its derivative (which is proportional to the net current) have to be specified at a given point to yield a completely determined solution.

The actual solution to (2.12) involves some heavy notation, though it is algebraically trivial. It will not be repeated here since it is very well documented in [2]. It is assumed that this solution is known.

Figure 2.1 shows three adjacent QUANDRY nodes. Equation (2.12) is first solved for node $(\ell-1, m, n)$ subject to the homogeneous boundary conditions (one-dimensional flux and currents) at $u = u_\ell$. By integrating the resulting solution over the range $\left[u_{\ell-1}, u_\ell\right]$, and rearranging terms, one obtains the homogeneous one-dimensional flux at u_ℓ, $\hat{\varphi}^u_{\ell=1, m, n}(u_\ell)$, as a function of the surface averaged current, transverse leakages and volume averaged fluxes

$$\left[\hat{\varphi}^u_{\ell-1, m, n}(u_\ell)\right] = f_\lambda\left(\left[\hat{J}^u_{\ell-1, m, n}(u_\ell)\right], \left[\hat{\bar{\varphi}}_{\ell-1, m, n}\right], \left[\hat{S}^u_{\ell-2, m, n}\right], \left[\hat{S}^u_{\ell-1, m, n}\right], \left[\hat{S}^u_{\ell, m, n}\right]\right) \quad (2.13)$$

By similarly imposing the homogeneous boundary conditions at $u = u_\ell$ on node (ℓ, m, n), one obtains:

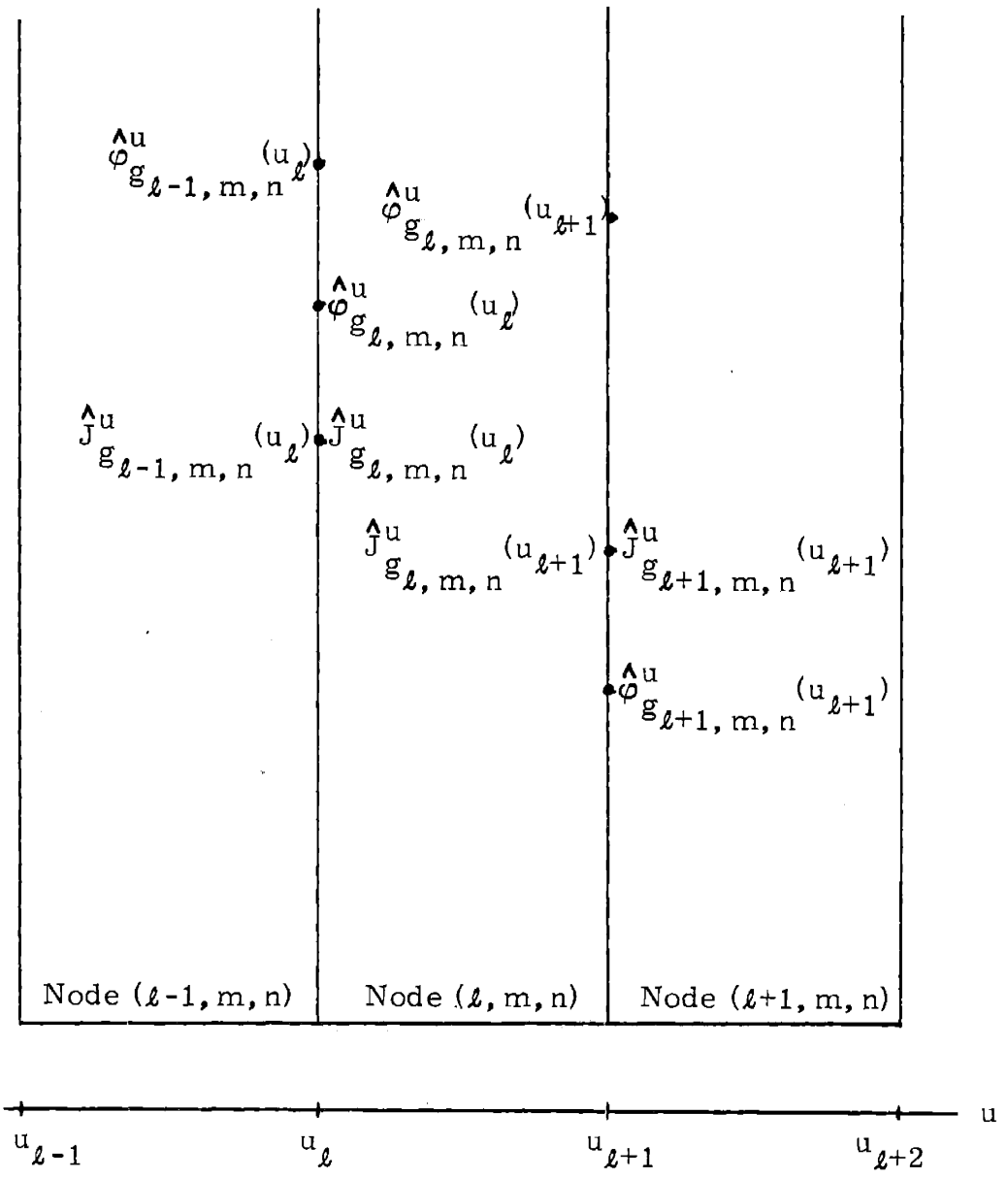

Fig. 2.1 Three adjacent QUANDRY nodes.

$$\left[\hat{\varphi}^{u}_{\ell,m,n}(u_\ell)\right] = g_\lambda\left(\left[\hat{J}^{u}_{\ell,m,n}(u_\ell)\right], \left[\bar{\hat{\varphi}}_{\ell,m,n}\right], \left[\hat{S}^{u}_{\ell-1,m,n}\right], \left[\hat{S}^{u}_{\ell,m,n}\right], \left[\hat{S}^{u}_{\ell+1,m,n}\right]\right) \quad (2.14)$$

By imposing the continuity condition (2.9), along with the net current continuity condition, the one-dimensional homogeneous fluxes appearing in (2.13) and (2.14) can be eliminated; the resulting relation will be of the form:

$$h_\lambda\left(\left[\hat{J}^{u}(u_\ell)\right], \left[\bar{\hat{\varphi}}_{\ell-1,m,n}\right], \left[\hat{S}^{u}_{\ell-2,m,n}\right], \left[\hat{S}_{\ell-1,m,n}\right], \left[\hat{S}_{\ell,m,n}\right], \left[\hat{S}_{\ell+1,m,n}\right]\right) = 0 \quad (2.15)$$

where

$$\left[\hat{J}^{u}(u_\ell)\right] = \left[\hat{J}^{u}_{\ell,m,n}(u_\ell)\right] = \left[\hat{J}^{u}_{\ell-1,m,n}(u_\ell)\right]$$

Though Equation (2.15) has been written in an implicit form, it is a linear relation (except for the eigenvalue dependence). It is particularly important to notice that currents can be expressed as functions of the other parameters in this relation. The same process can be repeated at $u = u_{\ell+1}$, and will yield a relation analogous to (2.15). By extracting the face-averaged net currents at u_ℓ and $u_{\ell+1}$ from these equations, and subtracting them to obtain the net leakage in the u-direction, the spatial coupling for direction u is found: this equation relates only net leakages and nodal fluxes; the face-averaged fluxes and net currents have been eliminated.

We have now found enough equations to determine fully a solution to the equivalence theory equations. The next section will discuss how

these equations are solved in the computer code QUANDRY, and will outline the possible problems associated with the numerical schemes used in QUANDRY.

2.3.4 Numerical Solution to the QUANDRY Equations

The combination of the nodal balance equation with the three directional coupling equations yields a system of the form:

$$[H]\,[\psi] = \frac{1}{\hat{\lambda}}\,[P]\,[\psi] \qquad (2.16)$$

where

$[\psi]$ = col $\left\{[\hat{\bar{\varphi}}],\ [\hat{\bar{L}}_x],\ [\hat{\bar{L}}_y],\ [\hat{\bar{L}}_z]\right\}$ is a 4 * G * I * J * K column vector, containing the nodal fluxes and net leakages in each direction;

[P] is a (4 * G * I * J * K) x (4 * G * I * J * K) square matrix, containing the fission production terms in the top left (G * I * J * K) * (G * I * J * K) square sub-matrix. Its elements are zero everywhere else.

[H] is a (4 * G * I * J * K) x (4 * G * I * J * K) square matrix whose elements result from the coupling equations derived in section 2.3.3. These elements depend on $\hat{\lambda}$. This last dependence of [H] on the global eigenvalue of the homogeneous problem creates a nonlinearity in Equation (2.16). Nevertheless, QUANDRY is generally successful in solving this eigenvalue problem by implementing the following four levels of iterations:

- an updating process, wherein the matrix [H] is recalculated every few (usually 5 to 10) outer iterations;
- a fission source iteration ("outer" iteration), accelerated through Wielandt's scheme [4], and used for determining

the maximum eigenvalue;

- within each outer iteration, "inner" iterations, using a modified Gauss-Seidel scheme [5], performed to invert [H];
- a cyclic Cheybychev Semi-Iterative method [5] to perform the flux iterations.

In the course of this investigation, some nodal schemes which involved the use of QUANDRY were found to be non-convergent. Though this non-convergence is not necessarily due to the QUANDRY numerical schemes, it seems important to point out where they may fail.

We already indicated the nonlinear nature of Equation (2.16). Under these conditions, there is no mathematical guarantee that QUANDRY will converge. Nevertheless, Smith [2] indicates that when a good estimate of the eigenvalue of the global homogeneous problem is known, the effects of updating the matrix [H] should be quite negligible. Unfortunately, in the case of iterative schemes, eigenvalues can vary widely from iteration to iteration, as shown in Chapter 3.

Cheng [6] pointed out that, as both energy groups are solved simultaneously during the flux iterations, diagonal dominance is not ensured, so that these iterations are not guaranteed to converge.

However, QUANDRY has been used very extensively at MIT, and the accumulated experience indicates that, if realistic input parameters are used, it never fails to converge.

2.4 The Generation of Approximate Equivalence Theory Parameters

2.4.1 Introduction

The "exact" equivalence theory parameters are defined by Equation (2.8):

$$\hat{\Sigma}_{\alpha g_{i,j,k}} = \frac{\int_{V_{i,j,k}} \varphi_g(\underline{r})\, \Sigma_{\alpha g}(\underline{r})\, dr}{V_{i,j,k}\, \bar{\varphi}_{g_{i,j,k}}}$$

This relation involves the knowledge of the exact heterogeneous macroscopic cross sections $\Sigma_{\alpha g}(\underline{r})$, along with the knowledge of the spatial shape of the reference fluxes, $\varphi_g(\underline{r})/\bar{\varphi}_{g_{i,j,k}}$. How two-group macroscopic cross sections are obtained will be discussed in the next section.

Determining the shape of the reference fluxes is probably as difficult as determining the fluxes themselves. Furthermore, there would be no advantage in using elaborate nodal methods if the reference solution was known anyway. It is therefore of primary interest to be able to generate an accurate and cheap approximation for the detailed shape of the reference fluxes. Section 2.4.3 will present and discuss the various methods which have been devised for that purpose.

2.4.2 Determination of 2-Group Heterogeneous Macroscopic Cross Sections

The general expression for a heterogeneous macroscopic cross section in group g is:

$$\Sigma_{\alpha g}(\underline{r}) = \frac{\int_{\Delta E_g} dE \sum_j n_j(\underline{r})\, \sigma_{\alpha j}(E)\, \varphi(\underline{r}, E)}{\int_{\Delta E_g} \varphi(\underline{r}, E)} \qquad (2.17)$$

where

$n_j(\underline{r})$ is the density of isotope j at point $\underline{r}$;

$\sigma_{\alpha j}(E)$ is the microscopic cross section for event α, for isotope j, at energy E;

$\varphi(\underline{r}, E)$ is the flux of neutrons with energy E at point $\underline{r}$.

The exact knowledge of all these quantities is necessary for the calculation of $\Sigma_{\alpha g}(\underline{r})$. Unfortunately, their determination is clearly an impossible task: for example, calculating $\varphi(\underline{r}, E)$ would require solving the continuous diffusion equation. Furthermore, the isotope densities, $n_j(\underline{r})$, are a function of all time-dependent pointwise fluxes. Ultimately, the knowledge of microscopic cross sections and depletion dependent phenomena is not perfect; even though the capacities of digital computers increase rapidly, the basic experimental determination of these physical quantities remains a final limit to the precision of Reactor Physics calculations.

Numerous approximate methods have been devised for the estimation of macroscopic cross sections [1, 8, 9]. They generally rely on assuming the separability of $\varphi(\underline{r}, E)$ with respect to space and energy. The energy component is then approximated by known shapes, or obtained from spectrum calculations.

The implementation of energy collapsing procedures in the equivalence theory framework has been studied only superficially [10]. In the rest of this investigation, it will be assumed that the 2-group heterogeneous macroscopic cross sections of all materials involved are known.

2.4.3 The Determination of Approximate Equivalence Theory Parameters

2.4.3.1 Problem Definition

The most common approach to approximating the shape of the reference flux is to solve the diffusion equation within each node, applying some set of assumed boundary conditions. This set of boundary

conditions should obey two rules: first, it should be general enough so that just a few of these local calculations are sufficient to solve the global problem; second, and most important for the accuracy of the results, it should respect the physics of the problem, in order not to introduce artificial distortions.

Partial incoming or outgoing currents, net surface currents, or surface fluxes, if defined on all faces of the node, each constitute a set of boundary conditions sufficient to determine a unique solution to the diffusion equation within the node. Each of these sets of boundary conditions can be described entirely by the magnitude and the shape of the corresponding physical quantity. Therefore, any assumption made for approximating the reference flux shape will consist of choosing the magnitude or the shape (or both) of the quantity imposed on each boundary. Consequently, there will be two classes of approximate methods for determining homogenized parameters; the first category will consist of those methods where both the shape and magnitude of the boundary condition are chosen: these methods will be essentially non-iterative. The second category will contain all methods where only the mathematical form of the shape of the boundary condition is chosen; its magnitude has to be determined through an iterative process.

A simple test can be used for determining the accuracy of a given approximation, without having to implement it in a sometimes complicated procedure: if, for example, the shape of some boundary condition is assumed, the diffusion equation should be solved within a node, imposing the reference magnitude along with the chosen shape on its boundaries. A comparison of the reference flux shape within the node with the flux shape obtained through this process will indicate the quality of the

approximation.

2.4.3.2 Non-iterative Schemes for the Approximation of Equivalence Theory Parameters: "Assembly" Homogenized Parameters

"Assembly" homogenized parameters are obtained by assuming that the net current across the boundaries of each individual assembly are zero ($\underline{J} \cdot \underline{n} = 0$) in all energy groups. Smith [3] introduced this method for BWR's when he noticed that reference discontinuity factors depend essentially on the type (defined as a function of void fraction and burnup) of assembly considered, and little on the position of the assembly in the core. In this connection it should be noted that the presence of a large gap of water between the fuel and the assembly boundaries (see Appendix 1) isolates individual assemblies from each other.

For each type of assembly an eigenvalue calculation is done with the $\underline{J} \cdot \underline{n} = 0$ boundary condition. The resulting heterogeneous fluxes, $\varphi_g^A(x,y)$, are used along with Equation (2.8) to obtain "assembly cross sections" (AXS). Because of the zero current boundary condition, the homogeneous fluxes within the node are spatially flat; hence the "assembly discontinuity factor" (ADF) on a face is the ratio of the average heterogeneous flux on this face, to the node-averaged heterogeneous flux.

The first two columns of Tables 2.1 and 2.2 show the nodal results obtained from different homogenization schemes for the LSH-BWR benchmark, a strongly heterogeneous and tilted core, and the CISE benchmark, a more homogeneous core. Both these benchmarks are described in Chapter 3 and in Appendix 1.

Table 2.1 LSH-BWR nodal results

Nodal Scheme	FWC	ADF-AXS	J N1S1	J N5S2
Error in eigenvalue	-0.29%	-0.08%	0.05%	-0.16%
Maximum error in nodal powers	22.6%	9.48%	3.42%	38.8%
Average error in nodal powers	5.90%	3.16%	1.06%	12.2%

Note: NnSs means n nodes, and s segments on each surface are used for generating response matrices.

Table 2.2 CISE nodal results

Nodal Scheme	FWC	ADF-AXS	J_{in} (cluster) N1S2	J_{in} (cluster) N5S2	J N1S1	J N5S2
Error in eigenvalue	-0.16%	-0.03%	-1.67%	-1.25%	0.09%	-0.10%
Maximum error in nodal powers	+9.86%	-3.06%	47.8%	9.54%	2.87%	1.09%
Average error in nodal powers	4.19%	0.98%	15.2%	3.50%	0.97%	0.33%

The notation is the same as in Table 2.1.

The standard flux weighted constants (FWC) yield high errors in nodal powers. The use of "assembly" parameters (ADF-AXS) clearly improves the nodal solution, but the precision obtained is still only marginally acceptable.

The failure of ADF-AXS to yield excellent results is clearly related to the inadequacy of the $\underline{J} \cdot \underline{n} = 0$ approximation: while this approximation is physically acceptable far from any strong heterogeneity, assemblies close to control rods or to the water reflector are subject to very important currents of neutrons across their faces.

An immediate generalization of the notion of assembly parameters is to impose the $\underline{J} \cdot \underline{n} = 0$ condition not on assembly boundaries, but on some arbitrary location, where the condition seems to be physically acceptable. This generalization was done for PWR's by Hoxie [7], with the notion of "extended assemblies".

Extended assemblies are constituted of some peripheral fuel assemblies, along with a part of the water reflector and, in PWR's, they also include a portion of the steel baffle surrounding the core. An eigenvalue calculation, with $\underline{J} \cdot \underline{n} = 0$ boundary conditions, is then performed for that portion of the core; by avoiding the imposition of a non-realistic zero-current condition on the fuel-reflector interface, this method enabled Hoxie to improve results obtained from "normal" assembly calculations.

This method could conceivably be applied to the analysis of BWR's by using large sets of assemblies surrounding all important heterogeneities (control rods and fuel-reflector interface). However, the number of heterogeneous calculations involved (as many as half the fueled assemblies) would make this scheme unattractive. Some partial

use of the concept underlying this procedure will nevertheless be made in the course of this investigation.

We conclude that non-iterative methods for determining approximate equivalence parameters are not sufficient to yield uniformly accurate nodal results in BWR's. In order to obtain improved accuracy, more sophisticated schemes must be used.

2.4.3.3 Iterative Schemes for the Approximation of Equivalence Theory Parameters Based on Partial or Net Surface Currents

Assembly calculations based on $\underline{J} \cdot \underline{n} = 0$ boundary conditions fail to yield correct homogenized parameters because these boundary conditions do not take into account many of the interassembly effects.

Smith [3] noticed that if the actual boundary conditions that exist on the surface of an assembly were known, a fixed source cell calculation could be performed to obtain exact equivalence parameters. Unfortunately, the determination of these exact boundary conditions is as difficult as the determination of the reference heterogeneous fluxes. Nevertheless, the observation that such fixed-source calculations could produce the exact equivalence parameters led Smith to devise an iterative scheme in which the needed boundary conditions at each iteration are obtained from the magnitude predicted at the previous iteration, along with an assumed shape. Later, Cheng [6] introduced the use of pretabulated response matrices for these schemes, in order to reduce significantly the number of fixed-source calculations to be performed.

Cheng first investigated the use of partial incoming current response matrices. These matrices were generated either for one node (a node being either an assembly or a cluster of 4 assemblies), or a

cross-shaped cluster of five nodes. The use of a cluster of five nodes was intended to suppress the effects of the approximation made on the shape of the partial currents on the boundaries of the central node. In both cases, the shape of the partial currents was represented by either one or two flat segments on each surface. Upon testing these methods, Cheng obtained very large errors in both eigenvalue and nodal powers (see Table 2.2, columns 3 and 4). He related these large errors to the inadequacy of the spatial approximations applied to partial surface currents. In particular, discontinuity factors for peripheral nodes were greatly in error, which resulted in significant discrepancies in the power densities of these nodes.

Noticing that the shape of net currents was much smoother than the shape of partial currents, Cheng then investigated the use of response matrices based on net surface currents. The different approximations used were the same as for the case of partial surface currents (one or five nodes, one or two flat segments). Results for the LSH-BWR and CISE benchmarks are given in the last two columns of Tables 2.1 and 2.2, respectively. Although these results are often very good, they do not appear to be totally consistent. For example, these iterative schemes do not always improve the ADF-AXS results. Furthermore, Cheng found that the global-local iteration process associated with these schemes often fails to converge. Such erratic behavior makes this particular approach of limited use.

To understand why these relatively sophisticated schemes fail to predict correct equivalence theory parameters, we applied the test suggested in section 2.4.3.1 to estimate how well different shape approximations reproduce the reference fluxes within a node when

reference magnitudes are used. It was shown [11] that unless a quadratic shape was assumed for the net surface currents, the heterogeneous fluxes could not be obtained with satisfactory precision. Unfortunately, there is no known way of inferring the parameters that specify the required quadratic shape from only nodal results. Thus iterative schemes based on net surface currents seem not to be a fruitful approach to the problem of finding homogenized group parameters and discontinuity factors for a heterogeneous node.

2.5 Summary

In this chapter we first described the nodal equivalence theory, and showed that there exist homogenized parameters which will reproduce any reference solution to the neutron transport equation. The implementation of the equivalence theory in the computer code QUANDRY was then described. Finally, different approximate methods for estimating homogenized parameters were examined, and it was shown that for BWR benchmark problems both non-iterative methods, which supress the coupling effects between adjacent nodes, and iterative schemes, which represent this coupling through surface partial- and net-currents, fail to yield correct homogenized parameters.

CHAPTER 3

HOMOGENIZATION TECHNIQUES BASED ON SURFACE FLUX RESPONSE MATRICES

3.1 Introduction

In Chapter 2 we described a simple method, based on zero net-currents boundary condition assembly calculations, for determining approximate equivalence-theory parameters, and we also described more sophisticated iterative schemes, based on partial- and net-current response matrices. We pointed out that these schemes fail to yield good homogenized parameters because of the inadequacy of the assumptions made for the shape of the boundary conditions used for determining these parameters.

In this chapter we shall first describe the two-dimensional BWR benchmarks for which new homogenization schemes will be tested. In section 2 the possibilities of approximating the assembly boundary conditions by polynomial shapes will be examined, and we shall show that the most feasible scheme consists of assuming a quadratic shape for the surface form function (the ratio of the heterogeneous surface flux to the assembly surface flux). Section 3 will describe how this quadratic shape can be derived from a nodal solution, by interpolating cornerpoint fluxes. Section 4 will discuss the response matrices based on this assumption, and will show how a consistent iterative scheme using these matrices can be implemented. This scheme will be tested for realistic benchmarks in section 5. Finally, the extension of homogenization schemes to three-dimensional calculations will be discussed in section 6.

3.1.1 Two-Dimensional BWR Benchmarks

The axial flux distribution in a BWR core is smooth everywhere, except at the tip of inserted control rods. Therefore, the main difficulties for assembly homogenization lie in the radial planes of the core. Consequently, the benchmarks chosen for testing new homogenization schemes are all two-dimensional; these benchmarks are explicitly described in Appendix 1. An extension to the axial direction will be examined in section 6 of this chapter.

3.1.1.1 The CISE BWR Benchmark Problem

The CISE BWR benchmark problem [13] represents a simplified model of a two-dimensional BWR core. It consists of 208 fuel assemblies (both fresh and burned) surrounded by a 15-cm water reflector. It does not exhibit any void pattern. The fuel assemblies consist of a central homogeneous fuel region, surrounded by a water gap and control rod blades. Though some heterogeneities (such as water holes, burnable poison pins and enrichment zones) are not represented explicitly, the most important heterogeneities, as far as homogenization is concerned, are represented. These are the control rod blades and the water gap. Thus, the CISE BWR benchmark serves as a realistic test of any homogenization scheme.

The reference solution for the CISE BWR benchmark was obtained from a fine-mesh QUANDRY run. 64 mesh points were used in each assembly. It is important to note that this meshing is sufficient for the QUANDRY solution to be spatially converged, whereas a PDQ7 [17] solution using this same meshing would not be spatially converged.

3.1.1.2 The LSH BWR Benchmark Problem

The LSH BWR (Loretz-Smith-Henry) benchmark problem was

designed at MIT in order to be a very severe test for the homogenization schemes being studied there, and is described in Appendix 1. It consists of 160 fuel assemblies surrounded by a 30.62 cm water reflector. The central region of the core is partially voided (40% and 70% void fractions), and two control rods are present in each quarter-core. Their location is such that groups of two very close control rods exist around each symmetry-line of the core. That particular feature creates very strong flux tilts in the core. The fuel assemblies are those characteristic of the Vermont Yankee reactor, where most heterogeneities are explicitly represented; i.e., the different enrichment zones, the water hole, the gadolinium pins, the wide and narrow gaps and the control rod blades are all represented as distinct regions. The can surrounding the fuel regions is not modeled, though it is accounted for in the calculation of the heterogeneous diffusion theory parameters.

Two reference solutions are available for this benchmark; a fine-mesh QUANDRY solution, for which 169 mesh points were used in each assembly, and a fine-mesh PDQ7 solution, where 324 mesh points were used in each assembly. While the first solution is spatially converged, the second is not (as can be seen from the results shown in Appendix 6). Nevertheless, it is an essential feature of equivalence theory to be able to reproduce any solution of the diffusion equation. Therefore, both of these references are valid, as far as the testing of homogenization procedures is concerned.

3.1.1.3 The MVY BWR Benchmark Problem

The MVY BWR (Modified Vermont Yankee) benchmark problem models the bottom section (water inlet) of the Vermont Yankee reactor and is described in Appendix 1. It consists of 368 fuel assemblies

surrounded by a water reflector. The assembly configuration and the heterogeneous cross sections are the same as those described for the LSH BWR benchmark. These assemblies differ only slightly from those used to model the real Vermont Yankee core: the model used in this thesis assumes that the fuel cross sections are only enrichment dependent, whereas a more precise modeling would require these cross sections to be position dependent, to account for spectral effects.

Some previous testing at MIT [14] has shown that the Vermont Yankee core is a very severe problem for usual homogenization schemes: standard flux weighted constants yield errors in nodal powers as large as 26%, while the use of ADF-AXS reduces these errors to around 10%. This is only marginally acceptable, though it is better than the results from the tuned nodal code SIMULATE [15]. The presence of an important number of control rods, and particularly the proximity of one of these rods to the water reflector, creates very large flux gradients throughout the core.

The reference solution for the MVY BWR benchmark problem is a fine-mesh PDQ7 solution, where 324 mesh points are used in each assembly.

3.2 Polynomial Approximations for Assembly Boundary Conditions

The determination of equivalence theory parameters requires the knowledge of approximated boundary conditions for each assembly. These approximated boundary conditions should have the following properties:

1. The fluxes resulting from solving the diffusion equation within each assembly, subject to these particular boundary conditions, should be a close approximation to the reference

fluxes.

2. These boundary conditions should have some properties of additivity, namely, the sum of two such boundary conditions should still have the same mathematical form as the two original boundary conditions. This property is essential for the very existence of response matrices based on these particular boundary conditions.
3. The mathematical form of this approximation can be implemented from the sole knowledge of a nodal solution to the global problem.

The second condition quoted eliminates the majority of the usual analytic functions: trigonometric functions, exponentials, logarithms, do not have the necessary additivity properties. For example, the sum of two sine functions is generally not a sine function. On the other hand, polynomials of degree smaller or equal to n form a ring for the usual addition and multiplication by a scalar. They are, therefore, natural candidates for approximating assembly boundary conditions.

The first condition has less obvious implications: for example, it is hard to judge a priori if a poor approximation for some surface currents will result in poor heterogeneous fluxes within the assembly. Appendix 3 contains some graphs of the actual boundary conditions along assembly faces: net and partial surface currents, albedos and surface fluxes. The behavior of these quantities in the fast energy group is generally very smooth, so that any shape approximation which is sufficiently accurate in the thermal group can be immediately extended to the fast group. The first eight graphs show these quantities, in the thermal group, along two interfaces between fueled assemblies and water

reflector, for the LSH BWR benchmark (the PDQ7 reference calculation was used; the partial and net currents were calculated by D. K. Parsons). The six first graphs, which represent in- and out-going partial currents, net currents and albedos (φ/J) clearly demonstrate the impossibility of a polynomial fit to these quantities. The next two graphs represent the heterogeneous fluxes and a new quantity, called the form function, and defined as the ratio of the heterogeneous flux to the heterogeneous assembly surface flux:

$$F_g(x,y) = \frac{\varphi_g(x,y)}{A_g(x,y)} \qquad (3.1)$$

Both the flux and form function appear to be quadratic in shape along the considered faces.

The following twelve graphs in Appendix 3 represent the heterogeneous flux and the form function, along a one-dimensional cut of the MVY BWR benchmark, ranging from the center of the core to the middle of its reflector. The quadratic nature of the form function is obvious, whereas the heterogeneous flux is poorly fit by a quadratic, especially along rodded faces.

There is strong evidence that the quadratic form function assumption is the best candidate for being implemented in an iterative scheme. Physically, this fact is not surprising: currents are proportional to the derivative of the fluxes, and are therefore very likely to have sharp variations; the fluxes themselves are subject to very large gradients near strong heterogeneities such as control rods; but once these fluxes are divided by the assembly fluxes, the dependence on local heterogeneities is supressed, and only the smooth global tilt of the core should appear.

It will be shown in the next section that the quadratic form function approximation satisfies the third condition stated earlier. It should also be noted that there appears to be no way of determining accurate quadratic shapes for partial and net surface currents, if only a nodal solution is known.

3.3 The Interpolation of Cornerpoint Fluxes

In this section we shall discuss mainly the theoretical background and the theoretical limitations of the cornerpoint fluxes interpolation scheme which has been developed at MIT [7, 14]. The actual equations which result from this theory are very simple, and are explicitly presented in Appendix 4 of this thesis.

3.3.1 Problem Description

Definition (3.1) for the form function implies the existence of two different form functions along a face common to two non-identical assemblies (these two form functions correspond to the two different assembly fluxes along this face). Furthermore, once the quadratic approximation is made for each of these form functions, two distinct heterogeneous flux shapes are defined along this face, as the quadratic approximation cannot reproduce exactly the pointwise fluxes. This very un-physical situation leads us to blend the two assembly flux shapes along this face in a unique "average assembly flux shape":

$$A_{av}(x) = \frac{1}{2}\left(\frac{A_1(x)}{\overline{A}_1} + \frac{A_2(x)}{\overline{A}_2}\right) \qquad (3.2)$$

where

x is the dimensional variable along the considered face;

$A_1(x)$ and $A_2(x)$ are the two assembly fluxes along that face;

$\overline{A}_1$ and $\overline{A}_2$ are the averages of the assembly fluxes over that face.

The assembly flux shapes vary relatively little with the exposure and void fraction of the considered assembly. It is therefore quite natural to use the blending process described by Equation (3.2).

The definition of a quadratic form function for each face requires three pieces of information (or equations) for each face. Two are readily obtained: the preservation of the average flux on that face (determined by a nodal calculation) leads to a first equation; the continuity of the heterogeneous flux at the cornerpoint leads to another equation. There is only one degree of freedom left to be eliminated. This will be done by the source-free condition.

3.3.2 The Source-free Condition

It is physically exact to state that each assembly cornerpoint is source-free [16]. This condition is implemented in a mathematical form by drawing a small square box around each cornerpoint (see Fig. 3.1) and requiring the contour integral of the net transverse currents, $\oint J_g \cdot \underline{n}$, to be zero at the limit of an infinitely small box. These currents are estimated from the derivative of the approximate flux shapes defined on the four faces converging at that cornerpoint. The resulting equations lead to a linear system in each energy group, where each cornerpoint flux is related to its four closest neighbors. Such a system is easily solved by an accelerated Gauss-Seidel iterative scheme.

Unfortunately, the fact of having used approximate flux shapes to determine net currents creates two essential problems:

1. The derivative of a good approximation is not necessarily a good approximation to the original derivative: even if the quadratic form function approximation is a very close fit to the reference form function, the derivative used in the

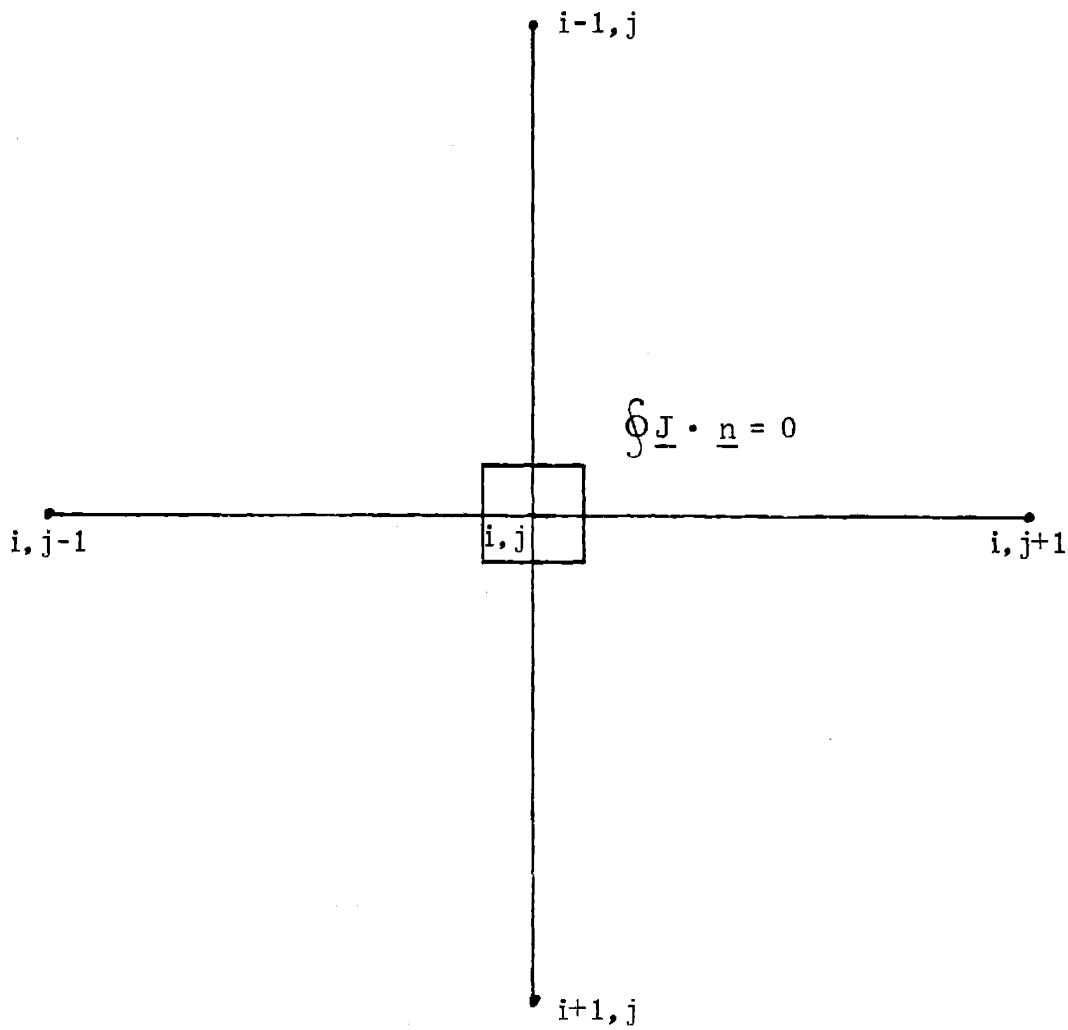

Fig. 3.1 The source-free condition.

source-free condition may yield a very bad approximation to the reference currents.

2. The reference net currents transverse to an assembly face are continuous across this face, whereas the approximate net currents are not necessarily continuous. This leads to a situation where the equation resulting from the source-free condition depends on the shape of the box used to implement this condition.

Two interesting limit-cases appear: when a rectangular box is used, and is being "flattened" in only one dimension, the resulting equation will impose the continuity of the net current in that same dimension, and no effects of currents transverse to that direction will be accounted for.

Some results for this cornerpoint flux interpolation scheme will be described in section 5 of this chapter. It will be seen that, although some serious theoretical limitations have been pointed out, the results are generally quite good.

3.4 An Iterative Scheme Based on Surface Flux Response Matrices

3.4.1 Definition of Surface Flux Response Matrices

It was stated in the second section of this chapter that polynomials of degree n, and particularly quadratics, have additivity properties which enable them to be implemented in a response matrix scheme. Specifically, it is very easy to show (using this additivity property along with the superposition principle for the solution of the diffusion equation and the continuity of surface fluxes) that, for a given global eigenvalue, λ, the heterogeneous flux at each point of an assembly is a linear function of the cornerpoint fluxes and average surface fluxes on the boundaries of

that assembly, provided the quadratic form function assumption is made:

$$\varphi_g(x,y) = \sum_{g'=1}^{G} \left[\sum_{IF=1}^{4} \bar{\varphi}_{g'}^{IF} \, a_{\lambda_{g'g}}^{IF}(x,y) + \sum_{IC=1}^{4} \varphi_{g'}^{IC} \, b_{\lambda_{g'g}}^{IC}(x,y) \right] \tag{3.3}$$

where

$\bar{\varphi}_{g'}^{IF}$ is the average flux in group g' on face IF;

$\varphi_{g'}^{IC}$ is the flux in group g' at cornerpoint IC;

$a_{\lambda_{g'g}}^{IF}(x,y)$ is the flux in group g' at point (x, y), resulting from a fixed-source problem for the eigenvalue λ, where all surface form functions are quadratic, and all cornerpoint fluxes and average surface fluxes are zero, except $\bar{\varphi}_{g'}^{IF}$ which is one.

$b_{\lambda_{g'g}}^{IC}(x,y)$ is the flux in group g' at point (x, y), resulting from a fixed-source problem for the eigenvalue λ, where all surface form functions are quadratic, and all cornerpoint fluxes and average surface fluxes are zero, except $\varphi_{g'}^{IC}$ which is one.

As the volume averaged fluxes, volume averaged reaction rates and face averaged transverse currents depend linearly on the heterogeneous fluxes (via the integration and derivation operators, which are linear), these quantities also depend linearly on the cornerpoint and face-averaged fluxes. Therefore, it is possible to define a response matrix R_λ so that:

$$[N.Q.] = [R_\lambda]\,[\omega] \tag{3.4}$$

where

$[\varphi]$ is an 8G column vector containing cornerpoint fluxes and face-averaged fluxes;

[N.Q.] is a 10G column vector containing all nodal quantities: the 4 face-averaged currents, the volume averaged fluxes, and the integrated reaction rates (transport, absorption, removal, nu-fission and fission).

Consequently, $[R_\lambda]$ is a 10G x 8G rectangular matrix. Its elements are defined in Appendix 5. It is important to notice that it is necessary and sufficient to know λ, the heterogeneous macroscopic cross sections and a model to solve the diffusion equation, in order to define $[R_\lambda]$ exactly.

3.4.2 The Generation of Surface Flux Response Matrices

It was shown in Chapter 2 that "exact" equivalence theory parameters have to be generated with the same model as is used in the reference calculation. It was also stated that they exist for any "reference" solution, even if this solution is not spatially converged. Specifically, the model which has to be used in both the reference calculations and the determination of equivalence theory parameters includes not only a relation between fluxes and currents, but also some information on the degree of spatial truncation allowed. For example, if the reference solution is a PDQ7 run [17], the homogenized parameters should be calculated with the same formalism (diffusion theory finite differences), and using the same geometrical meshing.

Unfortunately, the codes QUANDRY and PDQ7 do not contain any practical option for doing fixed flux boundary condition calculations. However, the diffusion theory, mesh-centered, finite-differences code "CITATION" [18] allows for such a boundary condition. The details of

the generation of surface flux response matrices using "CITATION" are given in Appendix 5. The general principle of the method being used is to impose successively on one face of the assembly, and in each energy group, a flat, linear and quadratic form function, while the flux is set to zero on the three other faces.

Unfortunately, the use of "CITATION" to generate response matrices does not guarantee consistency with a reference solution (point-centered) calculated by PDQ7, which is the standard of the industry. Therefore, a diffusion-theory, point-centered, finite differences code was written, with the sole purpose of generating surface flux response matrices using the PDQ7 difference equations. This code, along with its implementation in a scheme generating response matrices, is described in Appendix 5. The general principle used for the generation of these matrices is to set up for each input quantity of the matrices (i.e., for each cornerpoint flux and average surface flux) a fixed source problem which yields the flux shapes that result when this particular quantity is set to one, and the 15 other inputs are set to zero. Thus, any inconsistency due to the different finite differences models is eliminated. Furthermore, although the point centered code being used is very rudimentary (it does not use any acceleration scheme), the cost of generating a surface flux response matrix using this code is approximately equivalent to the cost of generating this matrix with "CITATION".

3.4.3 The Interpolation of Surface Flux Response Matrices

The purpose of response matrices is to permit the pre-tabulation of a large number of fixed-source calculations for one type of assembly. Unfortunately, these matrices depend on all position-dependent cross sections, which vary individually throughout the life of an assembly, so

that the tabulation process can become lengthy and expensive. Some matrix interpolation scheme is necessary to reduce the cost of that process.

On physical grounds, it is expected that a few state variables (power level, xenon concentration, temperature, void fraction, void history, average exposure, and eigenvalue) describe fairly accurately the neutronic properties of an assembly. The variations of these properties (and, consequently, of response matrices) with the state variables depicted, are expected to be smooth. It is not the purpose of this thesis to establish multidimensional interpolation formulas for response matrices. Nevertheless, the smoothness of the dependency of the matrices on the state variables makes it very likely that tables of matrices can be easily generated for interpolation purposes. The λ dependency of the response matrices has been studied, for PWR's, by K. Parsons [12] who found that this dependency could be very well approximated by a quadratic function. This same approximation will be used in this thesis. The benchmark problems for which the response matrix homogenization technique is tested in this chapter are all steady state beginning of life cores, so that the response matrices will not have to be interpolated versus the void fractions and average exposures of the corresponding assemblies. Chapter 5 will describe some aspects of the effects of fuel burnup on the generation of response matrices.

3.4.4 The Implementation of Surface Flux Response Matrices in an Iterative Scheme

3.4.4.1 The Non-selective Use of Response Matrices

Figure 3.2 summarizes the different steps of an iterative scheme based on surface flux response matrices. As response matrices are

Fig. 3.2 Description of the iterative scheme.

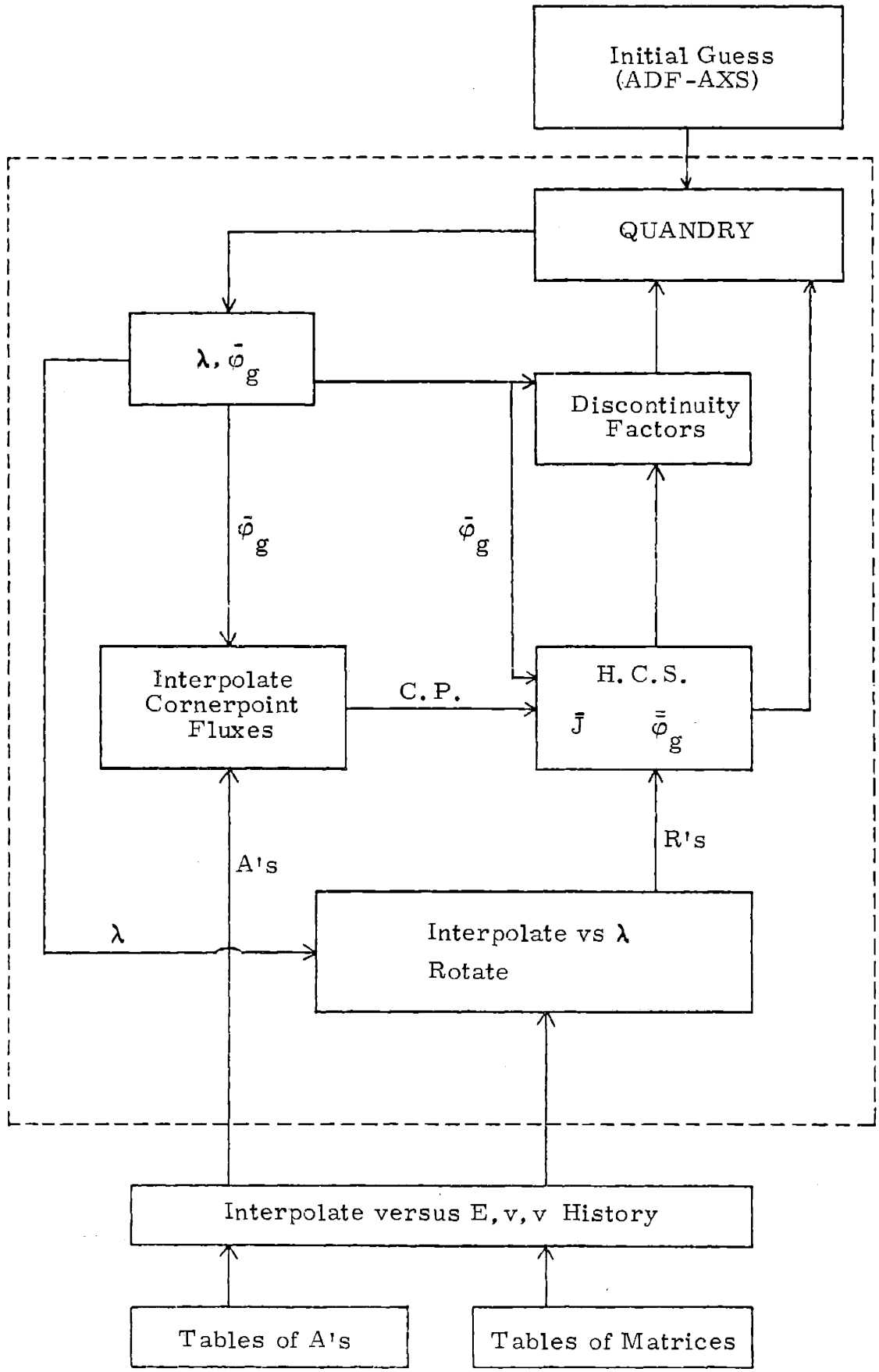

used for determining equivalence theory parameters for all assemblies, this scheme is called "non-selective".

Some preliminary calculations have to be performed before the iterations can start: assembly surface fluxes (used in the cornerpoint flux interpolation scheme) and response matrices have to be interpolated for the state variables of each assembly (this interpolation should be included in the iterative process in the case when feedback or transient effects are taken into account). Also, an initial guess for the equivalence theory parameters has to be found: a relatively good guess is to choose the assembly discontinuity factors and cross sections for each node (they can be pre-tabulated and interpolated versus the state variables of each assembly). The effect of this initial guess on the convergence of the iterative scheme will be discussed in section 5 of this chapter.

The iterative scheme itself consists of using this guess, or the homogenized parameters resulting from a previous iteration, along with the nodal code QUANDRY, to get a new estimate of the nodal solution. The homogeneous face-averaged fluxes predicted by QUANDRY are then multiplied by the corresponding discontinuity factors. Thus, heterogeneous face-averaged fluxes are obtained for each face. Only the global eigenvalue and the heterogeneous face-averaged fluxes predicted by this calculation are used in the following steps. The heterogeneous face-averaged fluxes are used, along with the interpolated assembly surface fluxes, to interpolate, group by group, the cornerpoint fluxes. In parallel to that interpolation process, the global eigenvalue is used to interpolate, in a quadratic manner, the surface flux response matrices corresponding to the state variables of each assembly. The resulting matrices are then rotated, in order to correspond to the correct position-

ing of each assembly (beginning of life BWR assemblies have very little symmetry). The interpolated cornerpoint fluxes and the average heterogeneous surface fluxes from the earlier nodal solution are then used as input to the response matrices. A simple multiplication yields for each assembly: new homogenized cross sections, volume averaged fluxes, and a set of net surface currents. It should be noted here that these currents are in general physically incorrect, as can be seen from the fact that, along a single face, the net currents predicted by the matrices corresponding to the assemblies located on either side of that face will generally not be identical. This inconsistency will be further discussed in section 5.

The homogenized cross sections, net surface currents and volume averaged fluxes determined by the response matrix technique, and the global eigenvalue and average surface fluxes from the previous iteration are then used in equations of the type (2.13), which define the discontinuity factors, to determine new discontinuity factors. A QUANDRY nodal calculation is then performed with the new equivalence theory parameters. This process is then repeated until convergence.

The mathematical nature of the scheme described above is highly nonlinear. There is therefore no guarantee that it will converge. Furthermore, even if it does converge, the converged solution will be very hard to characterize mathematically.

The properties of this iterative scheme will be examined in section 5.

3.4.4.2 The Selective Use of Response Matrices

The generation of tables of response matrices is an expensive process: the discretization of the state variables describing each

assembly will lead to interpolation tables containing several thousand response matrices. Though this important financial investment can be depreciated over the whole lifetime of a reactor (or type of reactor), it is of paramount interest to reduce that tabulating effort as much as possible. One drastic way of doing so is to generate response matrices only for those nodes having the strongest heterogeneities, corresponding to the assemblies where the control blades are inserted. Other assemblies are generally well represented by the ADF-AXS parameters. An iterative scheme using response matrices for the rodded nodes, and pre-tabulated assembly homogenized parameters for all other nodes can be implemented in a manner equivalent to the scheme where response matrices are used for all nodes.

As was the case for the previous iterative scheme, no predictions based on mathematical properties can be made concerning the behavior of that "selective" scheme. Furthermore, it is not known if the fact of improving the homogenized parameters in the rodded nodes will also improve the nodal solution in the other nodes, or will merely renormalize the power levels in the non-rodded assemblies.

3.5 Numerical Testing of the Surface Flux Response Matrix Iterative Schemes

3.5.1 A Preliminary Test Problem

A very small and highly tilted BWR benchmark was designed in order to test our iterative schemes and understand their behavior. This benchmark is described in Appendix 1: it consists of 36 heterogeneous assemblies, with very dissimilar exposures and void fractions. 4 control rods are inserted in locations close to the center of the core, and the fluxes are set to zero on the external boundary: these characteristics,

though very artificial, create very strong tilts, thus making the homogenization problem a difficult one. The assemblies are idealized BWR assemblies, where the central fuel region is partially homogenized but still consists of three different fuel enrichment zones and four gadolinium pins (see Fig. A1.5.2). The control rod blades and the water gaps are represented explicitly.

The reference solution for the preliminary test problem is a fine-mesh QUANDRY run, where 144 meshes are used in each assembly. The response matrices were generated with CITATION, using 576 meshes per assembly: this finer meshing is intended to ensure a correct spatial convergence. The assembly surface fluxes and equivalence theory parameters were obtained from fine-mesh QUANDRY runs where 576 meshes were used in each assembly.

When the surface flux response matrix iterative scheme was described, it was stated that the matrices corresponding to two neighboring assemblies do not predict the same currents on the face common to the two assemblies. In particular, response matrices do not necessarily predict zero net surface currents on faces where this is a physically imposed condition. Consequently, there exist two distinct approaches for implementing the iterative scheme:

Method A: This method consists of using the net currents predicted by the response matrices in the calculation of the discontinuity factors.

Method B: This option consists of averaging the net currents predicted by the response matrices for two adjacent assemblies. Also, the physical zero net current boundary condition is implemented explicitly.

Both methods were tested for the small benchmark described earlier, using response matrices for all nodes. Figure 3.3 shows the eigenvalue obtained at each iteration for both methods: clearly Method B diverges, while Method A converges in an oscillatory fashion. This behavior can be explained on physical grounds: the net currents, reaction rates and node-averaged fluxes predicted by the response matrices obey an exact neutronic balance for each individual node, although the surface currents implied by this balance may not match when more than one node is considered. Thus, when these surface currents are averaged, balance is destroyed, so that the resulting discontinuity factors are inherently in contradiction with the nodal balance equation (2.7). Divergence results. Accordingly, in the rest of this investigation only Method A will be used.

It is extremely important for the study of any iterative scheme to determine whether the converged solution, if it exists, depends on the initial guess used to start the iterations: if there is such a dependence, the whole scheme is of very little interest, as no prediction can be made concerning its outcome. On the other hand, if the converged solution is unique, it is generally also the solution to a simpler equation, which helps in understanding its physical nature. To test for uniqueness, two distinct initial guesses were used for the preliminary test problem: the approximated assembly homogenized parameters, and the reference homogenized parameters. The converged solutions were identical.

The nodal solutions are summarized in Table 3.1. While the assembly homogenized parameters yield a maximum and average error in nodal power of 9.85% and 3.63%, respectively, these quantities are 4.51% and 1.75% for the converged response matrix solution: a very significant

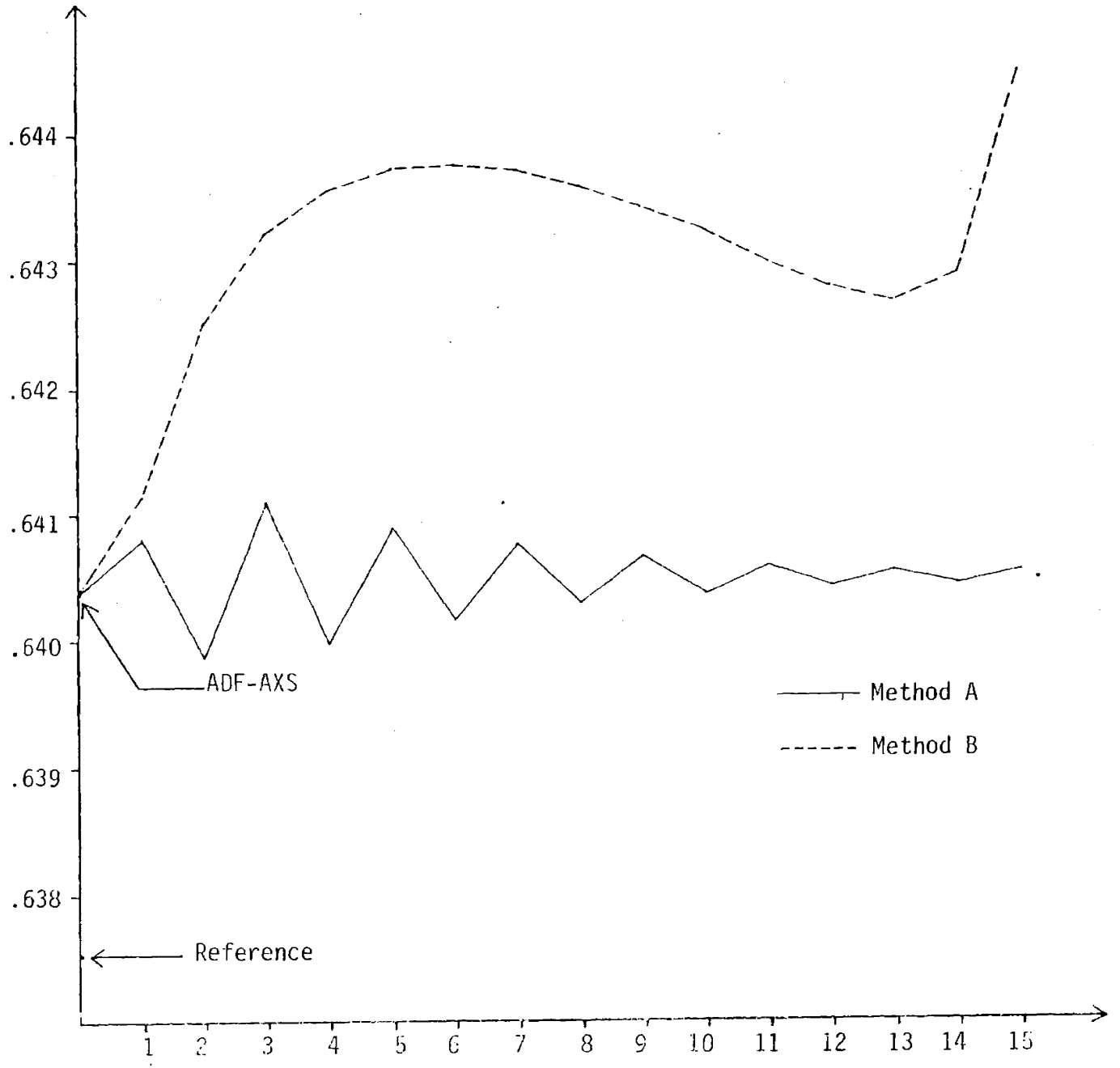

Fig. 3.3 Eigenvalue convergence for the Preliminary Test Problem

Table 3.1 Nodal results for the preliminary test benchmark

	ADF-AXS	First Iteration	Converged Solution	Average of 3rd and 4th Iterations
Error in eigenvalue	+0.45%	+0.51%	+0.46%	+0.47%
Maximum error in nodal powers	9.85%	4.00%	4.51%	4.23%
Average error in nodal powers	3.63%	1.66%	1.75%	1.71%
Maximum error in homogenized cross sections	3.90%	1.14%	0.96%	0.99%
Maximum error in thermal surface fluxes	14.1%	6.4%	5.0%	4.9%

improvement is obtained from the use of the iterative scheme. The improvement is even more evident when the homogenized cross sections and the thermal surface fluxes are considered. Complete nodal results are given in Appendix 6.

A relatively poor eigenvalue was obtained. This seems to be due to the use of "CITATION" for generating response matrices. While the analytic nodal method, implemented in QUANDRY, ensures spatial convergence even with a relatively coarse meshing, the mesh-centered finite-differences scheme implemented in CITATION requires a very fine meshing in order to be spatially converged.

The iterative process showed a very slow convergence: 18 iterations were needed to converge fully. This feature could make the scheme marginally attractive, but, fortunately, the oscillatory fashion in which it converges can be used to obtain, after a few iterations, a good estimate of the converged solution: the results in Table 3.1 show that the average of 2 successive iterations is very close to the converged solution. However, these results also show that a single iteration is not sufficient to estimate the converged solution.

3.5.2 The CISE BWR Benchmark Problem

The reference run for the CISE BWR benchmark is a fine mesh QUANDRY calculation, where 64 meshes are used for each assembly. The surface flux response matrices were generated with the diffusion theory code CITATION and, in order to insure a correct spatial convergence, 576 meshes were used for each assembly. Assembly surface fluxes and homogenized parameters were obtained from QUANDRY runs, using the same 576 meshes for each assembly.

The behavior of the "non-selective" iterative scheme was investi-

gated, and the features discovered for the Preliminary Test Problem were checked. It was found that:

1. The converged solution does not depend on the initial guesses for the equivalence theory parameters.
2. The convergence is oscillatory, and the average of the third and fourth iterations is a very good estimate of the converged solution.

Furthermore, it was found that essentially the same converged solution was obtained, whether the flat or quadratic transverse leakage approximations were used in the nodal calculations of the iterative scheme. The discontinuity factors determined at each step by the iterative scheme account for both the heterogeneous nature of the CISE BWR assemblies and the transverse leakage approximation used in the global QUANDRY calculations. This is a further indication that the iterative scheme involves some inherent mathematical or physical property. Also, this behavior demonstrates a significant advantage for the surface flux response matrix method, since the "flat" global calculations are faster running and require less memory than the "quadratic" global calculations.

The nodal solutions for the CISE BWR benchmark are summarized in Table 3.2. Complete nodal results are given in Appendix 6. The values resulting from the iterative scheme exhibit a significant improvement over the ADF-AXS results: the maximum and average errors in nodal powers are reduced by a factor of 2, while the homogenized cross sections and the surface fluxes are improved by an even greater factor.

From an examination of the nodal powers, it appears that, while the use of assembly homogenized parameters results in high errors in

Table 3.2 Nodal results for the CISE BWR benchmark

	ADF-AXS Flat Leakage	ADF-AXS Quadratic Leakage	Average of 3rd and 4th iteration Flat Leakage	Average of 3rd and 4th iteration Quadratic Leakage
Error in eigenvalue	0.02%	0.05%	0.11%	0.11%
Maximum error in nodal power	3.46%	3.04%	1.83%	1.74%
Average error in nodal power	1.31%	0.90%	0.58%	0.54%
Maximum error in homogenized cross sections	3.03%	3.03%	0.73%	0.75%
Maximum error in surface fluxes:				
• fast	4.2%	3.4%	2.1%	2.1%
• thermal	10.3%	9.5%	3.1%	2.9%
Average error in surface fluxes:				
• fast	1.4%	1.0%	0.7%	0.7%
• thermal	3.1%	2.6%	0.8%	0.7%

rodded nodes, the iterative scheme predicts excellent nodal powers in these locations. This result indicates that the only approximation made in the iterative scheme, the quadratic form function approximation, is uniformly good, even in the presence of very strong heterogeneities.

3.5.3 The LSH BWR Benchmark Problem

Two reference solutions are available for the LSH-BWR benchmark. They result in two homogenization problems which are mathematically distinct, though they are physically identical. They will be called the CLSH (Converged LSH) and the NLSH (Non-converged LSH) benchmarks, depending on whether the fine-mesh QUANDRY solution or the fine-mesh PDQ7 solution is considered.

3.5.3.1 The CLSH BWR Benchmark Problem

This benchmark corresponds to the fine-mesh QUANDRY solution where 169 meshes are used in each assembly. The surface flux response matrices were generated with CITATION, using 576 meshes per assembly. The assembly surface fluxes and homogenized parameters were obtained from fine-mesh QUANDRY runs with the same 576 meshes.

The properties of the "non-selective" iterative scheme which were noticed in the study of the two previous benchmark problems were verified for the CLSH benchmark:

1. The converged solution does not depend on the initial guess for equivalence theory parameters.
2. The converged solution does not depend on the transverse leakage approximation used in the global QUANDRY calculations.
3. The convergence is oscillatory.

The oscillatory behavior of the convergence is illustrated in

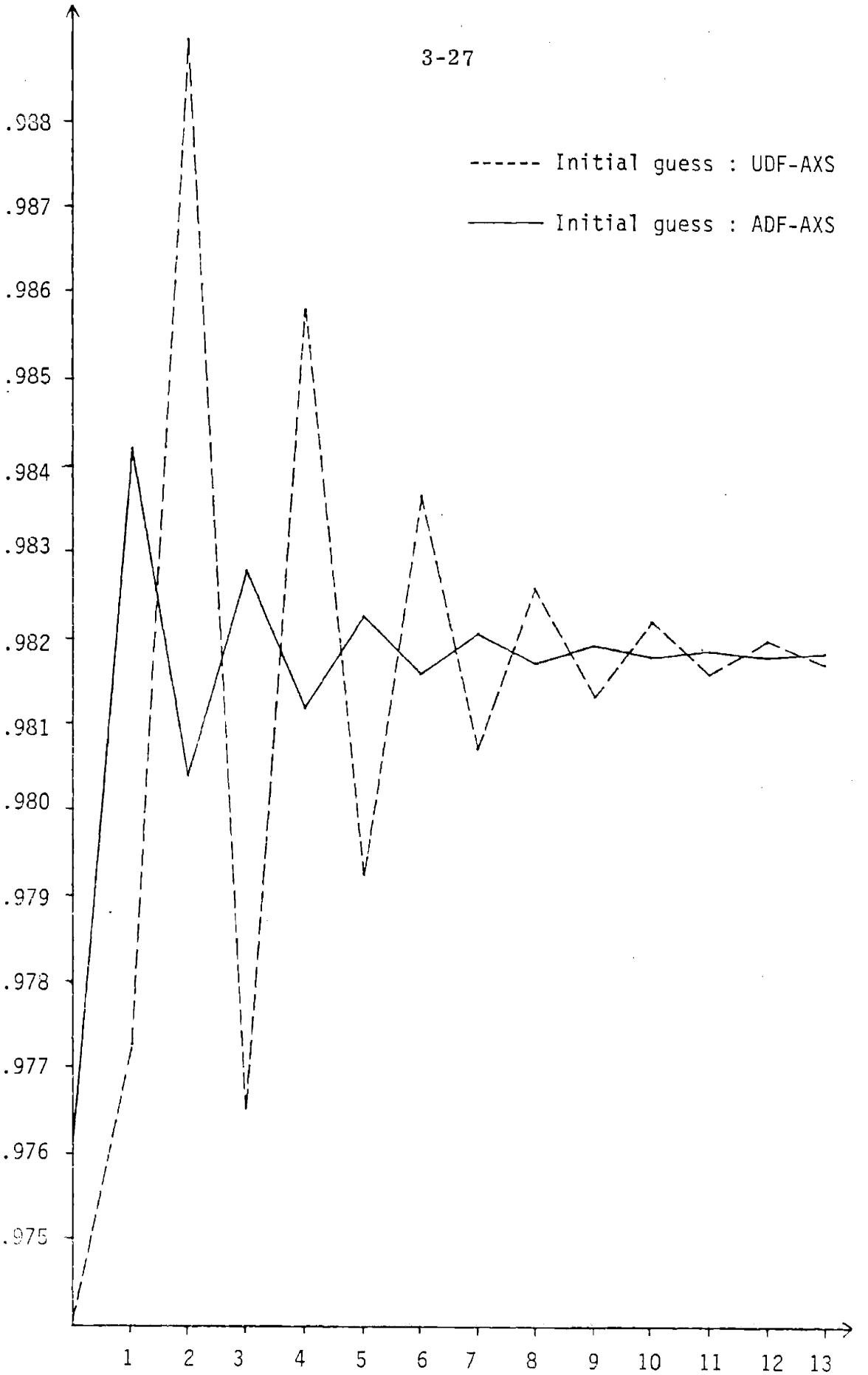

Fig. 3.4 Eigenvalue convergence for the CLSH BWR benchmark problem.

Fig. 3.4 which represents the eigenvalue predicted at each iteration for two different initial guesses. This figure suggests that the convergence is oscillatory-exponential: namely, if λ_n is the eigenvalue predicted at iteration n, the following relation

$$\frac{\lambda_n - \lambda_{n+1}}{\lambda_{n+1} - \lambda_{n+2}} = C \qquad (3.5)$$

(where C is a negative constant which does not depend on n) is expected to be verified for <u>any</u> n. λ will then converge towards:

$$\lambda_\infty = \frac{1}{1-C}(\lambda_k - C\lambda_{k+1}) \qquad (3.6)$$

where λ_k and λ_{k+1} are <u>any</u> two successive values of λ. The validity of Equations (3.5) and (3.6) was verified for the CLSH benchmark. Table 3.3 indicates that a few iterations, along with these relations, are sufficient for obtaining an excellent estimate of the converged solution.

The nodal results for this benchmark are summarized in Table 3-4. The use of standard flux-weighted constants leads to extremely high errors: the maximum error in nodal powers is 22.6%, which cannot be accepted if the nodal method is to be used for industrial purposes. The use of assembly homogenized parameters (ADF-AXS) reduces this maximum error to 9.61%, which is still only marginally acceptable. The "non-selective" response matrix technique results in a maximum error in nodal powers of only 1.06%, which is quite acceptable. Detailed nodal powers are presented in Appendix 6. They show that assembly homogenized parameters predict poor nodal powers for rodded nodes but predict accurate powers in other nodes. The "non-selective" response matrix homogenization scheme predicts powers that are

Table 3.3 The oscillatory-exponential convergence for the CLSH benchmark

C estimated from iterations:	1, 2, 3	2, 3, 4	3, 4, 5
$\frac{\lambda_e - \lambda_c}{\lambda_c}$	+0.0015%	-0.0002%	+0.0003%
$\left(\frac{\bar{\varphi}_e - \bar{\varphi}_c}{\bar{\varphi}_c}\right)_{max}$	1.72%	0.43%	0.13%

The $\bar{\varphi}$'s are the average surface fluxes.

Index c means "converged value"; index e means "estimated value".

Table 3.4 Nodal results for the CLSH-BWR benchmark

	UDF-AXS	ADF-AXS	Response Matrices
Error in eigenvalue	-0.29%	-0.05%	0.54%
Maximum error in nodal powers	22.6%	9.61%	1.06%
Average error in nodal powers	5.90%	3.26%	0.46%

uniformly good.

The eigenvalue predicted by the response matrix technique is quite poor. The error is 0.54%, while the corresponding error for the ADF-AXS calculation is only -0.05%. This is surprising in view of the excellent powers obtained from the response matrix technique. Two interpretations of this behavior are advanced:

1. This error could be intrinsic to the quadratic form function approximation.
2. The method used to generate response matrices and, in particular, the use of CITATION, may not be accurate enough.

The NLSH benchmark, for which response matrices are generated by a scheme consistent with the reference solution, will permit us to determine which interpretation is the correct one.

3.5.3.2 The NLSH BWR Benchmark Problem

This benchmark corresponds to the fine-mesh PDQ7 solution for which 324 mesh points are used in each assembly. The surface flux response matrices, the assembly surface fluxes and the assembly homogenized parameters were all calculated using the same mathematical formalism and geometrical meshing as in the reference solution. Both the "selective" and "non-selective" iterative schemes presented earlier were tested. The corresponding nodal results are summarized in Table 3.5.

The "non-selective" scheme (i.e., the scheme where response matrices are used for determining equivalence theory parameters in all assemblies) predicts excellent nodal powers: the maximum and average errors are 2.50% and 0.81%, compared with 10.83% and 13.37% for

ADF-AXS. Also, the predicted eigenvalue is correct (the error is 0.18%, while it was 0.54% for the CLSH problem); this result strongly suggests that the cause of the high error in eigenvalue found for the CLSH problem lay in the scheme used to generate surface flux response matrices.

The cornerpoint fluxes interpolated from the various nodal solutions are the most significant measurements of the quality of the nodal solutions, as these fluxes are the most detailed information ever involved in the homogenization processes. The cornerpoint fluxes for the NLSH benchmark are shown in Appendix 6: while they are highly in error for the "FWC" and "ADF-AXS" homogenization schemes, the response matrix technique predicts them very well throughout the core. This result indicates the coherence of the response matrix scheme, in opposition to non-iterative schemes which do not perform uniformly well.

The "selective" scheme (i.e. the scheme where response matrices are used for determining equivalence theory parameters in the rodded assemblies only, and ADF-AXS are used in other assemblies) also predicts very good nodal powers: the maximum and average errors are 4.21% and 1.34%. A close examination of the predicted nodal powers shows that while this scheme greatly improves the power level of the rodded assemblies, in comparison with ADF-AXS, it merely renormalizes the powers in the other assemblies. An immediate consequence of that fact is that this scheme will predict a good power distribution if and only if the ADF-AXS approximation is consistently good in non-rodded regions. Unfortunately this can not be guaranteed.

Table 3.5 Nodal results for the NLSH benchmark

	UDF-AXS	ADF-AXS	Matrices "non-selective"	Matrices "selective"
Error in eigenvalue	-0.28%	-0.05%	0.18%	0.09%
Maximum error in nodal powers	24.60%	10.83%	2.50%	4.21%
Average error in nodal powers	6.25%	3.37%	0.81%	1.34%

Table 3.6 Nodal results for the MVY benchmark

	UDF-AXS	ADF-AXS	Matrices "non-selective"	Matrices "selective"
Error in eigenvalue	-0.41%	+0.04%	+0.005%	+0.22%
Maximum error in nodal powers	31.31%	-11.26%	-1.95%	-8.37%
Average error in nodal powers	5.37%	1.90%	0.66%	1.80%

3.5.4 The MVY BWR Benchmark

The reference solution, assembly fluxes, assembly homogenized parameters and response matrices for the MVY benchmark were generated in the PDQ7 formalism, using 324 meshes per assembly.

The nodal results are summarized in Table 3.6. The inadequacy of standard flux weighted constants is clearly demonstrated by the very high errors in the nodal powers they predict: the maximum error is 31.31%. The assembly homogenized cross sections and discontinuity factors considerably improve these nodal powers: the maximum error is reduced to 11.26%. This is still only marginally acceptable. The nodal results associated with the non-selective use of response matrices are excellent: for example, the maximum error in nodal powers is less than 2%. Also, the oscillatory-exponential behavior of the convergence, described by Equations (3.5) and (3.6), was checked, and the results given in Table 3.7 indicate that this behavior is a general property of the iterative scheme.

The selective use of response matrices led to disappointing results: while the power densities of the rodded assemblies are predicted with much greater accuracy than when ADF-AXS are used for all assemblies, the power densities in the non-rodded assemblies are merely renormalized. Consequently, some of the errors in the non-rodded assemblies are increased; finally, the average error in nodal powers for the "selective" iterative scheme and the assembly homogenization scheme are practically equal: they are 1.80% and 1.90% respectively. Thus the "selective" scheme appears to be of marginal interest.

3.5.5 Physical Interpretation of the Converged Solution

The uniqueness of the converged solution points strongly towards the existence of some physical property that characterizes this converged solution. It is not the purpose of this investigation to do a complete mathematical study of the surface flux response matrix iterative scheme. Nevertheless, the experience which has been accumulated about its behavior allows us to make an "educated guess" concerning the nature of this property: it is believed that the converged solution not only satisfies the nodal equations described in Chapter 2, but that it also is such that the currents predicted by the response matrices corresponding to two adjacent nodes are continuous.

This conjecture is practically impossible to demonstrate rigorously, as a high rate of convergence is necessary before large fluctuations in surface currents are eliminated (currents are very sensitive to even small variations in the nodal solution). Unfortunately, numerical truncation errors are such that this high rate of convergence cannot be reached.

3.5.6 Execution Time Comparison

The charges (on MIT's IBM 370/168) for various homogenization schemes applied to the NLSH and MVY benchmarks are summarized in Table 3.8. The figures indicated are only meaningful for comparative purposes. They include all system-related charges (CPU time, memory usage), but do not include the "overhead" costs (data files manipulations, printing, ...).

For all three homogenization schemes investigated, the main cost incurred is in the pre-tabulation of assembly calculations or response matrices. But, even if these tabulation costs are not depreciated over

Table 3.7 The oscillatory-exponential convergence for the MVY benchmark

C estimated from iterations	1, 2, 3	2, 3, 4	3, 4, 5
$\frac{\lambda_e - \lambda_c}{\lambda_c}$	+0.0009%	-0.0002%	+0.0002%
$\left(\frac{\bar{\varphi}_e - \bar{\varphi}_c}{\bar{\varphi}_c}\right)_{max}$	1.97%	0.59%	0.17%

Note: The notation is the same as in Table 3.3.

Table 3.8 Comparison of costs for non-iterative and iterative schemes

	NLSH	MVY
UDF-AXS or ADF-AXS	4 assembly calculations = 20.00 1 QUANDRY calculation = 00.70 Total: 20.70	2 assembly calculations = 10.00 1 QUANDRY calculation = 00.90 Total: 10.90
Response matrices	13 response matrices = 52 4 assembly calculations = 20 5 iterations = 7 Total: 79	7 response matrices = 28 2 assembly calculations = 10 5 iterations = 9 Total: 47
Reference	154	260

Note: The units used in this comparison are arbitrary.

the lifetime of a reactor, the homogenization schemes still improve significantly the computational efficiency of the core calculations.

3.6 Extension of Homogenization Methods to Three-Dimensional Calculations

3.6.1 The Estimation of Three-Dimensional Equivalence Theory Parameters

The homogenization schemes which were described and analyzed for two-dimensional benchmarks in the earlier sections of this chapter predicted equivalence theory parameters with an excellent accuracy. Unfortunately, their direct extension to three-dimensional calculations would be expensive. For example, the generation and tabulation of three-dimensional response matrices would require such storage capabilities that it is impossible with state of the art computing tools.

QUANDRY has never been applied to realistic three-dimensional BWR benchmarks, with heterogeneities in the radial and axial directions. The fluxes are smooth in the axial direction, except at the tip of inserted control rods. This property will be used for determining discontinuity factors. It is hoped that, if axial node boundaries are chosen to coincide with material discontinuities, each node will be homogeneous in the axial direction, and axial discontinuity factors will be close to one. Thus, accurate two-dimensional homogenization schemes should be sufficient to determine a good three-dimensional nodal solution.

3.6.2 Numerical Testing of Three-Dimensional Homogenization Schemes

The TRD BWR (Three Dimensional BWR) benchmark problem has been designed to test the validity of the unity axial discontinuity factor approximation. This benchmark consists of 9 assemblies, characteristic

of the central region of a BWR core. Zero net-current radial boundary conditions are imposed. The assemblies are based on the Vermont Yankee assemblies. However, the central fueled region (containing the fuel pins with different enrichments, the gadolinium pins and a water hole) is homogenized. Thus, some heterogeneities are eliminated; nevertheless, the most important heterogeneities, as far as homogenization is concerned (the water gaps and control rod blades), are explicitly represented. Four different regions of voiding are present in the core. The bottom section, corresponding to the water inlet, is not voided and the void fraction increases towards the top of the core. A control rod is inserted halfway and a 20 cm water reflector is present at each axial boundary of the core.

The reference solution for this benchmark is a fine-mesh PDQ7 run. The radial mesh layout is 13 x 13 in each assembly, and 57 meshes are used axially. A fine mesh (0.5 cm) is used in the vicinity of material discontinuities; a coarser mesh (4.0 cm) is used far from any axial discontinuity. The two-dimensional homogenized parameters (ADF-AXS) were calculated with PDQ7, using the same 13 x 13 mesh layout.

The nodal calculation was performed with one node per assembly in the radial direction and eight 15 cm segments in the axial direction of the fueled region; a 20-cm axial node size was used in the water reflector. Both FWC and ADF-AXS were used to approximate the radially homogenized parameters. The axial discontinuity factors were set to unity. Table 3.9 summarizes the nodal results. More complete nodal results are given in Appendix 6. As had been concluded for two-dimensional benchmarks, the superiority of ADF-AXS over FWC is

Table 3.9 Nodal results for the TRD-BWR benchmark

	Radial Homogenization Scheme	
	FWC	ADF-AXS
Error in eigenvalue	-0.12%	+0.056%
Maximum error in nodal power	10.54%	4.70%
Average error in nodal power	2.35%	1.14%

Table 3.10 Radially averaged nodal powers for the TRD-BWR benchmark

	Reference Average Power	Error from FWC	Error from ADF-AXS
Plane #1	0.7139	-2.97%	-0.87%
#2	1.109	-1.49%	+0.34%
#3	1.177	-0.97%	+0.07%
#4	1.299	+0.79%	+0.92%
#5	1.373	+1.96%	+1.15%
#6	1.056	+0.89%	-0.49%
#7	0.7524	+1.22%	-0.56%
#8	0.5158	-0.48%	-2.48%

clear: the maximum errors in nodal powers are 4.70% and 10.54% respectively.

Two tests were applied to examine the effects of the unity value assumed for the axial discontinuity factors. First, the average powers in each of the eight radial node-groupings were computed, and errors resulting from the nodal calculations were obtained. These results are shown in Table 3.10. As expected, ADF-AXS significantly improves the FWC results; furthermore, the axial power profile obtained from ADF-AXS is very close to the reference power profile. This is a strong indication that use of unity discontinuity factors in the axial direction is acceptable. The second test which was performed was to study two-dimensional cuts of the TRD BWR benchmark. The errors resulting from the FWC and ADF-AXS homogenization schemes in these sections are summarized in Table 3.11. The magnitude of these errors is comparable to that obtained for the three-dimensional analysis of the whole core.

These results support the adequacy of our homogenization schemes for the analysis of three-dimensional heterogeneous BWR cores. In particular, the use of unity axial discontinuity factors does not seem to affect the accuracy of the nodal results.

3.7 Summary

An iterative scheme, based on surface flux response matrices was formally introduced and was tested for realistic two-dimensional benchmarks. Results show that, if response matrices are being used to represent all the assemblies in the core, the maximum error in nodal power is always smaller than 3%, whereas conventional FWC and ADF-AXS yield errors as high as 25% and 12% respectively. The behavior of

Table 3.11 Nodal results for two-dimensional cuts of the TRD-BWR benchmark

Homogenization Scheme	FWC	ADF-AXS
Error in eigenvalue		
Region 1	-0.321%	-0.013%
Region 2 (rodded)	-0.37%	+0.008%
Region 2 (non-rodded)	-0.007%	-0.006%
Region 3	-0.003%	-0.0002%
Region 4	0%	0%
Maximum error in nodal power		
Region 1	6.40%	5.25%
Region 2 (rodded)	7.68%	3.55%
Region 2 (non-rodded)	0.10%	0.35%
Region 3	0.56%	0.31%
Region 4	0%	0%
Average error in nodal power		
Region 1	2.31%	1.38%
Region 2 (rodded)	2.79%	0.99%
Region 2 (non-rodded)	0.05%	0.16%
Region 3	0.21%	0.15%
Region 4	0%	0%

the iterative scheme was shown to be very consistent, and its execution time was shown to be one order of magnitude smaller than that needed with standard finite-differences schemes. Finally, it was shown that the extension of homogenization schemes to three dimensions was straightforward, since axial discontinuity factors may be set to unity.

The characteristics and reliability of the iterative scheme described make it of great value for the analysis of BWR's, and the initial investment, which consists of generating tables of response matrices, seems to be justified.

CHAPTER 4

FLUX RECONSTRUCTION TECHNIQUES BASED ON COARSE MESH NODAL METHODS

4.1 Introduction

In Chapter 3 it was demonstrated that relatively cheap and very accurate BWR homogenization schemes do exist: an iterative scheme based on surface flux response matrices resulted in reliable nodal solutions. The next stage in the development of nodal methods consists of finding a way to recapture cheaply the heterogeneous detail of the fluxes from the sole knowledge of some (not necessarily accurate) nodal solution.

In the course of designing and operating a nuclear reactor, various tasks can be assigned to heterogeneous flux reconstruction schemes. The most fundamental one is the prediction of the hottest pins in the core, a determination essential to the safety of the reactor. The most complex task is the accurate determination of all heterogeneous fluxes throughout the core. Implicitly, this task is aimed at the replacement of standard finite-differences methods by a sophisticated, and cheaper, homogenization-dehomogenization scheme. It is the purpose of this chapter to describe methods which will meet these two objectives.

Section 2 will discuss the relation between the accuracy of the nodal solution available and the necessary complexity of the reconstruction schemes used. Section 3 will show that excellent reconstructed fluxes can be obtained from the converged solution of the iterative scheme described in Chapter 3. Section 4 will describe more sophisticated reconstruction schemes which, when used in connection with the

cheap (but inaccurate) ADF-AXS parameters, still yield very good reconstructed fluxes. Finally, section 5 will discuss briefly the extension of these reconstruction schemes to three-dimensional calculations.

4.2 The Relation Between Homogenization and Reconstruction Schemes

The main difficulty in reconstructing heterogeneous fluxes is that nodal schemes predict only surface and volume averaged quantities, so that it is necessary to make some kind of assumption concerning the shape of the flux in order to recapture it. Numerous such assumptions have been implemented and tested in recent years, and two large classes can be distinguished among them:

1. The "overall shape approximations"

   These methods consist of assuming that the fluxes throughout the assemblies have a known mathematical form [16, 19, 20]. Some of these schemes, in particular the polynomial form function method developed by Khalil for PWR's, are very attractive, but they will not be tested in this investigation.

2. The "boundary shape approximations"

   These methods consist of assuming a precise mathematical form for some quantity on the boundary of the nodes [16, 20]. It has already been shown (Chapter 3) that the most practical scheme in the class involves assuming a quadratic shape for the surface form function.

The first class of methods has the advantage of being very cheap, since the chosen shapes for the heterogeneous fluxes can often be obtained by a simple multiplication. Unfortunately, some important limitations

exist for these methods, since the chosen shapes often lack the flexibility required to take into account such effects as the large neutron thermalization in the water reflector.

The second class of methods is relatively more expensive (about one order of magnitude), since a fine-mesh finite-differences calculation is required for each assembly. But, as only the boundary condition is approximated, local errors there will smooth out in the interior of the assembly; specially, the presence of a water gap in BWR assemblies involves important thermalizations, and it is expected that localized errors in surface fluxes will not propagate far inside the assembly.

The quality of the nodal solution clearly affects the precision of the reconstructed heterogeneous fluxes. While it is expected that an excellent nodal solution (such as the converged solution of our iterative scheme) will predict excellent boundary conditions, a relatively poor nodal solution (such as ADF-AXS) will predict poor boundary conditions. (It has already been shown (Chapter 3) that cornerpoint fluxes interpolated from the ADF-AXS nodal solution can be as much as 40% in error.)

The reconstruction strategy therefore depends on the nodal solution available. If a good solution is used, the nodal quantities predicted on the boundary of each assembly can be used to reconstruct accurately the fluxes within that assembly. If only a poor nodal solution is known, larger fixed-source calculations must be used, where the boundary conditions used are not applied at the surface of the assembly to be reconstructed, but rather at locations far away from that assembly. Thus, such local effects as poorly interpolated cornerpoint fluxes are expected to have a very limited influence on flux reconstruction.

4.3 Flux Reconstruction Techniques Based on the Converged Solution of the Iterative Scheme

4.3.1 The "One-Assembly" Flux Reconstruction Technique

A straightforward extension of the response matrix technique is to generate flux reconstruction matrices while calculating the matrices needed for the iterative scheme. The reconstruction matrices will relate group and point-wise heterogeneous fluxes within each assembly to face-averaged and cornerpoint fluxes:

$$[\varphi_{het}] = [R_c(\lambda)]\,[\varphi] \qquad (4.1)$$

where, for a two-dimensional reconstruction,

$[\varphi]$ is an 8 * G column vector containing cornerpoint and face-averaged fluxes;

$[\varphi_{het}]$ is an N * N * G column vector containing heterogeneous fluxes (N is the number of meshes in each direction for one assembly).

Thus, $[R_c(\lambda)]$ is an (N * N * G) * (8 * G) rectangular matrix, and depends on all the state variables of each assembly. Though $[R_c(\lambda)]$ is implicitly calculated in the process of determining $[R_\lambda]$, the response matrix described in Chapter 3 (Equation (3.4)), the storage requirements of tables of such large matrices are clearly excessive. For example, if an 18 x 18 mesh layout is used, the resulting $[R_c(\lambda)]$ will be 32 times bigger than the corresponding $[R_\lambda]$. Thus, it is not expected that reconstruction matrices will be pretabulated. It is more efficient to do a separate fixed-source calculation with quadratic form-function boundary conditions for each assembly to be reconstructed.

4.3.2 Numerical Testing

4.3.2.1 The CLSH Benchmark

For this benchmark problem, the fixed-source calculation used in the reconstruction process was performed with the code CITATION. The same meshing used for the generation of response matrices was used.

Because of the technical difficulty of implementing this reconstruction, only two representative assemblies were reconstructed: these are the sixth and seventh assemblies in the bottom row of the core. The seventh assembly is rodded and corresponds to the node where the maximum error in nodal power occurs for the response matrix homogenization scheme. The sixth assembly is not rodded, so that the heterogeneous flux distribution within its boundaries is expected to be very smooth.

The maximum errors in pin-wise reconstructed fluxes are given in Table 4.1. (It should be noted that only the fluxes in the fueled regions are being reconstructed, as the fluxes in the water gaps are of little interest.) The largest error in reconstructed fluxes is 3.37%, a satisfactory value, in view of the heterogeneity and strong tilt of the CLSH benchmark.

4.3.2.2 The NLSH Benchmark

The fixed-source calculations for this benchmark were performed using the same formalism and meshing as in the reference calculations.

All fueled assemblies in the core were reconstructed. The maximum errors in each group and assembly are shown in Table 4.2. While fluxes in the interior of the core are very well reproduced, reconstructed fluxes in the peripheral assemblies are relatively poor (the maximum error in the thermal flux is 7.46%).

Table 4.1 Errors in reconstructed fluxes for the CLSH benchmark

	Node #6	Node #7
Maximum error in reconstructed fast flux in fueled region.	-1.89%	-2.85%
Maximum error in reconstructed thermal flux in fueled region.	-2.68%	-3.37%

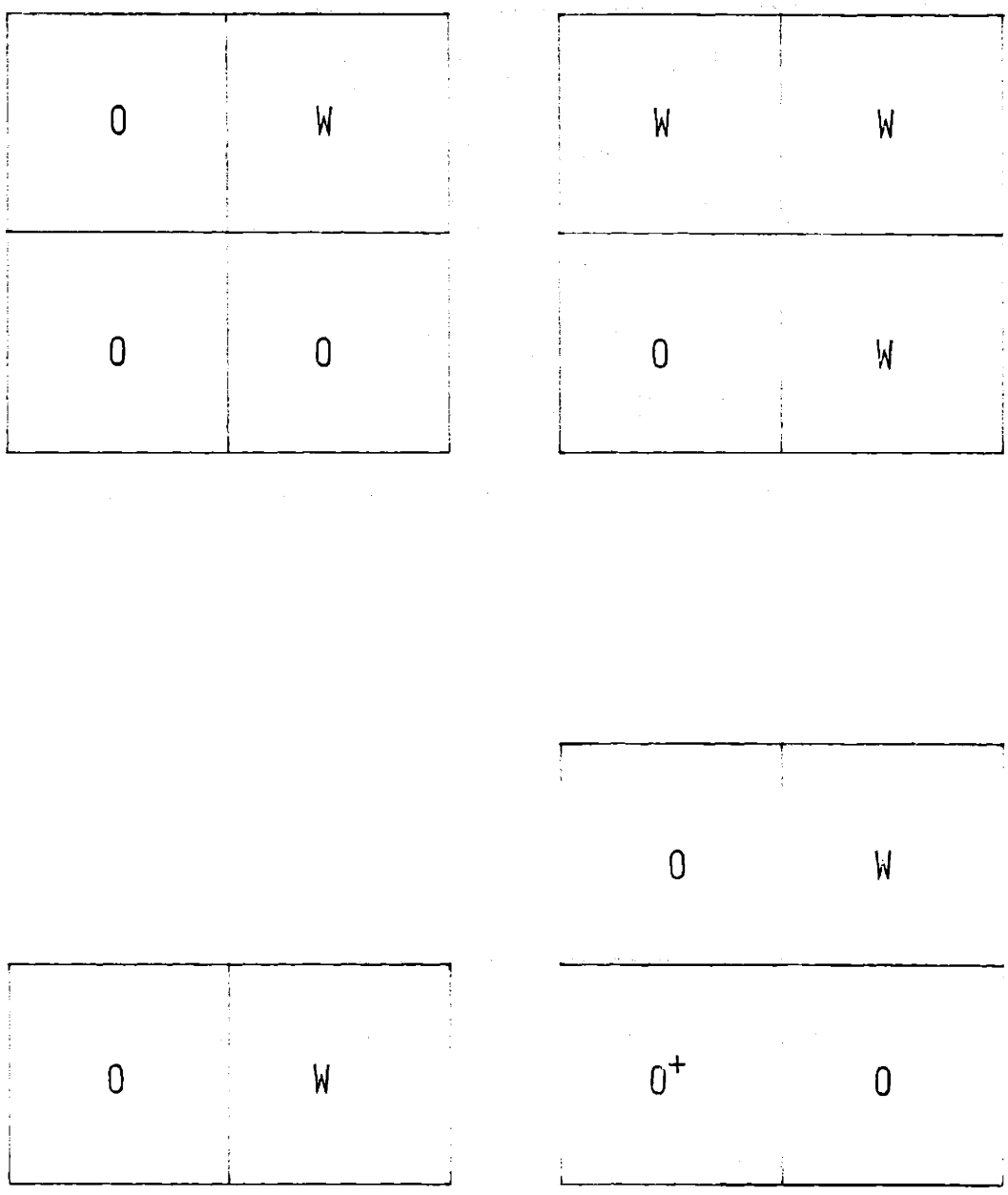

Note: All extended assemblies have zero current boundary conditions.

Fig. 4.1 Extended assemblies for the LSH benchmark.

Such poor reconstructed fluxes are related to a poor approximation of the heterogeneous surface fluxes by the quadratic form function method. Specifically, the use of assembly calculations, based on zero net current boundary conditions to reproduce the local heterogeneous nature of the flux, does not take into account the important neutron thermalization occurring in the water reflector.

These effects can be included in the reconstruction scheme by using "extended assemblies" to generate so-called "assembly flux shapes" in the periphery of the reflector. These extended assemblies are described in Fig. 4.1. They are composed of a set of 4 assemblies containing fuel and reflector nodes. The flux shapes resulting from eigenvalue calculations done for each of these sets are used to interpolate cornerpoint fluxes in the iterative process. It is important to note that these shapes are <u>not</u> used to generate new response matrices (the tabulation of response matrices which are not based on the usual assembly calculations can become very expensive). Nevertheless, the use of new flux shapes in the cornerpoint interpolation scheme results in a new converged nodal solution, which is summarized in Table 4.3 (detailed nodal power distributions are shown in Appendix 6). This nodal solution is very close to the solution obtained using the usual assembly flux shapes. The extended assembly flux shapes are then used for flux reconstruction. The results for all assemblies are shown in Table 4.4. The overall maximum error in reconstructed point-wise flux in the fuel is 4.76%. This is an excellent value; it is smaller than the maximum error in <u>nodal</u> power obtained from ADF-AXS.

Table 4.2 Maximum error for pin-wise flux reconstruction in the NLSH benchmark when "normal" assemblies are used

			-1.26% 4.41%	-1.89% 7.15%	-1.13% 4.76%	← error in reconstructed fast flux ← error in reconstructed thermal flux
		-0.33% -0.58%	-0.48% -1.54%	-0.60% 3.01%	-1.99% 4.74%	
	0.26% 0.49%	0.56% 1.46%	0.99% 1.58%	-3.55% -4.09%	-3.16% -5.45%	-3.82% 7.46%	-2.72% -4.38%
0.14% 0.47%	0.27% 0.52%	0.58% 1.52%	1.03% 2.30%	-3.16% -3.37%	-3.28% -4.26%	-3.75% -4.14%	-1.81% -4.57%

Table 4.3 Nodal results for the NLSH benchmark when extended assemblies are used

Error in eigenvalue	0.18%
Maximum error in nodal powers	2.88%
Average error in nodal powers	0.94%

Table 4.4 Maximum errors for pin-wise flux reconstruction in the NLSH benchmark, when extended assemblies are used

		-0.74% 1.65%	-1.85% -1.63%	-1.44% -1.15%	← fast group ← thermal group	
		-0.58% -1.44%	0.67% 3.05%	-3.43% 3.92%		
			-3.33% -3.91%	-3.01% -2.95%	-2.98% -3.45%	-2.64% -2.31%
			-2.95% -3.07%	-3.72% -3.89%	-3.84% -4.76%	-2.19% -2.49%

Note: In the central assemblies, the results are the same as in Table 4.2.

4.4 Flux Reconstruction Techniques Based on the ADF-AXS Nodal Solution

4.4.1 The "Four-" and "Nine-Assemblies" Reconstruction Techniques

The use of response matrices for determining equivalence theory parameters is relatively expensive. There is a strong incentive to develop reconstruction techniques based on cheaper nodal solutions.

The use of the ADF-AXS nodal solution seems particularly well suited for that purpose. Far from control rods, ADF-AXS predicts good face-averaged and cornerpoint fluxes (therefore giving good reconstructions with the straightforward technique); it also appears that the effect of control rods is very localized, so that one expects to get good reconstructions when using nodal information in locations relatively distant from the heterogeneity.

Accordingly a method has been devised in which quadratic fluxes are imposed not on the boundary of each node, but 3 such quadratics are imposed on each face of a set of 9 nodes, centered on the node to be reconstructed. A fine-mesh calculation is then performed, using the global eigenvalue predicted by the ADF-AXS run. The method is illustrated in Fig. 4.2.

This reconstruction method is fairly expensive. Furthermore, it is generally of no interest to reconstruct fluxes over full assemblies. For example, the value of the fluxes in pins very close to a control rod is of limited use.

Therefore, we devised a way to predict the power of the hottest pin in low power assemblies. As the location of that pin can generally be estimated fairly well, we surrounded the assembly to be reconstructed

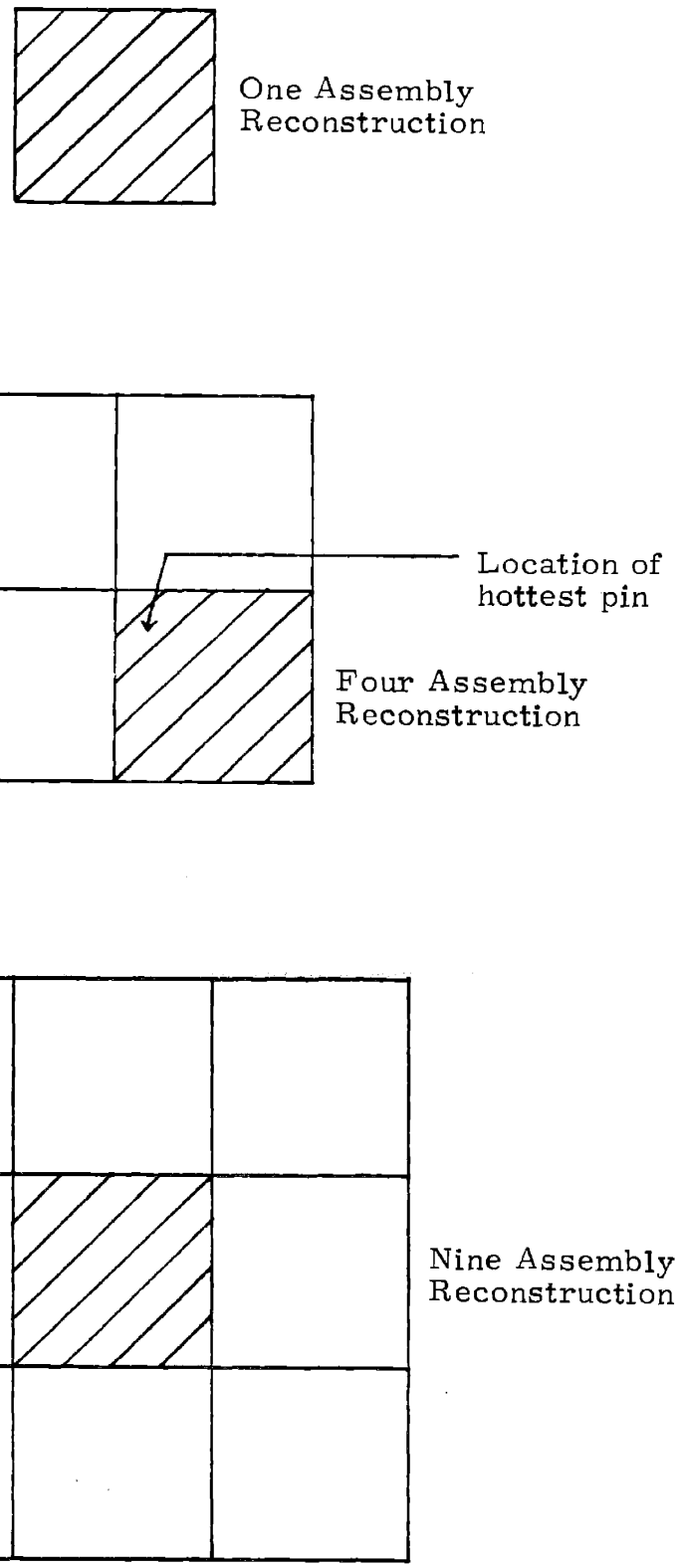

Fig. 4.2 Different reconstruction methods.

by three adjacent assemblies (see Fig. 4.2) so that the hottest pin is close to the center of the set. That way, we expect to suppress all local effects due to the interpolation of the cornerpoint closest to this hottest pin.

4.4.2 Numerical Testing

The hypothesis that the ADF-AXS nodal solution yields good reconstructed heterogeneous fluxes in assemblies located far from any heterogeneity was checked for the central assemblies (those with voids of 40% and 70%) of the NLSH benchmark. The results, shown in Table 4.5, are excellent.

The nine-assemblies reconstruction scheme was tested for two assemblies of the NLSH benchmark: a rodded assembly (the fifth assembly on the second row, #12), and a non-rodded assembly adjacent to the reflector (the eighth assembly on the second row, #15). Results for this reconstruction scheme, along with those corresponding to the "one-assembly" scheme, are given in Table 4.6. Node 12 is particularly well reconstructed. This is due to the fact that the boundary conditions for the reconstruction are relatively far from any significant heterogeneity and are therefore well predicted. Node 15 is in a globally overpredicted region, so that all boundary fluxes are overpredicted. Therefore, the reconstructed fluxes are overpredicted too. Nevertheless, all local effects (those due to the ADF-AXS approximation on this particular node, and those due to the cornerpoint interpolation) have been smoothed out, as can be seen from the fact that the minimum and maximum errors in reconstructed fluxes are very close.

The four-assembly reconstruction scheme, designed to predict the power of the hottest pin, was tested on node 12 in the NLSH bench-

Table 4.5 Maximum errors for pin-wise flux reconstruction in the central assemblies of the NLSH benchmark, when the ADF-AXS solution and the "one-assembly" reconstruction scheme are used.

		-0.55% 1.32%	-0.84% -2.44%	
	0.39% -0.31%	-0.48% 1.44%	1.77% 2.46%	
0.30% 0.37%	0.34% 0.29%	0.45% 1.57%	1.75% 2.48%	← fast flux ← thermal flux

mark and node 10 (tenth node in the first row) and node 35 (third node in the third row) of the MVY benchmark. The reconstruction results, shown in Table 4.7, are very good.

4.5 The Extension of Reconstruction Schemes to Three-Dimensional Calculations

It is not the purpose of this thesis to extend the two-dimensional reconstruction schemes described earlier, to three-dimensional calculations. Such work is currently underway at MIT.

Nevertheless, the smoothness of the fluxes in the axial direction makes it likely that the radial and axial behavior of the fluxes can be mathematically separated. If this fact is verified for realistic three-dimensional benchmarks, the extension of two-dimensional schemes will be straightforward.

4.6 Summary

In this chapter, flux reconstruction techniques based on imposing quadratic form functions on the boundary of one, four, or nine adjacent assemblies were described and tested.

It was shown that if the nodal solution resulting from the iterative scheme described in Chapter 3 was used, the one-assembly technique was sufficient to reconstruct heterogeneous fluxes within 5%. If the ADF-AXS nodal solution is to be used, the one-assembly technique gives excellent results in assemblies far from any significant heterogeneity and the nine-assembly technique yields good fluxes in all other assemblies, whereas the four-assembly technique is sufficient to predict very accurately the power in the hottest pin of each assembly.

Table 4.6 Maximum errors in flux reconstruction when using the ADF-AXS nodal solution

	One-Assembly Reconstruction	Nine-Assembly Reconstruction
Node #12 (LSH)		
Fast flux	-13.3%	0.81%
Thermal flux	-18.5%	0.83%
Node #15 (LSH)		
Fast flux	7.48%	5.94% (min: 4.86)
Thermal flux	13.1%	6.01% (min: 4.46)

Table 4.7 Maximum errors in hottest pin when using the ADF-AXS nodal solution and the "four assemblies" technique

	Assembly 12 (LSH)	Assembly 10 (MVY)	Assembly 35 (MVY)
Fast flux	-1.06%	-0.15%	-1.39%
Thermal flux	-0.95%	-0.01%	-1.21%

CHAPTER 5
THE APPLICATION OF NODAL METHODS TO DEPLETION CALCULATIONS

5.1 Introduction

In the earlier chapters of this thesis, homogenization and reconstruction schemes were described which, when applied to beginning-of-life BWR benchmarks composed of realistic assemblies, gave very satisfactory results.

The extension of these schemes to depletion calculations is not a straightforward procedure. Whereas exact heterogeneous cross sections are known for the beginning of life benchmarks, this is not the case when depletion effects are considered. Determining the exact heterogeneous cross sections throughout life would require the knowledge of all exact time-dependent pointwise fluxes, but nodal methods predict only approximate node-averaged quantities. Thus, some method has to be devised which will predict time-dependent equivalence theory parameters from the sole knowledge of a time-dependent nodal solution to the global problem.

Such a method, the "assembly-depletion" scheme, will be described in section 2. This method will be tested, both for the prediction of equivalence theory parameters and for flux reconstruction, in section 3. Feedback effects will not be tested.

5.2 The Assembly-Depletion Approximation

The most important limitation of nodal methods is the cost of generating and storing tables of response matrices or assembly homogenized parameters. Thus, the pretabulation of these quantities should

require as few interpolating parameters as possible. In particular, it would be extremely costly to take into account the global flux tilt of the reactor. Therefore, a simple approximation is needed for evaluating the time-dependent heterogeneous cross sections used in the process of generating equivalence theory parameters.

Because of the small magnitude of inter-assembly effects, the "assembly-depletion" approximation seems particularly well suited: each assembly is depleted with the $\underline{J} \cdot \underline{n} = 0$ boundary condition. Thus, assembly homogenized parameters and response matrices can be pre-tabulated versus the average assembly exposure. The same kind of tabulation should also be performed for the other state variables describing each assembly (void, void history, temperature, xenon concentration ...). Nevertheless, it is not the purpose of this thesis to study the effects of variations of these state variables. Thus, they will be assumed constant. The following procedure can be implemented at each time step of the depletion calculation.

1. Obtain, at beginning of time step, node-averaged powers, using known homogenized parameters or response matrices.
2. For each assembly, calculate average burnup, and interpolate new homogenized parameters or response matrices, using the zero current boundary condition "assembly depletions".
3. Calculate end of time-step nodal solution.

Compared to equivalent beginning of life nodal calculations, the depletion calculations performed that way include two new sources of errors. First, it is an inherent feature of the "assembly-depletion"

approximation that the flux tilts throughout the core are not taken into account. Therefore, heterogeneous cross sections used in the calculation of response matrices and ADF-AXS will not be predicted exactly. The second, and most important, source of error is that the nodal procedure leads to some error in average assembly exposures. Hence, the homogenized parameters and response matrices used at each time-step do not represent the exact physical state of the corresponding assembly.

Nevertheless, the variations of the heterogeneous cross sections with fuel burnup are generally very small [1, 8]. Consequently, even a large imprecision in the determination of pin or assembly-averaged burnup, is expected to have a relatively insignificant effect on the determination of homogenized parameters or response matrices.

5.3 Numerical Testing

5.3.1 Description of Benchmark Problems

The two depletable benchmarks described in this section are both small two-dimensional BWR cores. They are more explicitly described in Appendix 2.

5.3.1.1 The DEP1 BWR Benchmark Problem

The DEP1 BWR benchmark is a small and very tilted core. It consists of 32 fresh and burned fuel assemblies, some of which are partially voided. It is surrounded by a water reflector. A control rod is present in each half-core, and is located close to the reflector. That particular feature creates a very strong local tilt, thus increasing the difficulty of the homogenizations. The assemblies are those characteristic of the Vermont Yankee reactor.

The variations of the macroscopic cross sections with burnup were obtained from CASMO calculations [21] provided by Yankee Electric. We assumed that all cross sections vary quadratically with pin-wise burnups. No feedback effects were accounted for. The assumption that macroscopic cross sections vary only with pin-wise burnups is very simplistic, as some effects, like the spectral dependence of cross sections in adjacent pins, are neglected. Nevertheless, these are only second-order effects. Furthermore, the objective of this study is to compare nodal methods to fine-mesh finite-differences calculations. In that respect, an approximate cross-sectional model is sufficient for meaningful comparisons.

The reference solution for the DEP1 benchmark is a fine-mesh full core PDQ7 "one-shot" depletion. The depletion was performed for 10,000 hours at a reactor power level of 10^5 W/cm height. 969 mesh-points were used in each assembly. The "one-shot" assumption is not realistic, but is expected to be conservative: generally B.O.L. fluxes have larger gradients than fluxes in depleted cores; thus, the "one-shot" depletion generates more tilted burnups than a realistic depletion. Furthermore, if the same "one-shot" assumption is used to perform nodal calculations, comparisons between the nodal and finite-differences solutions are expected to be meaningful.

5.3.1.2 The DEP2 BWR Benchmark Problem

The DEP2 benchmark is a small and strongly tilted BWR core. It consists of 60 fuel assemblies, surrounded by a water reflector. All assemblies are heterogeneous and are those characteristic of the Vermont Yankee, where the length of the control rods has been slightly modified (see Appendix 2). The cross section behavior with burnup is the same as

that used in the DEP1 BWR benchmark.

Two successive, one-shot 10,000-hour depletions were performed and the assemblies were shuffled at the end of each cycle. The beginning of life core consisted of a central rodded region with burned fuel and 40% void fraction, surrounded by high void burned fuel. The outside of the fueled region consists of fresh assemblies, with 40% void. A one-shot depletion was performed for 10,000 hours at a full core power level of 197606 W. The resulting core was then shuffled, in order to bring the outer fresh fuel in a more central position. The mostly burned assemblies were eliminated, and fresh fuel was brought into the outer locations. The central rodded assemblies were kept in the same location. (No data was available for the variation of cross sections with void; thus each assembly was assumed to operate at its original void.) A new one-shot depletion of 10,000 hours was then performed, again at a power level of 197606 W, and the resulting core was then shuffled. The assemblies in the periphery were those which were located next to the "jag" of the core during the second depletion cycle, and had therefore been depleted under very strongly tilted conditions. The inner assemblies were the same as those used for the first reload core (they had been burned in peripheral positions during the first cycle).

The reference solution for the DEP2 benchmark is a full core CITATION run, where 256 meshes are used in each assembly.

5.3.2 Numerical Testing of Homogenization Methods

5.3.2.1 The DEP1 Benchmark

The assembly surface fluxes and homogenized parameters were obtained from PDQ7 calculations, using the same meshing as in the reference calculation. The surface flux response matrices were

generated with CITATION, using that same meshing.

Beginning of life nodal powers were predicted using both the ADF-AXS and the response matrix homogenization schemes. For each of these methods and for each assembly, a one-shot depletion was performed for 10,000 hours with PDQ7, for the nodal power predicted at beginning of life. These calculations led to a new set of homogenized parameters (corresponding to ADF-AXS B.O.L. nodal powers) and response matrices (corresponding to response matrix B.O.L. nodal powers).

Tables 5.1 and 5.2 give the B.O.L. and E.O.L. nodal powers and the errors corresponding to the two homogenization schemes used. Tables 5.3 and 5.4 summarize the nodal results.

The response matrix homogenization scheme results in only a marginal improvement on the ADF-AXS results. This seems to be due to the severity of this benchmark, which causes the quadratic form function approximation to be invalid. Nevertheless, both homogenization schemes predict very good nodal powers. This seems to be due to the small size of the core.

Although the end of life homogenized parameters and response matrices were generated from assembly depletions which reproduce neither the reference B.O.L. powers, nor the flux tilts, the nodal powers predicted by the two depletion schemes at E.O.L. are consistently better than at B.O.L. These results seem to indicate that the "assembly-depletion" approximation is accurate, even in the case of a highly tilted benchmark.

5.3.2.2 The DEP2 Benchmark

The assembly surface fluxes and homogenized parameters were

Table 5.1 B.O.L. nodal powers for the DEP1 benchmark

1.10895	1.00858	Reference
-1.17%	-2.68%	ADF-AXS
+3.07%	+1.33%	Response matrices
1.00765	1.11126	1.03922
- 2.05%	- 0.02%	+ 2.48%
+ 0.63%	- 0.92%	+ 0.36%
0.75218	0.97299	0.99917
- 0.17%	- 0.30%	3.89%
- 2.12%	- 2.16%	- 1.15%

Table 5.2 E.O.L. nodal powers for the DEP2 benchmark

1.12865 2.07% 0.00%	1.03486 0.50% -1.34%	References Response matrices ADF-AXS
0.98729 0.48% 0.04%	1.06904 - 0.56% 0.04%	1.05908 0.00% 1.13%
0.78219 -0.68% -0.47%	0.96354 -1.51% 1.01%	0.97535 -0.79% 2.01%

Table 5.3 Nodal results at B.O.L. for the DEP1 benchmark

	ADF-AXS	Response Matrices
Error in eigenvalue	-0.18%	+0.22%
Average error in nodal power	1.60%	1.47%
Maximum error in nodal power	3.89%	3.07%

Table 5.4 Nodal results at E.O.L. for the DEP1 benchmark

	ADF-AXS	Response Matrices
Error in eigenvalue	-0.07%	+0.20%
Average error in nodal power	0.90%	0.82%
Maximum error in nodal power	2.01%	2.07%

obtained from QUANDRY calculations, using the same meshing as in the reference calculations. The surface flux response matrices were generated with CITATION, using that same meshing.

The nodal powers were predicted at each time step, using both the ADF-AXS and the response matrix homogenization schemes. The assembly homogenized parameters and the response matrices were predicted, at each time step, from successive one-shot CITATION depletions performed with zero current boundary conditions, using the average nodal powers predicted at the earlier steps by the response matrix technique. As these nodal powers are generally better than those predicted by the ADF-AXS method, this approach is expected to yield better assembly homogenized parameters than those which would have been calculated from the nodal powers of the ADF-AXS run. Therefore, a comparison between the ADF-AXS and response matrices results is expected to overestimate the accuracy of the ADF-AXS results.

Nodal results for each time step are summarized in Table 5.5. No significant variations in the quality of the nodal results can be observed when the fueled assemblies are either depleted or shuffled. Thus, the "assembly-depletion" approximation seems to be adequate for predicting assembly homogenized parameters and response matrices.

5.3.3 Numerical Testing of Reconstruction Methods

A straightforward extension of the depletion schemes based on the "assembly-depletion" approximation is to use the local heterogeneous cross sections predicted by this approximation in the fixed source calculation involved in the reconstruction process. Only the "one-assembly" reconstruction scheme, used in conjunction with the response matrix

Table 5.5 Errors in nodal quantities at each time step of the DEP2 benchmark (in percents)

	B.O.L. 1	E.O.L. 1	B.O.L. 2	E.O.L. 2	B.O.L. 3
Maximum error in nodal power					
ADF-AXS	5.19	2.53	4.83	4.54	3.66
Response matrices	1.36	0.73	1.18	2.01	1.72
Average error in nodal power					
ADF-AXS	2.22	1.01	2.34	2.37	1.70
Response matrices	0.88	0.38	0.82	0.82	0.69
Error in eigenvalue					
ADF-AXS	-0.66	-0.29	-1.10	-0.18	-0.67
Response matrices	-0.64	-0.24	0.06	0.54	-0.19

solution, will be tested.

The heterogeneous cross sections of depleted assemblies are not predicted exactly by the "assembly depletions", as the flux tilts throughout the core are not taken into account when these depletions are performed (see section 5.2). More accurate cross sections could be predicted by reconstructing the heterogeneous fluxes throughout the core at each time step. These reconstructed fluxes would then be used for depleting each individual pin. Thus, flux tilts would be taken into account. Unfortunately, this approach would be very expensive. Not only would it require reconstructing all heterogeneous fluxes, but also each individual pin burnup would have to be calculated and stored. Thus, this approach does not seem to be fruitful.

5.3.3.1 The DEP1 Benchmark

The heterogeneous fluxes were reconstructed at B.O.L. and E.O.L., using the response matrix nodal solution. The pin-powers were reconstructed by using these reconstructed heterogeneous fluxes, and the pin-wise fission cross sections obtained from the "assembly-depletions".

Table 5.6 gives the maximum errors in reconstructed fluxes and powers at B.O.L. and E.O.L., and the maximum error in pin-wise thermal fission cross section in the fuel pins and in the gadolinium pins, due to the "assembly depletion" approximation.

The maximum errors in reconstructed fluxes and powers decrease during depletion. The errors in reconstructed powers decrease by a large amount; this is mainly due to a cancellation of errors; at the particular location where the maximum error in reconstructed power occurs, the flux is overpredicted and Σ_{f2} is underpredicted. Nevertheless,

Table 5.6 Errors in reconstruction for the DEP1 benchmark using nodal quantities from response matrices

	B.O.L.	E.O.L.
Maximum error in:		
Reconstructed flux		
• fast	4.66%	3.60%
• thermal	8.62%	6.66%
Reconstructed powers	8.31%	5.13%
Thermal fission xs		
• in fuel	-	-1.57%
• in gadolinium	-	4.87%

the absolute sum of the maximum error in thermal flux (6.66%) and the maximum error in Σ_{f2} in the fuel (1.57%) is still smaller than the maximum error in reconstructed power at B.O.L.

The large error in Σ_{f2} of the gadolinium pins is due to the sharp variations of this cross section with burnup. Fortunately, these pins lie far inside the assemblies, where the reconstructed fluxes are always very accurate.

5.3.3.2 The DEP2 Benchmark

The heterogeneous pin-wise fluxes and the pin-wise powers were reconstructed for all five time steps. CITATION was used to perform the fixed-source calculations. Quadratic form functions were imposed on the assembly boundaries. Maximum errors for these reconstructions are given in Table 5.7. At all time steps, the maximum error in reconstructed thermal flux and pin power occurs in the pin closest to the top right corner of assembly #9 (this is the fourth assembly in the third row).

The maximum errors in reconstructed fluxes and powers in the gadolinium pins are relatively large. However, it should be noted that these errors occur in low power nodes.

In order to obtain better reconstructed fluxes, "extended assemblies", described in Fig. 5.1, were used to generate the "assembly" fluxes involved in the cornerpoint interpolation scheme and in the reconstruction scheme, while "normal" assembly calculations were used to generate response matrices and perform assembly depletions. Thus, the cost of using extended assemblies was minimal.

The concept of extended assemblies was tested for the first three time steps of the DEP2 BWR benchmark. Nodal results are summarized in Table 5.8, while reconstruction results are given in Table 5.9.

Table 5.7 Maximum errors in reconstruction of heterogeneous quantities for the DEP2 benchmark (in percents)

	B.O.L. 1	E.O.L. 1	B.O.L. 2	E.O.L. 2	B.O.L. 3
Maximum error in reconstructed:					
Fast flux in assembly 9	1.99	-1.59	1.66	-2.38	-1.97
Thermal flux in assembly 9	10.5	8.70	10.3	7.74	9.54
Fast flux in other assemblies	-3.44	-2.38	-3.17	-3.04	-3.60
Thermal flux in other assemblies	7.08	5.59	7.16	5.61	6.37
Pin power in fuel in assembly 9	9.77	7.27	9.70	5.53	8.37
Pin power in other assemblies	6.27	3.40	6.54	-4.98	-4.98
Pin power in gadolinium fuel rod	-	13.0	12.1	10.5	9.83

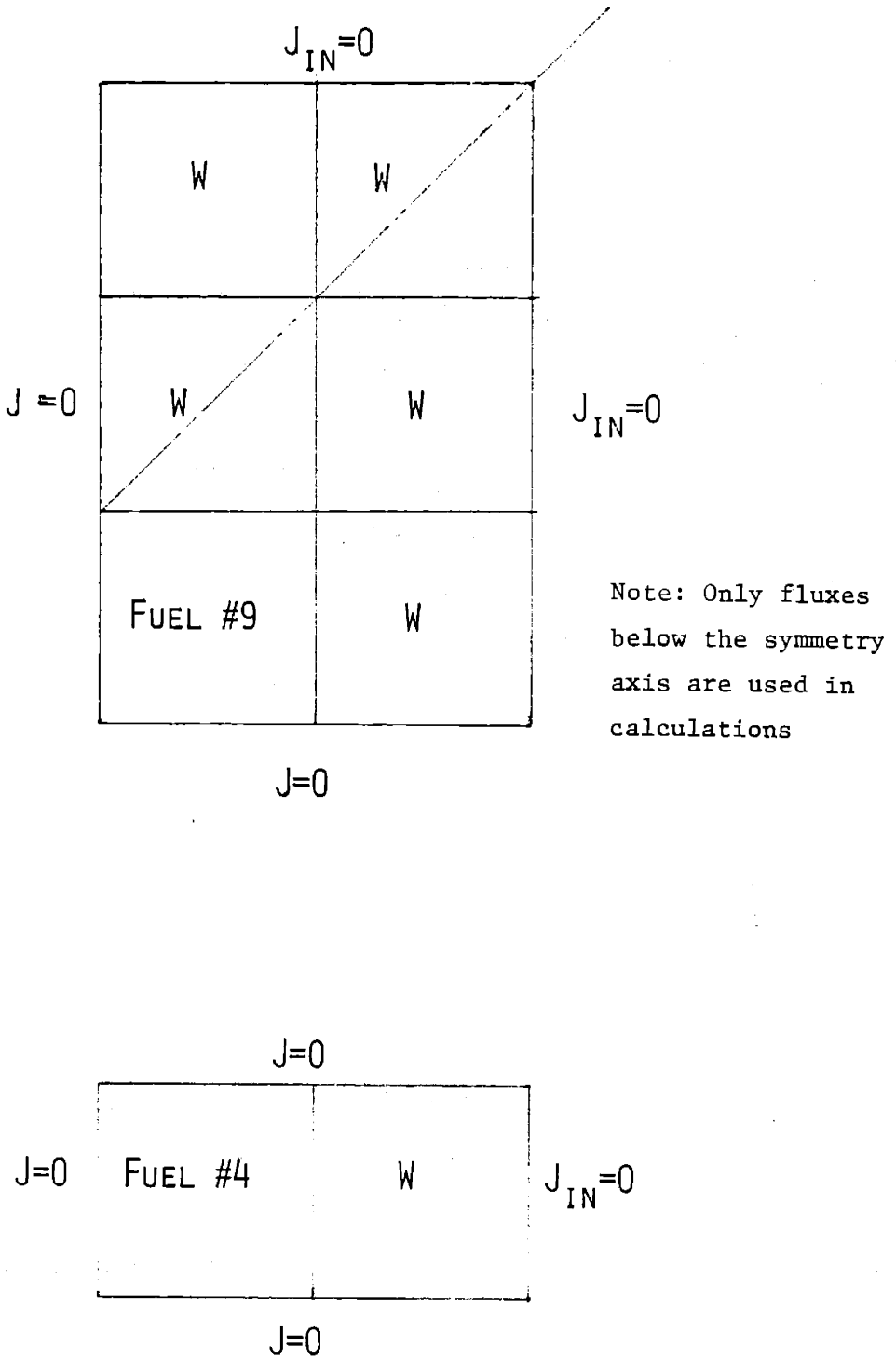

Fig. 5.1 Extended assemblies for the DEP2 benchmark.

Table 5.8 Errors in nodal quantities when using "extended assemblies" in the DEP2 benchmark

(in percents)

	B.O.L. 1	E.O.L. 1	B.O.L. 2
Maximum error in nodal power	0.98	1.28	1.21
Average error in nodal power	0.65	0.59	0.60
Error in eigenvalue	-0.59	-0.21	0.00

Table 5.9 Errors in reconstruction of heterogeneous quantities when using "extended assemblies" in the DEP2 benchmark

(in percents)

	B.O.L.1	E.O.L. 1	B.O.L. 2
Maximum error in reconstructed:			
Fast flux in assembly 9	1.55	-1.14	-4.22
Thermal flux in assembly 9	3.58	4.08	3.86
Fast flux in other assemblies	-3.05	-2.03	-3.29
Thermal flux in other assemblies	3.28	-5.17	-3.84
Pin power in fuel	3.40	4.55	-3.90

These results show a very significant improvement from those in Tables 5.5 and 5.7 corresponding to the use of "normal" assemblies.

The high errors encountered when reconstructing power in gadolinium pins are due to the sharp variation of the thermal fission cross section in the gadolinium fuel with burnup. In assembly 9, where the fluxes are very strongly tilted, "assembly depletions" predict poorly the burnup of the gadolinium pins; this will result in very inaccurate fission cross sections.

To correct this problem while still using the "assembly depletion" approximation to generate response matrices, one can use the pin powers reconstructed at each time step to keep track of the burnup of each gadolinium pin. This burnup can then be used to estimate the fission cross sections entering in the power reconstruction, while all other calculations (global local iterations and flux reconstruction) are done using only the results of "assembly depletions". Thus, the cost of this method can be kept minimal.

With this scheme used for the first depletion cycle, the highest error in reconstructed power in gadolinium pins was reduced from 13% to 3.1%.

The results show the consistency of the depletion scheme being tested. The reconstructed results are not significantly affected throughout either single-cycle depletions or when shuffling of the fuel is performed.

5.4 Summary

In this chapter a nodal depletion scheme, based on depleting each assembly with zero net-current boundary conditions was described.

It was shown that this approximation does not significantly affect

the precision of the homogenization schemes used (ADF-AXS and response matrices). With a few inexpensive modifications, the same conclusion was reached for the "one-assembly" reconstruction scheme.

CHAPTER 6

SUMMARY

6.1 Overview of the Investigation

The goal of this research was to apply the nodal equivalence theory and the analytic nodal method to the analysis of Boiling Water Reactors. First, it was necessary to develop homogenization procedures which would predict accurate equivalence theory parameters. The next step was to infer local fuel pin power densities from the nodal results.

In Chapter 1, it was shown that standard flux weighted constants do not preserve the nodal quantities of interest, because they do not allow for enough degrees of freedom. However, "equivalence theory", which is an extension of the usual diffusion theory model, shows that there exist homogenized parameters which reproduce the nodal quantities of interest.

Equivalence theory was formally derived in Chapter 2. The unique feature of that model is that it allows for the solution of the homogeneous problem to be discontinuous at nodal interfaces. Unfortunately, the reference solution is necessary to define "exact" parameters based on equivalence theory. Hence, approximate methods for determining them must be used in practical cases.

Such approximate methods were reviewed. The ADF-AXS method, developed by Smith [3], is a cheap and simple scheme, but its accuracy is only marginally acceptable for BWR applications. Consequently, more sophisticated methods were developed, wherein equivalence theory parameters are computed by local fixed-source calcula-

tions. Cheng [6] implemented fixed-source calculations based on partial or net surface currents in iterative schemes. These schemes appeared not to be a fruitful approach to the problem of obtaining homogenized parameters. It was shown that their failure was related to the inadequacy of the spatial approximation made for the boundary conditions of the fixed-source calculations.

Hence, various approximate boundary conditions were examined in Chapter 3. It was shown that a practical alternative consists of assuming that the heterogeneous surface fluxes are the product of an "assembly flux" and of a quadratic form function. The parameters of this quadratic can be obtained by interpolating cornerpoint fluxes. Response matrices based on this approximation were implemented in an iterative scheme. Numerical tests show that a few iterations are sufficient to predict very accurate assembly powers. The maximum error for average nodal powers generated in this way is generally less than 3%. Furthermore, this scheme was shown to improve consistently the ADF-AXS results. For two-dimensional cases the computational efficiency of the method appears to be at least one order of magnitude greater than that achieved by solving the global heterogeneous problem by a standard finite-differences method.

The extension of these homogenization schemes to three-dimensional calculations was shown to be straightforward. A numerical test demonstrated that axial discontinuity factors are well approximated by unity.

In Chapter 4, different heterogeneous flux reconstruction schemes were described. The general procedure adopted was to perform fixed source calculations with quadratic form functions imposed on the

boundaries of a set of one, four, or nine adjacent assemblies. It was shown that if the solution of the surface flux response matrix iterative scheme is available, detailed fluxes can be reconstructed to within 5% of reference values everywhere in the core using the one-assembly method. If the ADF-AXS nodal solution is used, a nine-assembly method predicts reconstructed fluxes within 6% of the reference solution. However, it is fairly expensive. On the other hand, a four-assembly method can be used along with the ADF-AXS nodal solution to determine the power of the hottest pin in each assembly. These powers are predicted very accurately.

In Chapter 5, the effects of fuel depletion and assembly shuffling were examined. A cheap way to estimate assembly homogenized parameters and response matrices had to be found if these effects are considered. Accordingly, the "assembly-depletion" approximation was described and was shown to be sufficient for predicting equivalence theory parameters throughout the life of a reactor.

Thus, cheap and efficient ways of predicting nodal powers and heterogeneous fluxes have been developed. They imply a relatively important initial investment. Nevertheless we strongly suggest that they be used for all BWR analysis.

6.2 Recommendations for Future Research

6.2.1 Improved Cornerpoint Flux Interpolation Schemes

Serious doubts about the theoretical validity of the cornerpoint flux interpolation scheme used for this investigation were raised in section 3.3.2. Specifically, the outcome of that scheme depends on the shape of the box used to implement the source-free condition. It seems highly desirable to develop methods which are more theoretically

defensible.

6.2.2 Tabulation and Interpolation of Response Matrices

The tabulation and interpolation of response matrices has been discussed in section 3.4.3. It was stated that a few state variables (void, void history, power level, temperature, xenon concentration, average exposures) are expected to describe well the physical properties of an assembly. Furthermore, it was expected that the variations of the response matrices with these state variables would be smooth. Nevertheless, no systematic way of interpolating response matrices has been studied in this thesis. Such a study is very important, in particular when feedback effects are considered and transient analyses are performed.

6.2.3 Three-Dimensional Flux Reconstructions

The smoothness of the flux in the axial direction suggests that the two-dimensional flux reconstruction method can be extended to the third dimension without having to perform expensive three-dimensional calculations. Nevertheless, cases such as partially inserted control blades should be studied.

6.2.4 The Analytic Generation of Response Matrices

The response matrices used in this investigation were based on an assumed shape of the flux on the boundaries of each assembly. Thus, expensive fixed-source calculations had to be performed to generate these matrices. An alternative to that method would be to find an analytic approximation for the fluxes within the assembly. Response matrices based on this approximation could then be generated analytically, and would therefore be very cheap. An investigation of this scheme is underway at M.I.T.

6.2.5 Improved Depletion Studies

Two important assumptions were made for the depletable benchmarks analyzed in Chapter 5: "one-shot" depletions were performed, and the heterogeneous cross sections were assumed to vary only with pin-wise burnups. It was argued that if the same two assumptions are used in the nodal calculations, comparison of finite-differences and nodal solutions would be meaningful. This argument needs to be further investigated, by performing more realistic depletion calculations.

REFERENCES

1. A. F. Henry, Nuclear Reactor Analysis, MIT Press, Cambridge, MA, 1975.

2. K. S. Smith, "An Analytic Nodal Method for Solving the Two-Group, Multidimensional, Static and Transient Neutron Diffusion Equation", N.E. Thesis, Department of Nuclear Engineering, MIT, Cambridge, MA, March 1979.

3. K. S. Smith, "Spatial Homogenization Methods for Light Water Reactor Analysis", Ph.D. Thesis, Department of Nuclear Engineering, MIT, Cambridge, MA, June 1980.

4. E. L. Wachspress, Iterative Solution of Elliptic Systems and Applications to the Neutron Diffusion Equations of Reactor Physics, Prentice-Hall, Englewood Cliffs, N.J., 1966.

5. R. S. Varga, Matrix Iterative Analysis, Prentice-Hall, Englewood Cliffs, N.J., 1962.

6. A. Y. C. Cheng, "Homogenization of BWR Assemblies by Response Matrix Methods", Ph.D. Thesis, Department of Nuclear Engineering, M.I.T., Cambridge, MA, May 1981.

7. C. L. Hoxie, "Application of Equivalence Theory to the Neutronic Analysis of PWR's", Ph.D. Thesis, Department of Nuclear Engineering, MIT, Cambridge, MA, June 1982.

8. J. R. Lamarsh, Nuclear Reactor Theory, Addison Wesley, Reading, MA, 1972.

9. J. Bussac and P. Reuss, Traité de Neutronique, Hermann, Paris, France, 1978.

10. B. W. Hagemeier, "Approximate Methods for Obtaining a One-Group Nodal Solution with Two-Group Parameters", S.M. Thesis, Department of Nuclear Engineering, MIT, Cambridge, MA, August 1982.

11. P. J. Finck, "Heterogeneous Flux Reconstruction Based on Surface Currents Response Matrices", A Special Problem in Nuclear Engineering Submitted to Professor A. F. Henry, MIT, Cambridge, MA, August 1981.

12. D. K. Parsons, "Application of Response Matrix Methods to PWR Analysis", S.M. Thesis, Department of Nuclear Engineering, MIT, Cambridge, MA, June 1982.

13. G. P. Bottoni, R. Gaundalini, G. Vimercati, and P. Peroni, "Neutronic Aspects of the LWR Core Simulator CETRA", ANS/ENS, May 1979.

REFERENCES (continued)

14. P. J. Finck, C. L. Hoxie, H. S. Khalil, D. K. Parsons, A. F. Henry, "The Application of Nodal Methods to Light Water Reactors", ANS Topical Meeting on Advances in Reactor Physics and Core Thermal Hydraulics, Kiamesha Lake, N.Y., September 1982.

15. D. M. VerPlanck, "Manual for the Reactor Analysis Program SIMULATE", Yankee Atomic Electric Company, 1978.

16. K. Koebke and M. R. Wagner, "The Determination of the Pin Power Distribution in a Reactor Core on the Basis of Nodal Coarse Mesh Calculations", Atomkernenergie (ATKE), Bol. 30, 1977.

17. C. J. Pfeifer, PDQ-7 Reference Manual II, WAPD-TM947 (L), Bettis Atomic Power Laboratory, 1971.

18. T. B. Fowler, D. R. Vondy, and G. W. Cunningham, "Nuclear Reactor Core Analysis Code:CITATION", ORNL-TM-2406, Oak Ridge National Laboratory, 1969.

19. H. S. Khalil, "The Application of Nodal Methods to PWR Analysis", Ph.D. Thesis, Department of Nuclear Engineering, MIT, Cambridge, MA, January 1983.

20. F. Nissen, "Determination of Local Pin Powers in the Framework of Nodal Coarse-Mesh Solutions", Risø-R-474, Risø National Laboratory, Denmark, August 1982.

21. A. Ahlin, M. Edenius, H. Haggblom, CASMO-A Fuel Assembly Burnup Program, AE-RF-76-4158, April 1978.

22. J. J. Dorning, "Modern Coarse-Mesh Methods - A Development of the 70's", ANS Proceedings of the Topical Meeting on Computational Methods in Nuclear Engineering", Williamsburg, VA, April 1979.

23. G. Greenman, "Derivation of an Analytic Nodal Method Employing the Quadratic Transverse Leakage Approximation", Special Problem in Nuclear Engineering Submitted to Professor A. F. Henry, MIT, Cambridge, MA, August 1977.

24. K. Koebke, "A New Approach to Homogenization and Group Condensation", paper presented at the IAEA Technical Committee Meeting on Homogenization Methods in Reactor Physics, Lugano, Switzerland, November 1978.

25. R. A. Loretz, "The Determination of Equivalent Diffusion Theory Parameters by Local Implementation of the Koebke Method", S.M. Thesis, Department of Nuclear Engineering, MIT, Cambridge, MA, August 1980.

REFERENCES (continued)

26. W. M. Stacey, Jr., Variational Methods in Nuclear Reactor Physics, Academic Press, New York, N.Y., 1974.

27. F. A. R. Schmidt, "Finite Element Application to Global Reactor Analysis", Proceedings of the International Topical Meeting on 'Advances in Mathematical Methods for the Solution of Nuclear Engineering Problems', Munich, West Germany, April 1981.

28. Z. Weiss, S. O. Lindahl, "High-Order Response Matrix Equations in Two-Dimensional Geometry", Nuclear Science and Engineering, Vol. 58, No. 2, 1975.

APPENDIX 1

DESCRIPTION OF BWR BENCHMARK PROBLEMS

A1.1 THE CISE BWR BENCHMARK PROBLEM

A1.2 THE LSH BWR BENCHMARK PROBLEM

A1.3 THE MVY BWR BENCHMARK PROBLEM

A1.4 THE TRD BWR BENCHMARK PROBLEM

A1.5 THE PRELIMINARY TEST PROBLEM

A1.1 THE CISE BWR BENCHMARK PROBLEM

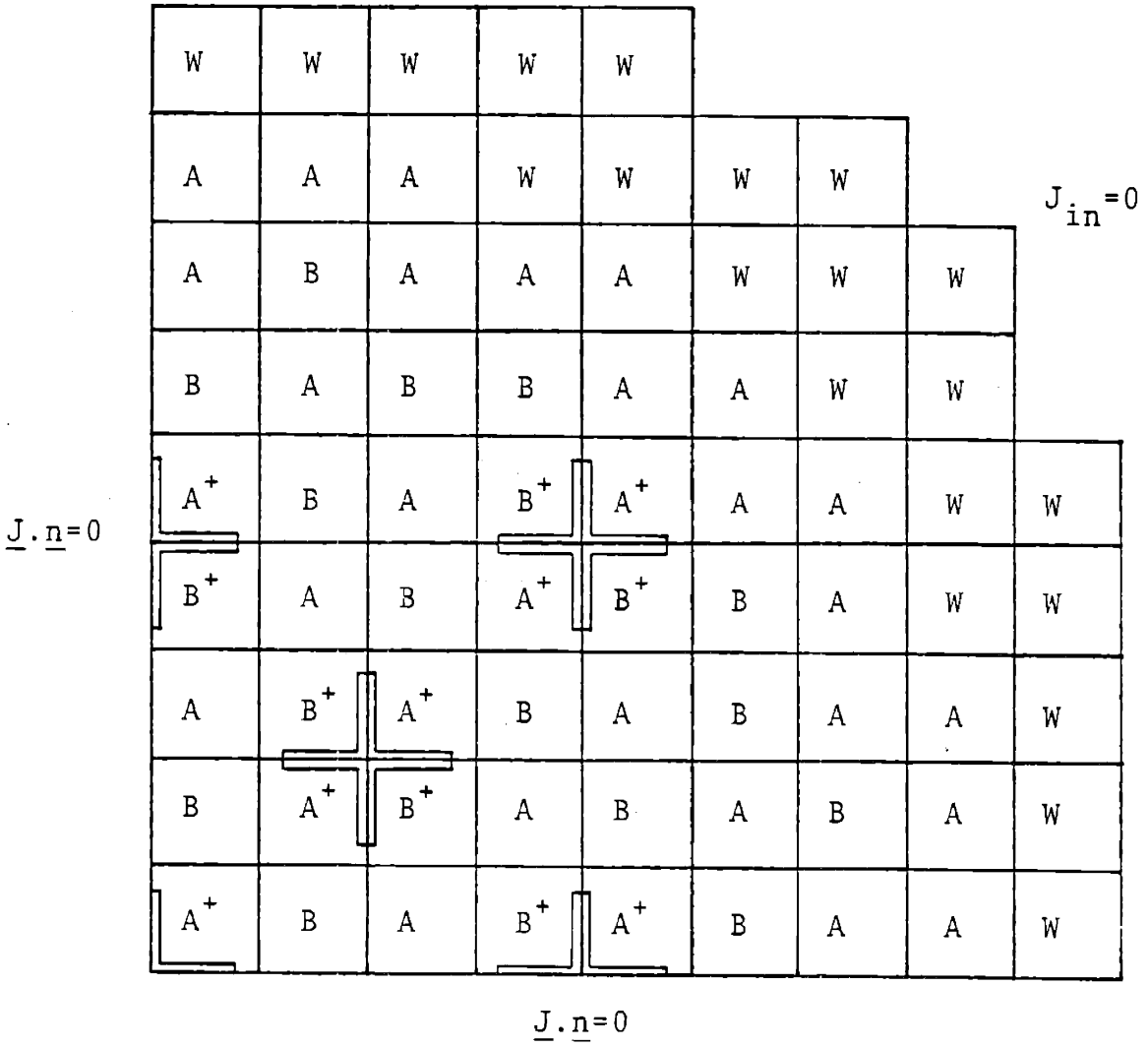

Fig. A1.1.1 Core layout for the CISE Benchmark Problem.

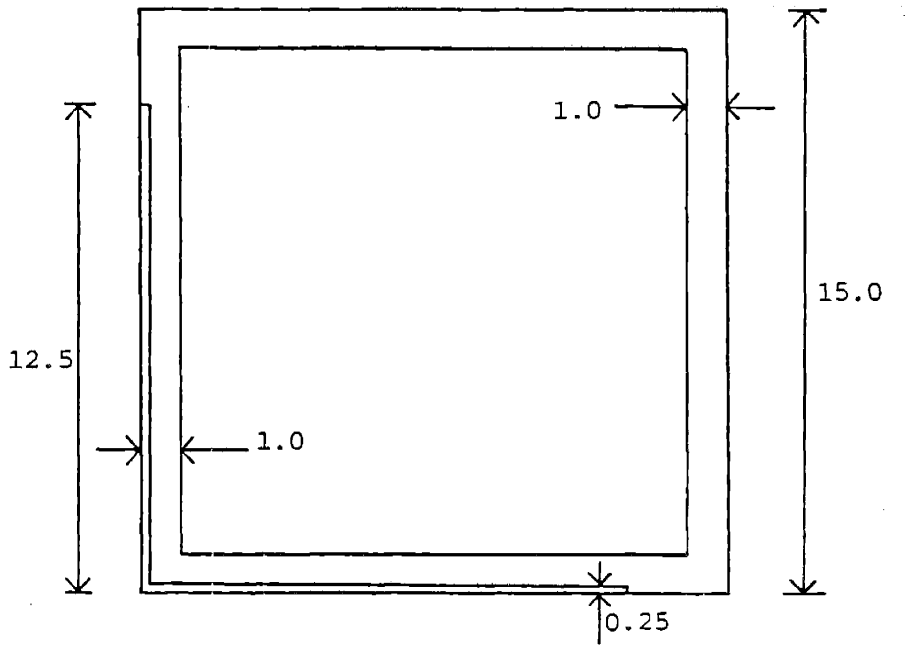

Fig. A1.1.2 Assembly description for the CISE Benchmark Problem.

Zone	A	A^+	B	B^+	REFL.
I	3	3	4	4	2
II	2	1	2	1	2
III	2	2	2	2	2

Table A1.1.1 Material Positions for Assemblies of the CISE Benchmark.

Composition	group	D_g (cm)	Σ_{ag_1} (cm^{-1})	$\nu\Sigma_{fg_1}$ (cm^{-1})	$\Sigma_{gg'_1}$ (cm^{-1})
1	1	3.00	0.08	0.0	0.0
(Control blade)	2	0.15	1.00	0.0	
2	1	2.00	0.0	0.0	0.04
(Water)	2	0.30	0.01	0.0	
3	1	1.80	0.008	0.006	0.012
(Fresh fuel)	2	0.55	0.085	0.110	
4	1	1.80	0.008	0.005	0.012
(Depleted fuel)	2	0.55	0.085	0.100	

$\chi_1 = 1.0$
$\chi_2 = 0.0$
$\nu = 2.5$

Table A1.1.2 Heterogeneous cross sections for the CISE Benchmark.

A1.2 THE LSH BWR BENCHMARK PROBLEM

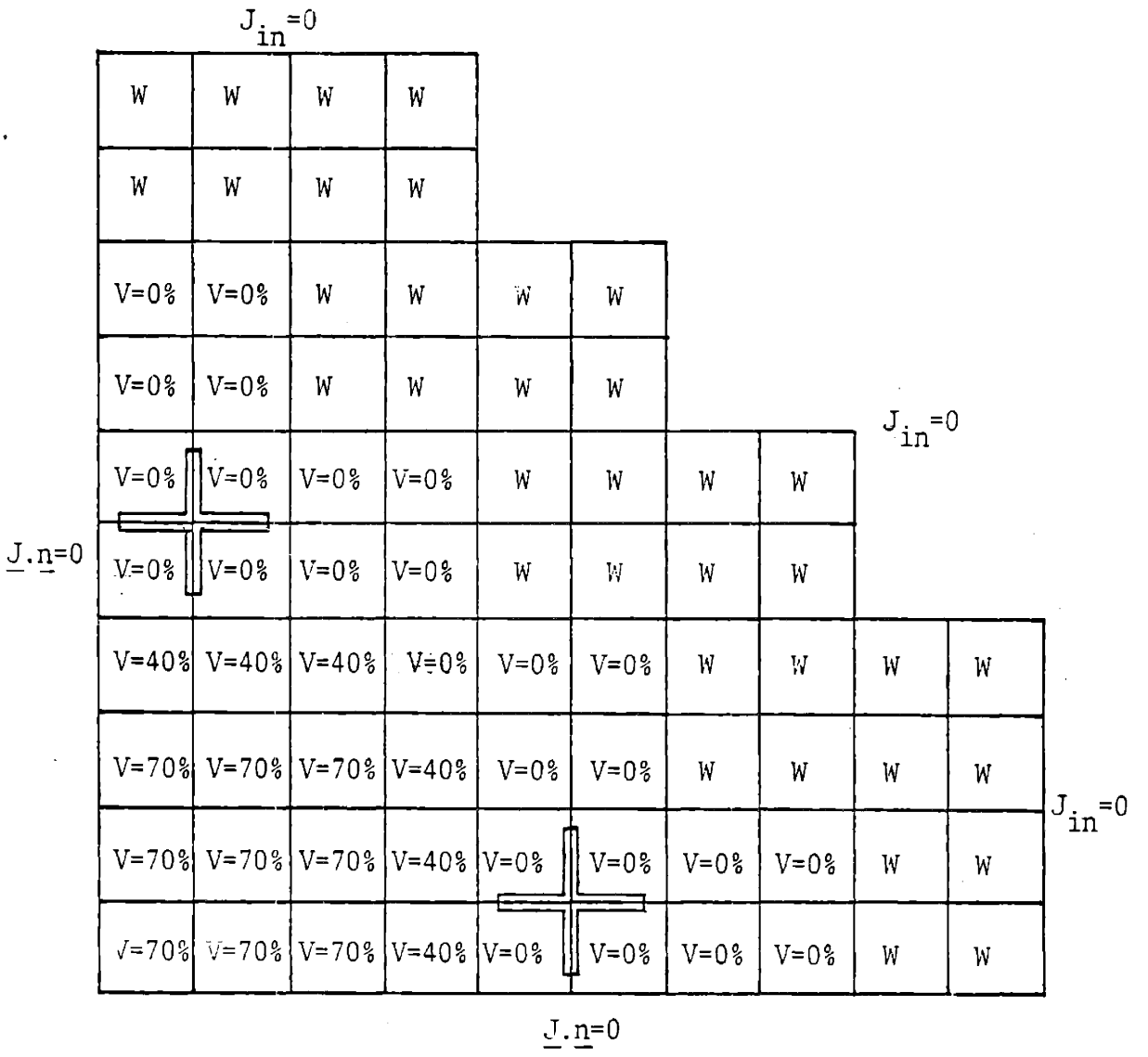

Fig. A1.2.1 Core layout for the LSH BWR Benchmark Problem.

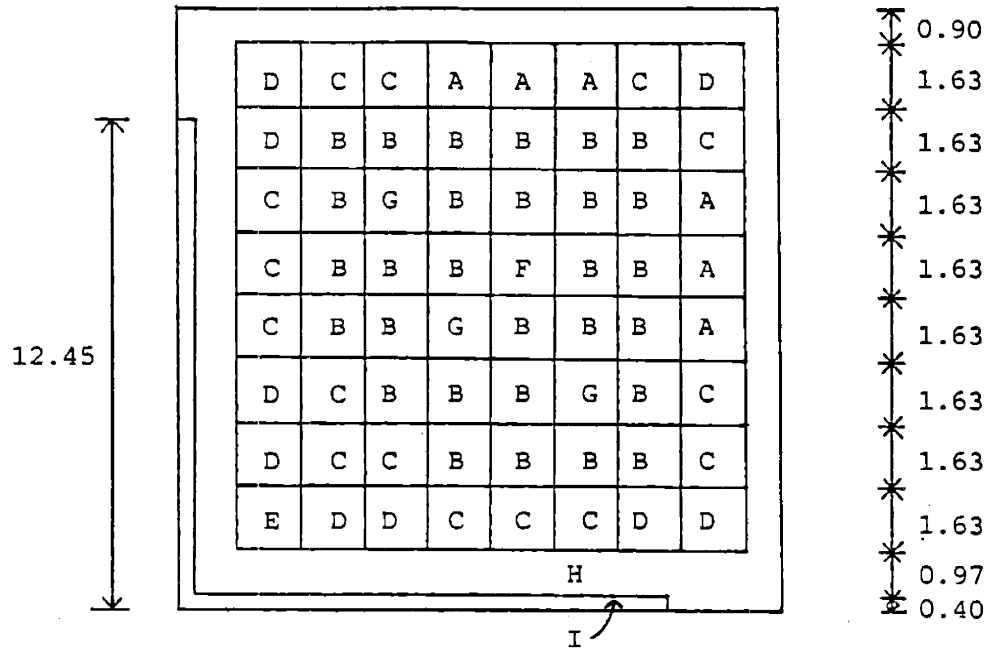

Fig. A1.2.2 Assembly description for the LSH BWR Benchmark.

	VOID FRACTION				
ZONE	0% (rodded)	0%	40%	70%	W
A	1	10	18	26	34
B	2	11	19	27	34
C	3	12	20	28	34
D	4	13	21	29	34
E	5	14	22	30	34
F	6	15	23	31	34
G	7	16	24	32	34
H	8	17	25	33	34
I	9	17	25	33	

Table A1.2.1 Material positions for assemblies of the LSH BWR Benchmark.

Table A1.2.2 Heterogeneous cross sections for the LSH BWR Benchmark Problem.

COMPOSITION	GROUP	DIFFUSION COEFFICIENT	TOTAL CROSS-SECTION	REMOVAL CROSS-SECTION	NU-FISSION CROSS-SECTION
1	1	1.42700E+00	2.62550E-02	1.66990E-02	6.65270E-03
	2	3.68080E-01	7.79120E-02	0.0	1.26440E-01
2	1	1.41060E+00	2.55200E-02	1.62170E-02	6.51540E-03
	2	3.79930E-01	7.51790E-02	0.0	1.26440E-01
3	1	1.39490E-01	2.57680E-02	1.66060E-02	5.59700E-03
	2	3.78210E-01	6.37000E-02	0.0	9.71490E-02
4	1	1.37490E+00	2.62460E-02	1.71350E-02	4.91400E-03
	2	3.80550E-01	5.46390E-02	0.0	7.79920E-02
5	1	1.34160E+00	2.59190E-02	1.67510E-02	4.27110E-03
	2	3.91690E-01	4.61890E-02	0.0	6.10660E-02
6	1	1.58160E+00	2.81970E-02	2.77330E-02	0.0
	2	3.07530E-01	8.69100E-03	0.0	0.0
7	1	1.39730E+00	2.90910E-02	1.62010E-02	5.89980E-03
	2	2.71070E-01	4.44140E-01	0.0	2.68800E-02
8	1	1.52290E+00	2.68460E-02	2.62490E-02	0.0
	2	3.12270E-01	8.75880E-03	0.0	0.0
9	1	1.11330E+00	8.74190E-03	3.75290E-03	0.0
	2	1.84010E-01	9.67260E-01	0.0	0.0
10	1	1.41630E+00	2.63780E-02	1.67780E-02	6.62050E-03
	2	3.68490E-01	8.00900E-02	0.0	1.25430E-01

Table A1.2.2 (continued)

COMPOSITION	GROUP	DIFFUSION COEFFICIENT	TOTAL CROSS-SECTION	REMOVAL CROSS-SECTION	NU-FISSION CROSS-SECTION
11	1	1.41780E+00	2.54260E-02	1.62050E-02	6.51950E-03
	2	3.76890E-01	7.79900E-02	0.0	1.22110E-01
12	1	1.41410E+00	2.62910E-02	1.72090E-02	5.69940E-03
	2	3.71370E-01	6.68700E-02	0.0	9.84880E-02
13	1	1.40190E+00	2.71220E-02	1.81040E-02	5.07070E-03
	2	3.71680E-01	5.76770E-02	0.0	7.95880E-02
14	1	1.39030E+00	2.81730E-02	1.91260E-02	4.58180E-03
	2	3.71310E-01	5.04670E-02	0.0	6.46670E-02
15	1	1.58420E+00	2.78650E-02	2.74030E-02	0.0
	2	3.09230E-01	8.64970E-03	0.0	0.0
16	1	1.40970E+00	2.87200E-02	1.60240E-02	5.88620E-03
	2	2.67700E-01	4.49050E-01	0.0	2.65000E-02
17	1	1.53100E+00	3.13090E-02	3.07390E-02	0.0
	2	2.94170E-01	9.16000E-03	0.0	0.0
18	1	1.68930E+00	1.91380E-02	9.99040E-03	6.33850E-03
	2	5.27170E-01	7.60250E-02	0.0	1.21900E-01
19	1	1.69710E+00	1.81410E-02	9.55690E-03	6.21530E-03
	2	5.38430E-01	7.37680E-02	0.0	1.18220E-01
20	1	1.68950E+00	1.89620E-02	1.03320E-02	5.46480E-03
	2	5.31530E-01	6.34410E-02	0.0	9.61500E-02

Table A1.2.2 (continued)

COMPOSITION	GROUP	DIFFUSION COEFFICIENT	TOTAL CROSS-SECTION	REMOVAL CROSS-SECTION	NU-FISSION CROSS-SECTION
21	1	1.67460E+00	1.95930E-02	1.09500E-02	4.85350E-03
	2	5.32680E-01	5.46350E-02	0.0	7.79930E-02
22	1	1.66130E+00	2.04500E-02	1.16880E-02	4.38500E-03
	2	5.32230E-01	4.77090E-02	0.0	6.36410E-02
23	1	1.97400E+00	1.98060E-02	1.94180E-02	0.0
	2	4.08610E-01	6.58170E-03	0.0	0.0
24	1	1.69900E+00	2.11310E-02	9.33020E-03	5.62870E-03
	2	3.60880E-01	4.38710E-01	0.0	2.79270E-02
25	1	1.60950E+00	2.82650E-02	2.77210E-02	0.0
	2	3.16570E-01	8.54980E-03	0.0	0.0
26	1	1.68940E+00	1.48870E-02	5.71000E-03	6.30570E-03
	2	5.25170E-01	7.80170E-02	0.0	1.23400E-01
27	1	1.69750E+00	1.40690E-02	5.46140E-03	6.19450E-03
	2	5.36580E-01	7.56550E-02	0.0	1.19800E-01
28	1	1.69000E+00	1.45590E-02	5.90060E-03	5.43910E-03
	2	5.29360E-01	6.54030E-02	0.0	9.80660E-02
29	1	1.67550E+00	1.49260E-02	6.24900E-03	4.83840E-03
	2	5.30250E-01	5.67280E-02	0.0	8.04220E-02
30	1	1.66280E+00	1.54660E-02	6.66170E-03	4.37940E-03
	2	5.29560E-01	4.99330E-02	0.0	6.65090E-02

Table A1.2.2 (continued)

COMPOSITION	GROUP	DIFFUSION COEFFICIENT	TOTAL CROSS-SECTION	REMOVAL CROSS-SECTION	NU-FISSION CROSS-SECTION
31	1	1.97440E+00	1.14830E-02	1.10950E-02	0.0
	2	4.08850E-01	6.57670E-03	0.0	0.0
32	1	1.70050E+00	1.57160E-02	4.14920E-03	5.65780E-03
	2	3.70520E-01	4.19950E-01	0.0	3.38370E-02
33	1	1.60990E+00	2.82560E-02	2.77120E-02	0.0
	2	3.16700E-01	8.54670E-03	0.0	0.0
34	1	2.01000E+00	3.56870E-02	3.51600E-02	0.0
	2	3.25900E-01	9.96300E-03	0.0	0.0

$\chi_1 = 1.0$

$\chi_2 = 0.0$

$\nu = 2.5$

Zone	Material
A	2.50 w/o fuel adjacent to can
B	2.50 w/o fuel in the interior
C	1.90 w/o fuel
D	1.49 w/o fuel
E	1.18 w/o fuel
F	the water rod
G	the gadolinium rods
H	the wide and narrow gaps
I	the control rod

Table A1.2.3 Material description for the LSH BWR Benchmark

A1.3 THE MVY BWR BENCHMARK PROBLEM

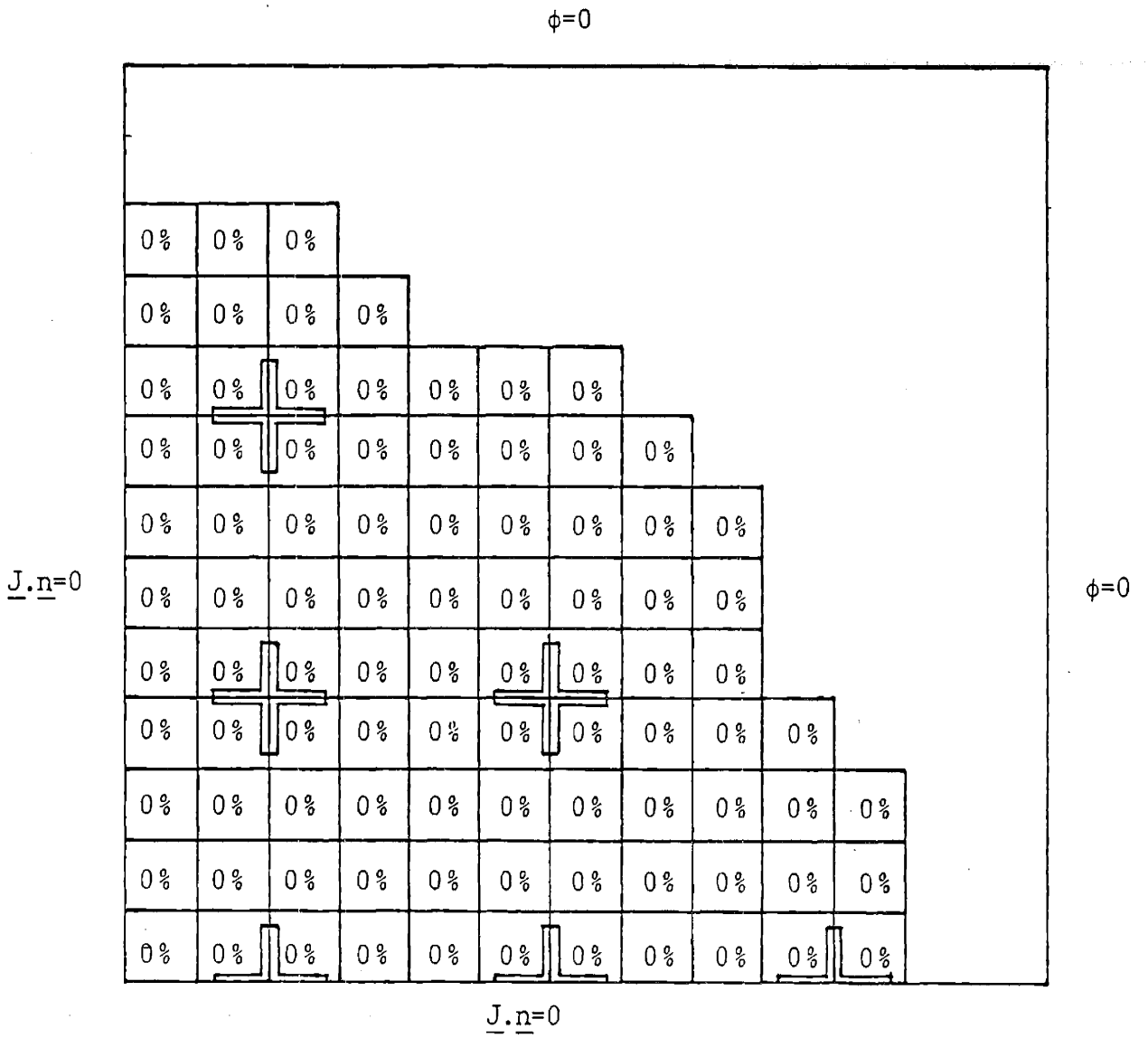

Fig. A1.3.1 Core layout for the MVY BWR Benchmark Problem.

Note: The assembly geometry and the heterogeneous cross sections are the same as for the LSH BWR Benchmark Problem.

A1.4 THE TRD BWR BENCHMARK PROBLEM

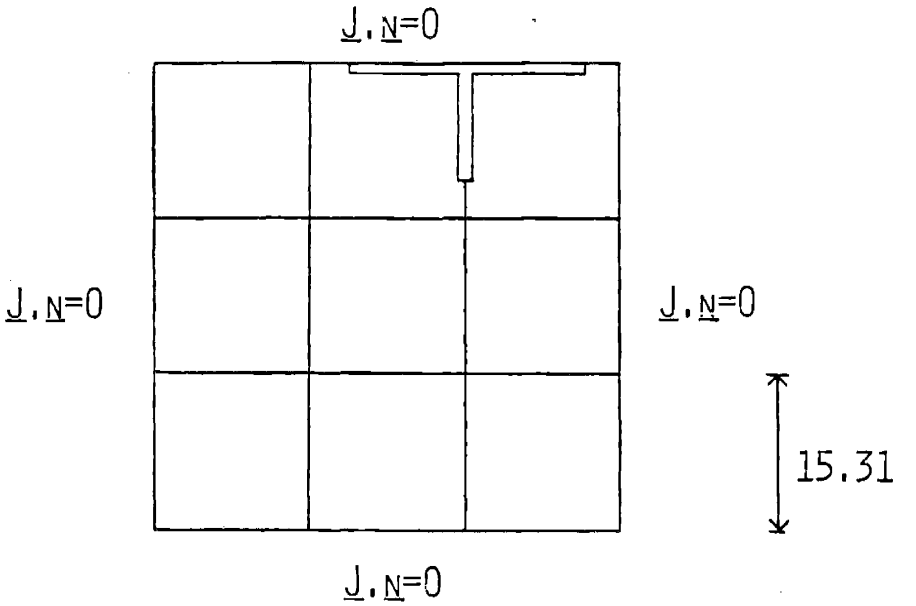

Fig. A1.4.1 Radial core layout for the TRD BWR Benchmark Problem.

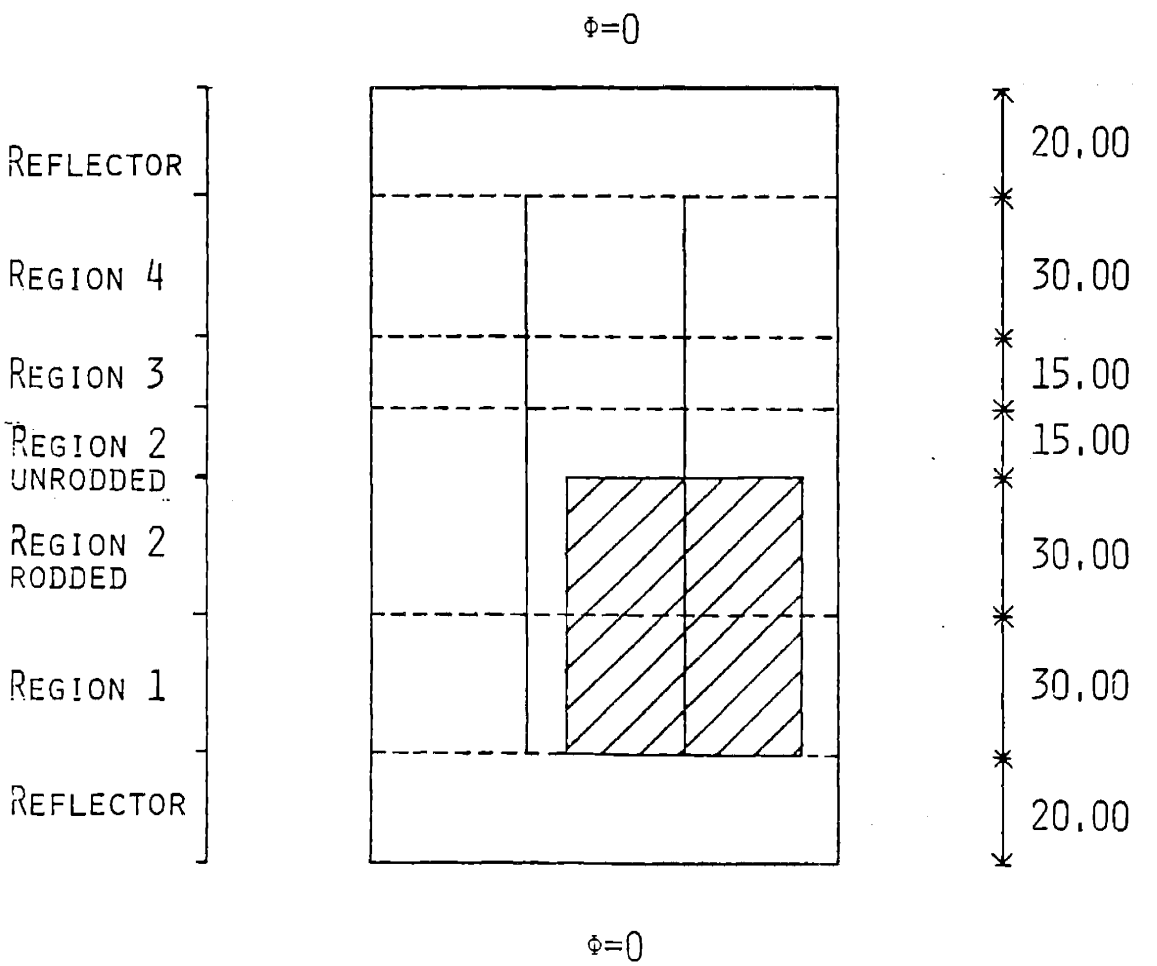

Fig. A1.4.2 Axial core layout for the TRD BWR Benchmark Problem.

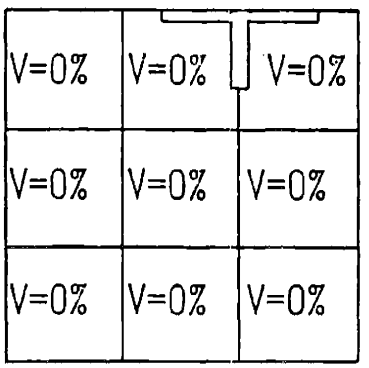

REGION 1

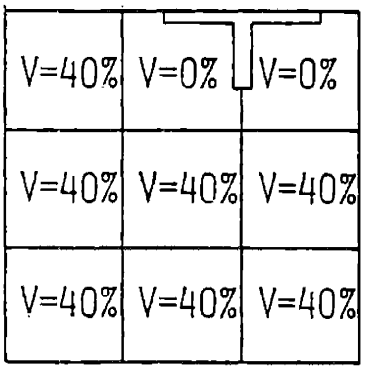

REGION 2

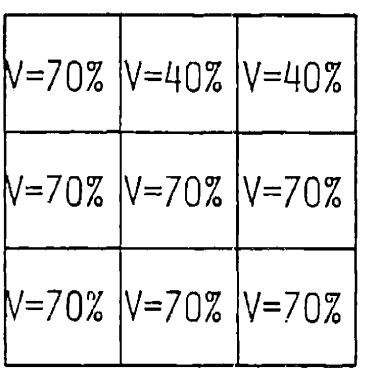

REGION 3

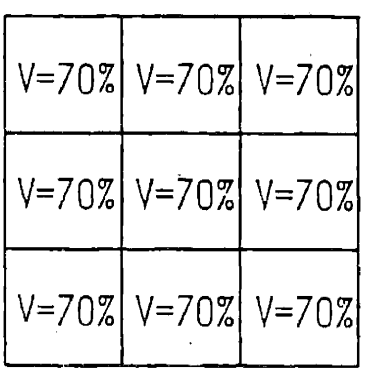

REGION 4

Fig. A1.4.3 Void fractions for the TRD BWR Benchmark.

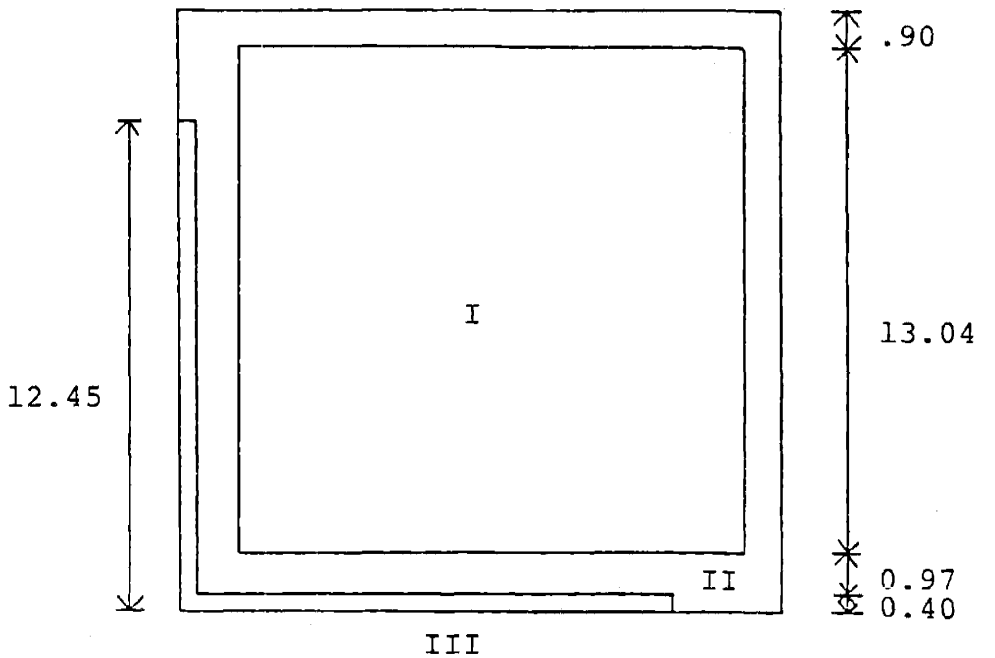

Fig. A1.4.4 Assembly description for the TRD BWR Benchmark.

	VOID FRACTION				
ZONE	0% (rodded)	0%	40%	70%	REFL.
I	1	4	6	8	10
II	2	5	7	9	10
III	3	5	7	9	10

Table A1.4.1 Material positions for assemblies of the TRD BWR Benchmark.

Compo.	Group	D_g	Σ_{tg}	Σ_{rg}	Σ_{fg}
1	1	1.406	.2596E-1	.1667E-1	.5963E-2
	2	.3735	.8025E-1	0.0	.1048
2	1	1.523	.2685E-1	.2625E-1	0.0
	2	.3123	.8559E-2	0.0	0.0
3	1	1.113	.8742E-1	.3750E-2	0.0
	2	.1840	.9673	0.0	0.0
4	1	1.417	.2618E-1	.1696E-1	.5983E-2
	2	.3696	.7986E-1	0.0	.1019
5	1	1.531	.3131E-1	.3074E-1	0.0
	2	.2942	.9160E-2	0.0	0.0
6	1	1.696	.1883E-1	.1015E-1	.5715E-2
	2	.5276	.7658E-1	0.0	.9909E-1
7	1	1.610	.2827E-1	.2772E-1	0.0
	2	.3166	.8550E-2	0.0	0.0
8	1	1.696	.1443E-1	.5739E-2	.5694E-2
	2	.5262	.7688E-1	0.0	.1006
9	1	1.610	.2826E-1	.2771E-1	0.0
	2	.3167	.8547E-2	0.0	0.0
10	1	2.010	.3569E-1	.3516E-1	0.0
	2	.3259	.9963E-2	0.0	0.0

Table A1.4.2 Heterogeneous cross sections for the TRD BWR Benchmark.

A1.5 THE PRELIMINARY TEST PROBLEM

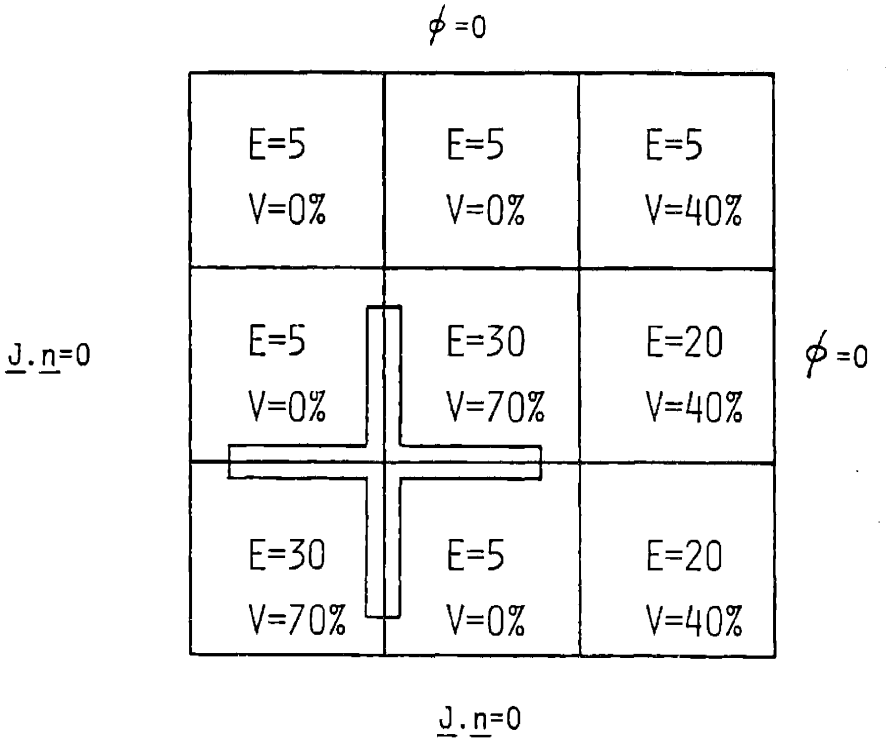

Fig. A1.5.1 Core layout for the preliminary Test Problem.

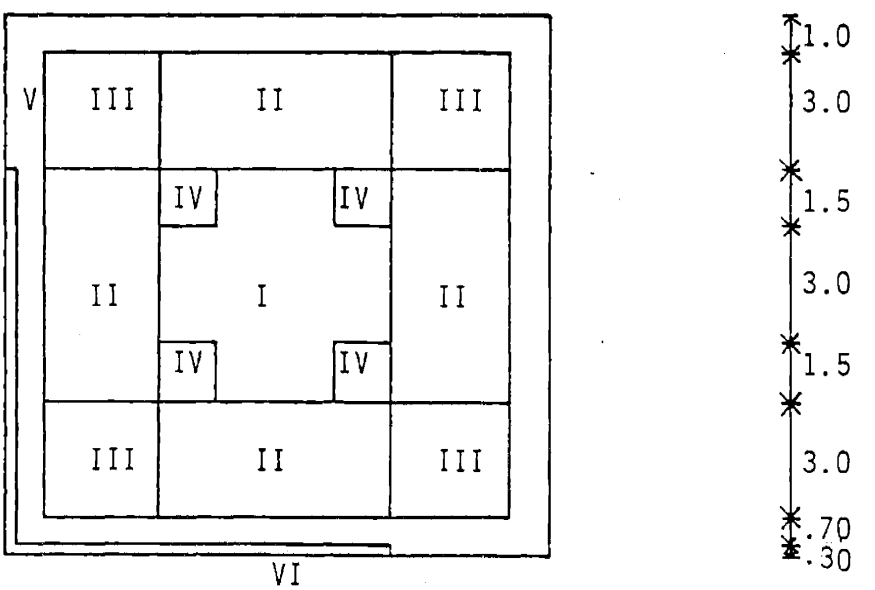

Fig. A1.5.2 Assembly description for the Preliminary Test Problem.

ASSEMBLY

ZONE	E=5 V=0%	E=5 V=0% (rodded)	E=20 V=40%	E=30 V=70%
I	1	6	12	17
II	2	7	13	18
III	3	8	14	19
IV	4	9	15	20
V	5	10	16	21
VI	5	11	16	22

Table A1.5.1 Material positions for assemblies of the preliminary Test Problem.

Table A1.5.2 Heterogeneous cross sections for the preliminary Test Problem.

Compo.	D_g	Σ_{tg}	Σ_{rg}	$\nu\Sigma_{fg}$	Σ_{fg}
1	1.71505	1.84927E-2	8.81354E-3	4.99860E-3	1.84674E-3
	5.11289E-1	8.46766E-2	0.00000000	1.19180E-1	4.43968E-2
2	1.69906	1.99288E-2	9.71929E-3	4.30283E-3	1.56236E-3
	5.11885E-1	7.17403E-2	0.0	9.26985E-2	3.37757E-2
3	1.68338	2.09624E-2	1.03746E-2	3.93319E-3	1.41348E-3
	5.13507E-1	6.46235E-2	0.00000000	7.86099E-2	2.82029E-2
4	1.73868	1.85938E-2	8.52619E-3	4.91940E-3	1.83287E-3
	5.11698E-1	9.15108E-2	0.0	1.25018E-1	4.69796E-2
5	1.60915	2.78535E-2	2.73058E-2	0.0	0.0
	3.14606E-1	8.60145E-3	0.0	0.0	0.0
6	1.98792	1.30264E-2	4.06734E-3	4.12817E-3	1.49970E-3
	7.47662E-1	7.95545E-2	0.00000000	1.07666E-1	3.89630E-2
7	1.95759	1.37564E-2	4.26446E-3	3.52284E-3	1.25997E-3
	7.59114E-1	6.82293E-2	0.0	8.53155E-2	3.02465E-2
8	1.93191	1.43559E-2	4.46617E-3	3.23760E-3	1.14956E-3
	7.66242E-1	6.21661E-2	0.00000000	7.39183E-2	2.59204E-2
9	2.01118	1.33169E-2	3.90106E-3	4.06286E-3	1.48788E-3
	7.48782E-1	8.48796E-2	0.0	1.11592E-1	4.07234E-2
10	1.67279	1.96026E-2	1.90530E-2	0.0	0.0
	3.70045E-1	7.43640E-3	0.0	0.0	0.0
11	1.14239	7.58520E-2	3.89653E-4	0.0	0.0
	2.03168E-1	9.58567E-1	0.0	0.0	0.0

Table A1.5.2 (continued)

12	1.42296	2.54540E-2	1.58941E-2	6.20089E-3	2.37656E-3
	3.68090E-1	8.66178E-2	0.0	1.30677E-1	5.17711E-2
13	1.41659	2.65477E-2	1.69087E-2	5.36251E-3	2.02871E-3
	3.63656E-1	7.49651E-2	0.0	1.06123E-1	4.14995E-2
14	1.40531	2.74979E-2	1.77605E-2	4.80538E-3	1.79981E-3
	3.63633E-1	6.66050E-2	0.0	8.91109E-2	3.44174E-2
15	1.42655	2.65288E-2	1.56848E-2	5.97769E-3	2.30796E-3
	3.33876E-1	2.28168E-1	0.0	9.82144E-2	3.88767E-2
16	1.53167	3.10730E-2	3.05027E-2	0.0	0.0
	2.93667E-1	9.18008E-3	0.0	0.0	0.0
17	1.41364	2.56225E-2	1.59592E-2	6.19485E-3	2.37655E-3
	3.71075E-1	8.62191E-2	0.00000000	1.30199E-1	5.15526E-2
18	1.39631	2.59559E-2	1.62703E-2	5.25298E-3	1.99088E-3
	3.70192E-1	7.43578E-2	0.0	1.05568E-1	4.12276E-2
19	1.37762	2.64745E-2	1.67106E-2	4.64045E-3	1.74209E-3
	3.72179E-1	6.59599E-2	0.00000000	8.86472E-2	3.41744E-2
20	1.41302	2.69276E-2	1.58926E-2	5.99273E-3	2.31689E-3
	3.38183E-1	2.24434E-1	0.0	9.79440E-2	3.87449E-2
21	1.52271	2.64480E-2	2.58513E-2	0.0	0.0
	3.12588E-1	8.75572E-3	0.0	0.0	0.0
22	1.18545	8.21421E-2	5.04714E-4	0.0	0.0
	1.99039E-1	9.98926E-1	0.0	0.0	0.0

APPENDIX 2

DESCRIPTION OF DEPLETABLE BWR BENCHMARK PROBLEMS

A2.1 THE DEP1 BWR BENCHMARK PROBLEM

A2.2 THE DEP2 BWR BENCHMARK PROBLEM

A2.1 THE DEP1 BWR BENCHMARK PROBLEM

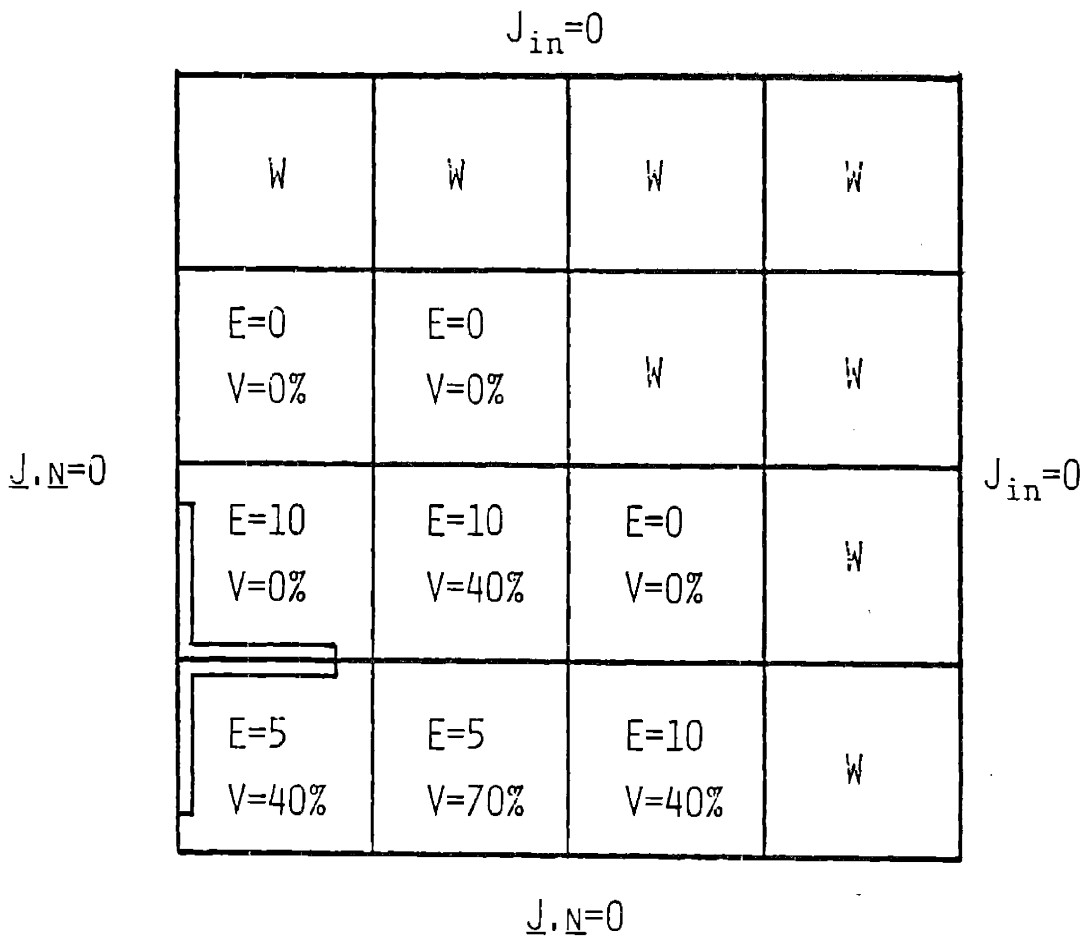

E = B.O.L. average exposure.

V = void fraction (constant throughout life)

Total Power = 10^5 W/cm height.

Depletion Time = 10,000 hours.

Fig. A2.1.1 Core layout for the DEP1 BWR Benchmark Problem.

Note: The assembly geometry is the same as for the LSH BWR benchmark problem.

Table A2.1.1 describes all heterogeneous cross sections for the DEP1 BWR Benchmark Problem in the PDQ7 format, for a mask at burnups 20,000, 10,000, and 0 MWD/MT.

```
401000,01
401001,A54C
401100,0+0,0+0,0+0
401200,0+0,0+0,0+0
40110102,.19666+00,.96210-2,.98690-2,.22800-2,.26075+1, 0.3204-10
40120102,.64863+00,.84320-01,0.0,.51010-01,.25368+01,.3204-10
* FUNCTION TABLES FOR MATERIAL A (V=40%, BURNUP=5, CONTROLLED)
130010,4,02,1,1,2,1
130011,.19602+00,.19634+00,.19666+00
130020,4,02,1,2,2,1
130021,.65744+00,.65569+00,.64863+00
130030,4,02,2,1,2,0
130031,.10548-01,.10154-01,.96210-02
130040,4,02,2,2,2,0
130041,.84522-01,.85990-01,.84320-01
130050,4,02,3,1,2,0
130051,.95167-02,.96305-02,.98690-02
130060,4,02,3,2,2,0
130061,.0,.0,.0
130070,4,02,4,1,2,0
130071,.18354-02,.20320-02,.22800-02
130080,4,02,4,2,2,0
130081,.43828-01,.48057-01,.51010-01
130090,4,02,5,1,2,0
130091,.27123+01,.26624+01,.26075+01
130100,4,02,5,2,2,0
130101,.26946+01,.26263+01,.25368+01
```

```
402000,02
402001,B54C
402100,0+0,0+0,0+0
402200,0+0,0+0,0+0
40210102,.19771+00,.89950-02,.92000-02,.22560-02,.26011+01,.32040-10
40220102,.62881+00,.82180-01,.0+0,.50220-01,.25309+01,.32040-10
* FUNCTION TABLES FOR MATERIAL B (V=40%, BURNUP=5, CONTROLLED)
130110,4,02,1,1,2,1
130111,.19617+00,.19684+00,.19771+00
130120,4,02,1,2,2,1
130121,.64536+00,.64040+00,.62881+00
130130,4,02,2,1,2,0
130131,.99153-02,.95211-02,.89950-02
130140,4,02,2,2,2,0
130141,.84181-01,.84826-01,.82180-01
130150,4,02,3,1,2,0
130151,.86332-02,.88464-02,.92000-02
130160,4,02,3,2,2,0
130161,.0,.0,.0
130170,4,02,4,1,2,0
130171,.17447-02,.19696-02,.22560-02
130180,4,02,4,2,2,0
130181,.42741-01,.47026-01,.50220-01
130190,4,02,5,1,2,0
130191,.27272+01,.26671+01,.26011+01
130200,4,02,5,2,2,0
130201,.27187+01,.26362+01,.25309+01
```

Table A2.1.1 Heterogeneous cross sections for the DEP1 BWR Benchmark Problem.

Table A2.1.1 (continued)

```
403000,03
403001,C54C
403100,0+0,0+0,0+0
403200,0+0,0+0,0+0
40310102,.20020+00,.91140-02,.93720-02,.18840-02,.26327+01,.32040-10
40320102,.62941+00,.71120-01,.0,.40510-01,.25648+01,.32040-10
* FUNCTION TABLES FOR MATERIAL C (V=40%, BURNUP=5, CONTROLLED)
130210,4,02,1,1,2,1
130211,.19912+00,.19966+00,.20020+00
130220,4,02,1,2,2,1
130221,.63877+00,.63706+00,.62941+00
130230,4,02,2,1,2,0
130231,.10414-01,.98812-02,.91140-02
130240,4,02,2,2,2,0
130241,.70883-01,.72337-01,.71120-01
130250,4,02,3,1,2,0
130251,.89212-02,.90680-02,.93720-02
130260,4,02,3,2,2,0
130261,.0,.0,.0
130270,4,02,4,1,2,0
130271,.13984-02,.15856-02,.18840-02
130280,4,02,4,2,2,0
130281,.31313-01,.35859-01,.40510-01
130290,4,02,5,1,2,0
130291,.27911+01,.27245+01,.26327+01
130300,4,02,5,2,2,0
130301,.28054+01,.27079+01,.25648+01
```

```
404000,04
404001,D54C
404100,0+0,0+0,0+0
404200,0+0,0+0,0+0
40410102,.20288+00,.92450-02,.96420-02,.16460-02,.26580+01,.32040-10
40420102,.62598+00,.63070-01,.0,.33730-01,.25974+01,.32040-10
* FUNCTION TABLES FOR MATERIAL D (V=40%, BURNUP=5, CONTROLLED)
130310,4,02,1,1,2,1
130311,.20165+00,.20227+00,.20288+00
130320,4,02,1,2,2,1
130321,.63371+00,.63267+00,.62598+00
130330,4,02,2,1,2,0
130331,.10820-01,.10195-01,.92450-02
130340,4,02,2,2,2,0
130341,.64049-01,.64708-01,.63070-01
130350,4,02,3,1,2,0
130351,.92400-02,.93472-02,.96420-02
130360,4,02,3,2,2,0
130361,.0,.0,.0
130370,4,02,4,1,2,0
130371,.12520-02,.13805-02,.16460-02
130380,4,02,4,2,2,0
130381,.25938-01,.29369-01,.33730-01
130390,4,02,5,1,2,0
130391,.28202+01,.27618+01,.26580+01
130400,4,02,5,2,2,0
130401,.28504+01,.27644+01,.25974+01
```

Table A2.1.1 (continued)

```
405000,05
405001,E54C
405100,0+0,0+0,0+0
405200,0+0,0+0,0+0
40510102,.20730+00,.93490-02,.90850-02,.14030-02,.26828+01,.32040-10
40520102,.60584+00,.55090-01,.0,.27430-01,.26424+01,.32040-10
* FUNCTION TABLES FOR MATERIAL E (V=40%, BURNUP=5, CONTROLLED)
130410,4,02,1,1,2,1
130411,.20435+00,.20608+00,.20730+00
130420,4,02,1,2,2,1
130421,.60692+00,.61232+00,.60584+00
130430,4,02,2,1,2,0
130431,.11296-01,.10818-01,.93490-02
130440,4,02,2,2,2,0
130441,.55329-01,.57165-01,.55090-01
130450,4,02,3,1,2,0
130451,.89201-02,.87463-02,.90850-02
130460,4,02,3,2,2,0
130461,.0,.0,.0
130470,4,02,4,1,2,0
130471,.12680-02,.11160-02,.14030-02
130480,4,02,4,2,2,0
130481,.21717-01,.21991-01,.27430-01
130490,4,02,5,1,2,0
130491,.27235+01,.28309+01,.26828+01
130500,4,02,5,2,2,0
130501,.26948+01,.28725+01,.26424+01
```

```
406000,06
406001,G54C
406100,0+0,0+0,0+0
406200,0+0,0+0,0+0
40610102,.19677+00,.10300-01,.90600-02,.22060-02,.25834+01,.32040-10
40620102,.70472+00,.21210+00,.0,.38400-01,.25328+01,.32040-10
* FUNCTION TABLES FOR MATERIAL G (V=40%, BURNUP=5, CONTROLLED)
130510,4,02,1,1,2,1
130511,.19398+00,.19486+00,.19677+00
130520,4,02,1,2,2,1
130521,.63831+00,.64896+00,.70472+00
130530,4,02,2,1,2,0
130531,.10452-01,.10221-01,.10300-01
130540,4,02,2,2,2,0
130541,.80849-01,.10743+00,.21210+00
130550,4,02,3,1,2,0
130551,.83498-02,.85794-02,.90600-02
130560,4,02,3,2,2,0
130561,.0,.0,.0
130570,4,02,4,1,2,0
130571,.16679-02,.19034-02,.22060-02
130580,4,02,4,2,2,0
130581,.43944-01,.46284-01,.38400-01
130590,4,02,5,1,2,0
130591,.27219+01,.26582+01,.25834+01
130600,4,02,5,2,2,0
130601,.27121+01,.26411+01,.25328+01
```

Table A2.1.1 (continued)

```
407000,07
407001,A00NC
407100,0+0,0+0,0+0
407200,0+0,0+0,0+0
407101,02,.23557+00,.95800-02,.16820-01,.25850-02,.25625+01,.32040-10
407201,02,.90678+00,.80370-01,.0,.51860-01,.24238+01,.32040-10
* FUNCTION TABLES FOR MATERIAL A (V=0%, BURNUP=0, NON CONTROLLED)
130610,4,02,1,1,2,1
130611,.23471+00,.23516+00,.23557+00
130620,4,02,1,2,2,1
130621,.93397+00,.92701+00,.90678+00
130630,4,02,2,1,2,0
130631,.11058-01,.10419-01,.95800-02
130640,4,02,2,2,2,0
130641,.87939-01,.88187-01,.80370-01
130650,4,02,3,1,2,0
130651,.16208-01,.16391-01,.16820-01
130660,4,02,3,2,2,0
130661,.0,.0,.0
130670,4,02,4,1,2,0
130671,.19550-02,.22339-02,.25850-02
130680,4,02,4,2,2,0
130681,.45100-01,.50095-01,.51860-01
130690,4,02,5,1,2,0
130691,.27085+01,.26408+01,.25625+01
130700,4,02,5,2,2,0
130701,.26803+01,.25777+01,.24238+01
```

```
408000,08
408001,B00NC
408100,0+0,0+0,0+0
408200,0+0,0+0,0+0
408101,02,.23540+00,.92000-02,.16240-01,.25420-02,.25649+01,.32040-10
408201,02,.88676+00,.78270-01,.0,.50490-01,.24223+01,.32040-10
* FUNCTION TABLES FOR MATERIAL B (V=0%, BURNUP=0, NON CONTROLLED)
130710,4,02,1,1,2,1
130711,.23261+00,.23323+00,.23540+00
130720,4,02,1,2,2,1
130721,.92439+00,.91848+00,.88676+00
130730,4,02,2,1,2,0
130731,.10508-01,.99251-02,.92000-02
130740,4,02,2,2,2,0
130741,.87280-01,.89037-01,.78270-01
130750,4,02,3,1,2,0
130751,.15261-01,.15489-01,.16240-01
130760,4,02,3,2,2,0
130761,.0,.0,.0
130770,4,02,4,1,2,0
130771,.19368-02,.22060-02,.25420-02
130780,4,02,4,2,2,0
130781,.44546-01,.50333-01,.50490-01
130790,4,02,5,1,2,0
130791,.27123+01,.26479+01,.25649+01
130800,4,02,5,2,2,0
130801,.26828+01,.25901+01,.24223+01
```

Table A2.1.1 (continued)

```
409000,09
409001,COONC
409100,0+0,0+0,0+0
409200,0+0,0+0,0+0
409101,02,.23590+00,.90600-02,.17250-01,.22060-02,.25848+01,.32040-10
409201,02,.89993+00,.67110-01,.0,.40730-01,.24230+01,.32040-10
* FUNCTION TABLES FOR MATERIAL C (V=0%, BURNUP=0, NON CONTROLLED)
130810,4,02,1,1,2,1
130811,.23458+00,.23494+00,.23590+00
130820,4,02,1,2,2,1
130821,.92678+00,.92206+00,.89993+00
130830,4,02,2,1,2,0
130831,.10821-01,.10098-01,.90600-02
130840,4,02,2,2,2,0
130841,.74648-01,.75891-01,.67110-01
130850,4,02,3,1,2,0
130851,.16504-01,.16652-01,.17250-01
130860,4,02,3,2,2,0
130861,.0,.0,.0
130870,4,02,4,1,2,0
130871,.16560-02,.18884-02,.22060-02
130880,4,02,4,2,2,0
130881,.34405-01,.39557-01,.40730-01
130890,4,02,5,1,2,0
130891,.27550+01,.26832+01,.25848+01
130900,4,02,5,2,2,0
130901,.27375+01,.26256+01,.24230+01
```

```
410000,10
410001,DOONC
410100,0+0,0+0,0+0
410200,0+0,0+0,0+0
410101,02,.23810+00,.90000-02,.18150-01,.19500-02,.26021+01,.32040-10
410201,02,.89920+00,.57880-01,.0,.32910-01,.24236+01,.32040-10
* FUNCTION TABLES FOR MATERIAL D (V=0%, BURNUP=0, NON CONTROLLED)
130910,4,02,1,1,2,1
130911,.23657+00,.23693+00,.23810+00
130920,4,02,1,2,2,1
130921,.92498+00,.92180+00,.89920+00
130930,4,02,2,1,2,0
130931,.11143-01,.10316-01,.90000-02
130940,4,02,2,2,2,0
130941,.67020-01,.67821-01,.57880-01
130950,4,02,3,1,2,0
130951,.17448-01,.17528-01,.18150-01
130960,4,02,3,2,2,0
130961,.0,.0,.0
130970,4,02,4,1,2,0
130971,.14895-02,.16701-02,.19500-02
130980,4,02,4,2,2,0
130981,.28311-01,.32622-01,.32910-01
130990,4,02,5,1,2,0
130991,.27858+01,.27168+01,.26021+01
131000,4,02,5,2,2,0
131001,.27849+01,.26713+01,.24236+01
```

Table A2.1.1 (continued)

```
411000,11
411001,E00NC
411100,0+0,0+0,0+0
411200,0+0,0+0,0+0
411101,02,.23998+00,.90300-02,.19170-01,.17520-02,.26170+01,.32040-10
411201,02,.89993+00,.50610-01,.0,.26740-01,.24237+01,.32040-10
* FUNCTION TABLES FOR MATERIAL E (V=0%, BURNUP=0, NON CONTROLLED)
131010,4,02,1,1,2,1
131011,.23878+00,.23914+00,.23998+00
131020,4,02,1,2,2,1
131021,.92364+00,.92132+00,.89993+00
131030,4,02,2,1,2,0
131031,.11579-01,.10651-01,.90300-02
131040,4,02,2,2,2,0
131041,.60153-01,.60445-01,.50610-01
131050,4,02,3,1,2,0
131051,.18569-01,.18587-01,.19170-01
131060,4,02,3,2,2,0
131061,.0,.0,.0
131070,4,02,4,1,2,0
131071,.13532-02,.14915-02,.17520-02
131080,4,02,4,2,2,0
131081,.23083-01,.26562-01,.26740-01
131090,4,02,5,1,2,0
131091,.28100+01,.27474+01,.26170+01
131100,4,02,5,2,2,0
131101,.28270+01,.27147+01,.24237+01
```

```
412000,12
412001,G00NC
412100,0+0,0+0,0+0
412200,0+0,0+0,0+0
412101,02,.23708+00,.13860-01,.16070-01,.22930-02,.25573+01,.32040-10
412201,02,.12579+01,.45300+00,.0,.10720-01,.24244+01,.32040-10
* FUNCTION TABLES FOR MATERIAL G (V=0%, BURNUP=0, NON CONTROLLED)
131110,4,02,1,1,2,1
131111,.22976+00,.23159+00,.23708+00
131120,4,02,1,2,2,1
131121,.90834+00,.96017+00,.12579+01
131130,4,02,2,1,2,0
131131,.10926-01,.11253-01,.13860-01
131140,4,02,2,2,2,0
131141,.70775-01,.14938+00,.45300+00
131150,4,02,3,1,2,0
131151,.14661-01,.15032-01,.16070-01
131160,4,02,3,2,2,0
131161,.0,.0,.0
131170,4,02,4,1,2,0
131171,.17709-02,.20125-02,.22930-02
131180,4,02,4,2,2,0
131181,.46348-01,.42873-01,.10720-01
131190,4,02,5,1,2,0
131191,.27279+01,.26559+01,.25573+01
131200,4,02,5,2,2,0
131201,.26983+01,.26364+01,.24244+01
```

Table A2.1.1 (continued)

```
413000,13
413001,A14NC
413100,0+0,0+0,0+0
413200,0+0,0+0,0+0
413101,02,.19677+00,.99710-02,.95810-02,.20800-02,.26486+01,.32040-10
413201,02,.65359+00,.85730-01,.0,.48870-01,.26028+01,.32040-10
* FUNCTION TABLES FOR MATERIAL A (V=40%, BURNUP=10, NON CONTROLLED)
131210,4,02,1,1,2,1
131211,.19609+00,.19633+00,.19677+00
131220,4,02,1,2,2,1
131221,.65630+00,.65661+00,.65359+00
131230,4,02,2,1,2,0
131231,.10911-01,.10509-01,.99710-02
131240,4,02,2,2,2,0
131241,.80863-01,.83973-01,.85730-01
131250,4,02,3,1,2,0
131251,.93723-02,.94367-02,.95810-02
131260,4,02,3,2,2,0
131261,.0,.0,.0
131270,4,02,4,1,2,0
131271,.16170-02,.18141-02,.20800-02
131280,4,02,4,2,2,0
131281,.37921-01,.43259-01,.48870-01
131290,4,02,5,1,2,0
131291,.27698+01,.27140+01,.26486+01
131300,4,02,5,2,2,0
131301,.27731+01,.26984+01,.26028+01
```

```
414000,14
414001,B14NC
414100,0+0,0+0,0+0
414200,0+0,0+0,0+0
414101,02,.19482+00,.91910-02,.90260-02,.21080-02,.26428+01,.32040-10
414201,02,.64675+00,.85680-01,.0,.49640-01,.25907+01,.32040-10
* FUNCTION TABLES FOR MATERIAL B (V=40%, BURNUP=10, NON CONTROLLED)
131310,4,02,1,1,2,1
131311,.19389+00,.19435+00,.19482+00
131320,4,02,1,2,2,1
131321,.65234+00,.65198+00,.64675+00
131330,4,02,2,1,2,0
131331,.10056-01,.96872-02,.91910-02
131340,4,02,2,2,2,0
131341,.81279-01,.84639-01,.85680-01
131350,4,02,3,1,2,0
131351,.86965-02,.88108-02,.90260-02
131360,4,02,3,2,2,0
131361,.0,.0,.0
131370,4,02,4,1,2,0
131371,.16411-02,.18426-02,.21080-02
131380,4,02,4,2,2,0
131381,.38574-01,.44295-01,.49640-01
131390,4,02,5,1,2,0
131391,.27618+01,.27076+01,.26428+01
131400,4,02,5,2,2,0
131401,.27604+01,.26863+01,.25907+01
```

Table A2.1.1 (continued)

```
415000,15
415001,C14NC
415100,0+0,0+0,0+0
415200,0+0,0+0,0+0
415101,02,.19643+00,.95740-02,.98490-02,.17880-02,.26829+01,.32040-10
415201,02,.64876+00,.73430-01,.0,.39040-01,.26383+01,.32040-10
* FUNCTION TABLES FOR MATERIAL C (V=40%, BURNUP=10, NON CONTROLLED)
131410,4,02,1,1,2,1
131411,.19586+00,.19619+00,.19643+00
131420,4,02,1,2,2,1
131421,.65095+00,.65114+00,.64876+00
131430,4,02,2,1,2,0
131431,.10660-01,.10200-01,.95740-02
131440,4,02,2,2,2,0
131441,.69585-01,.71777-01,.73430-01
131450,4,02,3,1,2,0
131451,.96607-02,.97218-02,.98490-02
131460,4,02,3,2,2,0
131461,.0,.0,.0
131470,4,02,4,1,2,0
131471,.14256-02,.15655-02,.17880-02
131480,4,02,4,2,2,0
131481,.29707-01,.33870-01,.39040-01
131490,4,02,5,1,2,0
131491,.28017+01,.27536+01,.26829+01
131500,4,02,5,2,2,0
131501,.28166+01,.27424+01,.26383+01
```

```
416000,16
416001,D14NC
416100,0+0,0+0,0+0
416200,0+0,0+0,0+0
416101,02,.19818+00,.98500-02,.10470-01,.15890-02,.27149+01,.32040-10
416201,02,.64712+00,.65460-01,.0,.32410-01,.26779+01,.32040-10
* FUNCTION TABLES FOR MATERIAL D (V=40%, BURNUP=10, NON CONTROLLED)
131510,4,02,1,1,2,1
131511,.19760+00,.19806+00,.19818+00
131520,4,02,1,2,2,1
131521,.64928+00,.64913+00,.64712+00
131530,4,02,2,1,2,0
131531,.11113-01,.10583-01,.98500-02
131540,4,02,2,2,2,0
131541,.63756-01,.64630-01,.65460-01
131550,4,02,3,1,2,0
131551,.10330-01,.10371-01,.10470-01
131560,4,02,3,2,2,0
131561,.0,.0,.0
131570,4,02,4,1,2,0
131571,.13219-02,.14145-02,.15890-02
131580,4,02,4,2,2,0
131581,.25456-01,.28239-01,.32410-01
131590,4,02,5,1,2,0
131591,.28210+01,.27828+01,.27149+01
131600,4,02,5,2,2,0
131601,.28492+01,.27866+01,.26779+01
```

Table A2.1.1 (continued)

```
417000,17
417001,E14NC
417100,0+0,0+0,0+0
417200,0+0,0+0,0+0
417101,02,.19996+00,.10270-01,.11220-01,.14200-02,.27451+01,.32040-10
417201,02,.64625+00,.58250-01,.0,.26480-01,.27205+01,.32040-10
* FUNCTION TABLES FOR MATERIAL E (V=40%, BURNUP=10, NON CONTROLLED)
131610,4,02,1,1,2,1
131611,.19940+00,.19985+00,.19996+00
131620,4,02,1,2,2,1
131621,.64799+00,.64748+00,.64625+00
131630,4,02,2,1,2,0
131631,.11662-01,.11087-01,.10270-01
131640,4,02,2,2,2,0
131641,.58048-01,.57933-01,.58250-01
131650,4,02,3,1,2,0
131651,.11132-01,.11171-01,.11220-01
131660,4,02,3,2,2,0
131661,.0,.0,.0
131670,4,02,4,1,2,0
131671,.12339-02,.12890-02,.14200-02
131680,4,02,4,2,2,0
131681,.21511-01,.23181-01,.26480-01
131690,4,02,5,1,2,0
131691,.28334+01,.28049+01,.27451+01
131700,4,02,5,2,2,0
131701,.28742+01,.28250+01,.27205+01
```

```
418000,18
418001,G14NC
418100,0+0,0+0,0+0
418200,0+0,0+0,0+0
418101,02,.19223+00,.95920-02,.87700-02,.20970-02,.26218+01,.32040-10
418201,02,.64712+00,.96630-01,.0,.51090-01,.25719+01,.32040-10
* FUNCTION TABLES FOR MATERIAL G (V=40%, BURNUP=10, NON CONTROLLED)
131710,4,02,1,1,2,1
131711,.19119+00,.19164+00,.19223+00
131720,4,02,1,2,2,1
131721,.65308+00,.65170+00,.64712+00
131730,4,02,2,1,2,0
131731,.10449-01,.10108-01,.95920-02
131740,4,02,2,2,2,0
131741,.88450-01,.91139-01,.96630-01
131750,4,02,3,1,2,0
131751,.83780-02,.85123-02,.87700-02
131760,4,02,3,2,2,0
131761,.0,.0,.0
131770,4,02,4,1,2,0
131771,.16009-02,.18109-02,.20970-02
131780,4,02,4,2,2,0
131781,.40468-01,.46518-01,.51090-01
131790,4,02,5,1,2,0
131791,.27444+01,.26892+01,.26218+01
131800,4,02,5,2,2,0
131801,.27429+01,.26684+01,.25719+01
```

Table A2.1.1 (continued)

```
419000,19
419001,A57NC
419100,0+0,0+0,0+0
419200,0+0,0+0,0+0
419101,02,.16793+00,.89130-02,.49640-02,.21460-02,.26025+01,.32040-10
419201,02,.44749+00,.80970-01,.0,.49800-01,.25402+01,.32040-10
* FUNCTION TABLES FOR MATERIAL A (V=70%, BURNUP=5, NON CONTROLLED)
131810,4,02,1,1,2,1
131811,.16740+00,.16752+00,.16793+00
131820,4,02,1,2,2,1
131821,.45178+00,.45450+00,.44749+00
131830,4,02,2,1,2,0
131831,.98433-02,.94718-02,.89130-02
131840,4,02,2,2,2,0
131841,.78693-01,.83153-01,.80970-01
131850,4,02,3,1,2,0
131851,.47136-02,.47386-02,.49640-02
131860,4,02,3,2,2,0
131861,.0,.0,.0
131870,4,02,4,1,2,0
131871,.15980-02,.18272-02,.21460-02
131880,4,02,4,2,2,0
131881,.39115-01,.45911-01,.49800-01
131890,4,02,5,1,2,0
131891,.27363+01,.26786+01,.26025+01
131900,4,02,5,2,2,0
131901,.27417+01,.26580+01,.25402+01
```

```
420000,20
420001,B57NC
420100,0+0,0+0,0+0
420200,0+0,0+0,0+0
420101,02,.16625+00,.80600-02,.47180-02,.21360-02,.26021+01,.32040-10
420201,02,.44144+00,.79580-01,.0,.49410-01,.25319+01,.32040-10
* FUNCTION TABLES FOR MATERIAL B (V=70%, BURNUP=5, NON CONTROLLED)
131910,4,02,1,1,2,1
131911,.16570+00,.16524+00,.16625+00
131920,4,02,1,2,2,1
131921,.43572+00,.45802+00,.44144+00
131930,4,02,2,1,2,0
131931,.88247-02,.85275-02,.80600-02
131940,4,02,2,2,2,0
131941,.77517-01,.83589-01,.79580-01
131950,4,02,3,1,2,0
131951,.44180-02,.44144-02,.47180-02
131960,4,02,3,2,2,0
131961,.0,.0,.0
131970,4,02,4,1,2,0
131971,.16241-02,.18360-02,.21360-02
131980,4,02,4,2,2,0
131981,.39009-01,.46608-01,.49410-01
131990,4,02,5,1,2,0
131991,.27256+01,.26759+01,.26021+01
132000,4,02,5,2,2,0
132001,.27240+01,.26500+01,.25319+01
```

Table A2.1.1 (continued)

```
421000,21
421001,C57NC
421100,0+0,0+0,0+0
421200,0+0,0+0,0+0
421101,02,.16750+00,.84940-02,.52010-02,.18420-02,.26325+01,.32040-10
421201,02,.44303+00,.69400-01,.0,.40280-01,.25645+01,.32040-10
* FUNCTION TABLES FOR MATERIAL C (V=70%, BURNUP=5, NON CONTROLLED)
132010,4,02,1,1,2,1
132011,.16729+00,.16703+00,.16750+00
132020,4,02,1,2,2,1
132021,.44594+00,.44919+00,.44303+00
132030,4,02,2,1,2,0
132031,.95691-02,.91415-02,.84940-02
132040,4,02,2,2,2,0
132041,.67048-01,.71240-01,.69400-01
132050,4,02,3,1,2,0
132051,.49702-02,.49678-02,.52010-02
132060,4,02,3,2,2,0
132061,.0,.0,.0
132070,4,02,4,1,2,0
132071,.14068-02,.15747-02,.18420-02
132080,4,02,4,2,2,0
132081,.30625-01,.36548-01,.40280-01
132090,4,02,5,1,2,0
132091,.27663+01,.27162+01,.26325+01
132100,4,02,5,2,2,0
132101,.27764+01,.26966+01,.25645+01
```

```
422000,22
422001,D57NC
422100,0+0,0+0,0+0
422200,0+0,0+0,0+0
422101,02,.16903+00,.87710-02,.55620-02,.16320-02,.26581+01,.32040-10
422201,02,.44074+00,.61700-01,.0,.33690-01,.25960+01,.32040-10
* FUNCTION TABLES FOR MATERIAL D (V=70%, BURNUP=5, NON CONTROLLED)
132110,4,02,1,1,2,1
132111,.16883+00,.16867+00,.16903+00
132120,4,02,1,2,2,1
132121,.44330+00,.44594+00,.44074+00
132130,4,02,2,1,2,0
132131,.10061-01,.95759-02,.87710-02
132140,4,02,2,2,2,0
132141,.60770-01,.63767-01,.61700-01
132150,4,02,3,1,2,0
132151,.53797-02,.53536-02,.55620-02
132160,4,02,3,2,2,0
132161,.0,.0,.0
132170,4,02,4,1,2,0
132171,.12850-02,.14114-02,.16320-02
132180,4,02,4,2,2,0
132181,.25875-01,.30477-01,.33690-01
132190,4,02,5,1,2,0
132191,.27912+01,.27461+01,.26581+01
132200,4,02,5,2,2,0
132201,.28103+01,.27405+01,.25960+01
```

Table A2.1.1 (continued)

```
423000,23
423001,E57NC
423100,0+0,0+0,0+0
423200,0+0,0+0,0+0
423101,02,.17033+00,.92300-02,.60260-02,.14630-02,.26863+01,.32040-10
423201,02,.43975+00,.55150-01,.0,.28060-01,.26311+01,.32040-10
* FUNCTION TABLES FOR MATERIAL E (V=70%, BURNUP=5, NON CONTROLLED)
132210,4,02,1,1,2,1
132211,.17029+00,.17022+00,.17033+00
132220,4,02,1,2,2,1
132221,.44171+00,.44333+00,.43975+00
132230,4,02,2,1,2,0
132231,.10687-01,.10145-01,.92300-02
132240,4,02,2,2,2,0
132241,.55292-01,.56739-01,.55150-01
132250,4,02,3,1,2,0
132251,.58828-02,.58561-02,.60260-02
132260,4,02,3,2,2,0
132261,.0,.0,.0
132270,4,02,4,1,2,0
132271,.11949-02,.12751-02,.14630-02
132280,4,02,4,2,2,0
132281,.21956-01,.25035-01,.28060-01
132290,4,02,5,1,2,0
132291,.28060+01,.27757+01,.26863+01
132300,4,02,5,2,2,0
132301,.28377+01,.27796+01,.26311+01
```

```
424000,24
424001,G57NC
424100,0+0,0+0,0+0
424200,0+0,0+0,0+0
424101,02,.16420+00,.91860-02,.45960-02,.20840-02,.25864+01,.32040-10
424201,02,.52116+00,.20980+00,.0,.38340-01,.25329+01,.32040-10
* FUNCTION TABLES FOR MATERIAL G (V=70%, BURNUP=5, NON CONTROLLED)
132310,4,02,1,1,2,1
132311,.16229+00,.16283+00,.16420+00
132320,4,02,1,2,2,1
132321,.45086+00,.46090+00,.52116+00
132330,4,02,2,1,2,0
132331,.92380-02,.90445-02,.91860-02
132340,4,02,2,2,2,0
132341,.10477+00,.17134+00,.20980+00
132350,4,02,3,1,2,0
132351,.41254-02,.42779-02,.45960-02
132360,4,02,3,2,2,0
132361,.0,.0,.0
132370,4,02,4,1,2,0
132371,.15685-02,.17938-02,.20840-02
132380,4,02,4,2,2,0
132381,.43144-01,.46060-01,.38340-01
132390,4,02,5,1,2,0
132391,.27243+01,.26613+01,.25864+01
132400,4,02,5,2,2,0
132401,.27181+01,.26429+01,.25329+01
```

Table A2.1.1 (continued)

```
425000,25
425001,A10C
425100,0+0,0+0,0+0
425200,0+0,0+0,0+0
425101,02,.23392+00,.10550-01,.16410-01,.21920-02,.26551+01,.32040-10
425201,02,.93058+00,.88840-01,.0,.49480-01,.26011+01,.32040-10
* FUNCTION TABLES FOR MATERIAL A (V=0%, BURNUP=10, CONTROLLED)
132410,4,02,1,1,2,1
132411,.23300+00,.23346+00,.23392+00
132420,4,02,1,2,2,1
132421,.93489+00,.93376+00,.93058+00
132430,4,02,2,1,2,0
132431,.11401-01,.11025-01,.10550-01
132440,4,02,2,2,2,0
132441,.85242-01,.87369-01,.88840-01
132450,4,02,3,1,2,0
132451,.16189-01,.16273-01,.16410-01
132460,4,02,3,2,2,0
132461,.0,.0,.0
132470,4,02,4,1,2,0
132471,.18142-02,.19829-02,.21920-02
132480,4,02,4,2,2,0
132481,.40824-01,.45040-01,.49480-01
132490,4,02,5,1,2,0
132491,.27493+01,.27048+01,.26551+01
132500,4,02,5,2,2,0
132501,.27342+01,.26714+01,.26011+01
```

```
426000,26
426001,B10C
426100,0+0,0+0,0+0
426200,0+0,0+0,0+0
426101,02,.23491+00,.10020-01,.15570-01,.22110-02,.26445+01,.32040-10
426201,02,.91075+00,.88810-01,.0,.50390-01,.25878+01,.32040-10
* FUNCTION TABLES FOR MATERIAL B (V=0%, BURNUP=10, CONTROLLED)
132510,4,02,1,1,2,1
132511,.23351+00,.23413+00,.23491+00
132520,4,02,1,2,2,1
132521,.91888+00,.91699+00,.91075+00
132530,4,02,2,1,2,0
132531,.10945-01,.10557-01,.10020-01
132540,4,02,2,2,2,0
132541,.85303-01,.87990-01,.88810-01
132550,4,02,3,1,2,0
132551,.15172-01,.15314-01,.15570-01
132560,4,02,3,2,2,0
132561,.0,.0,.0
132570,4,02,4,1,2,0
132571,.17623-02,.19579-02,.22110-02
132580,4,02,4,2,2,0
132581,.40414-01,.45518-01,.50390-01
132590,4,02,5,1,2,0
132591,.27565+01,.27045+01,.26445+01
132600,4,02,5,2,2,0
132601,.27468+01,.26759+01,.25878+01
```

Table A2.1.1 (continued)

```
427000,27
427001,C10C
427100,0+0,0+0,0+0
427200,0+0,0+0,0+0
427101,02,.23827+00,.10160-01,.15980-01,.18350-02,.26834+01,.32040-10
427201,02,.90728+00,.75980-01,.0,.39450-01,.26362+01,.32040-10
* FUNCTION TABLES FOR MATERIAL C (V=0%, BURNUP=10, CONTROLLED)
132610,4,02,1,1,2,1
132611,.23684+00,.23767+00,.23827+00
132620,4,02,1,2,2,1
132621,.91139+00,.91129+00,.90728+00
132630,4,02,2,1,2,0
132631,.11403-01,.10910-01,.10160-01
132640,4,02,2,2,2,0
132641,.71798-01,.74396-01,.75980-01
132650,4,02,3,1,2,0
132651,.15723-01,.15793-01,.15980-01
132660,4,02,3,2,2,0
132661,.0,.0,.0
132670,4,02,4,1,2,0
132671,.14393-02,.15803-02,.18350-02
132680,4,02,4,2,2,0
132681,.29261-01,.33772-01,.39450-01
132690,4,02,5,1,2,0
132691,.28130+01,.27642+01,.26834+01
132700,4,02,5,2,2,0
132701,.28277+01,.27568+01,.26362+01
```

```
428000,28
428001,D10C
428100,0+0,0+0,0+0
428200,0+0,0+0,0+0
428101,02,.24155+00,.10310-01,.16440-01,.16080-02,.27139+01,.32040-10
428201,02,.90139+00,.67710-01,.0,.32660-01,.26791+01,.32040-10
* FUNCTION TABLES FOR MATERIAL D (V=0%, BURNUP=10, CONTROLLED)
132710,4,02,1,1,2,1
132711,.23981+00,.24083+00,.24155+00
132720,4,02,1,2,2,1
132721,.90506+00,.90511+00,.90139+00
132730,4,02,2,1,2,0
132731,.11805-01,.11236-01,.10310-01
132740,4,02,2,2,2,0
132741,.65789-01,.66966-01,.67710-01
132750,4,02,3,1,2,0
132751,.16226-01,.16282-01,.16440-01
132760,4,02,3,2,2,0
132761,.0,.0,.0
132770,4,02,4,1,2,0
132771,.13247-02,.13947-02,.16080-02
132780,4,02,4,2,2,0
132781,.24859-01,.27673-01,.32660-01
132790,4,02,5,1,2,0
132791,.28264+01,.27998+01,.27139+01
132800,4,02,5,2,2,0
132801,.28531+01,.28131+01,.26791+01
```

Table A2.1.1 (continued)

```
429000,29
429001,E10C
429100,0+0,0+0,0+0
429200,0+0,0+0,0+0
429101,02,.24728+00,.10460-01,.15910-01,.13760-02,.27420+01,.32040-10
429201,02,.87443+00,.59370-01,.0,.26300-01,.27281+01,.32040-10
* FUNCTION TABLES FOR MATERIAL E (V=0%, BURNUP=10, CONTROLLED)
132810,4,02,1,1,2,1
132811,.24301+00,.24564+00,.24728+00
132820,4,02,1,2,2,1
132821,.87283+00,.87835+00,.87443+00
132830,4,02,2,1,2,0
132831,.12128-01,.11913-01,.10460-01
132840,4,02,2,2,2,0
132841,.61398-01,.59654-01,.59370-01
132850,4,02,3,1,2,0
132851,.15661-01,.15727-01,.15910-01
132860,4,02,3,2,2,0
132861,.0,.0,.0
132870,4,02,4,1,2,0
132871,.14906-02,.11958-02,.13760-02
132880,4,02,4,2,2,0
132881,.25678-01,.21440-01,.26300-01
132890,4,02,5,1,2,0
132891,.26860+01,.28324+01,.27420+01
132900,4,02,5,2,2,0
132901,.26040+01,.28696+01,.27281+01
```

```
430000,30
430001,G10C
430100,0+0,0+0,0+0
430200,0+0,0+0,0+0
430101,02,.23343+00,.10490-01,.15330-01,.21960-02,.26211+01,.32040-10
430201,02,.90752+00,.99890-01,.0,.51640-01,.25697+01,.32040-10
* FUNCTION TABLES FOR MATERIAL G (V=0%, BURNUP=10, CONTROLLED)
132910,4,02,1,1,2,1
132911,.23195+00,.23260+00,.23343+00
132920,4,02,1,2,2,1
132921,.91578+00,.91337+00,.90752+00
132930,4,02,2,1,2,0
132931,.11459-01,.11075-01,.10490-01
132940,4,02,2,2,2,0
132941,.91179-01,.94118-01,.99890-01
132950,4,02,3,1,2,0
132951,.14838-01,.14993-01,.15330-01
132960,4,02,3,2,2,0
132961,.0,.0,.0
132970,4,02,4,1,2,0
132971,.16970-02,.19135-02,.21960-02
132980,4,02,4,2,2,0
132981,.41433-01,.47157-01,.51640-01
132990,4,02,5,1,2,0
132991,.27408+01,.26853+01,.26211+01
133000,4,02,5,2,2,0
133001,.27326+01,.26615+01,.25697+01
```

A2.2 THE DEP2 BWR BENCHMARK

$J_{in}=0$

	W	W	W	W	W	
	E=0 V=40% Θ=0	E=0 V=40% Θ=0	E=0 V=40% Θ=0	W	W	
$J_{\perp N}=0$	E=10 V=70% Θ=0	E=10 V=70% Θ=0	E=0 V=40% Θ=0 H	E=0 V=40% Θ=0 I	W	$J_{in}=0$
	E=10 V=70% Θ=0	E=10 V=70% Θ=0 E	E=10 V=70% Θ=0 F	E=0 V=40% Θ=0 G	W	
	E=10 V=40% Θ=0 A	E=10 V=70% Θ=0 B	E=10 V=70% Θ=0 C	E=0 V=40% Θ=0 D	W	

$J_{\perp N}=0$

E = B.O.L. average exposure.

V = void fraction (constant throughout life).

θ = rotation angle (clockwise; equal to 0 in initial position).

Total Power = 0.197606 MW/cm height.

Depletion Time = 10,000 hours.

Fig. A2.2.1 Core layout for the first cycle of the DEP2 BWR Benchmark.

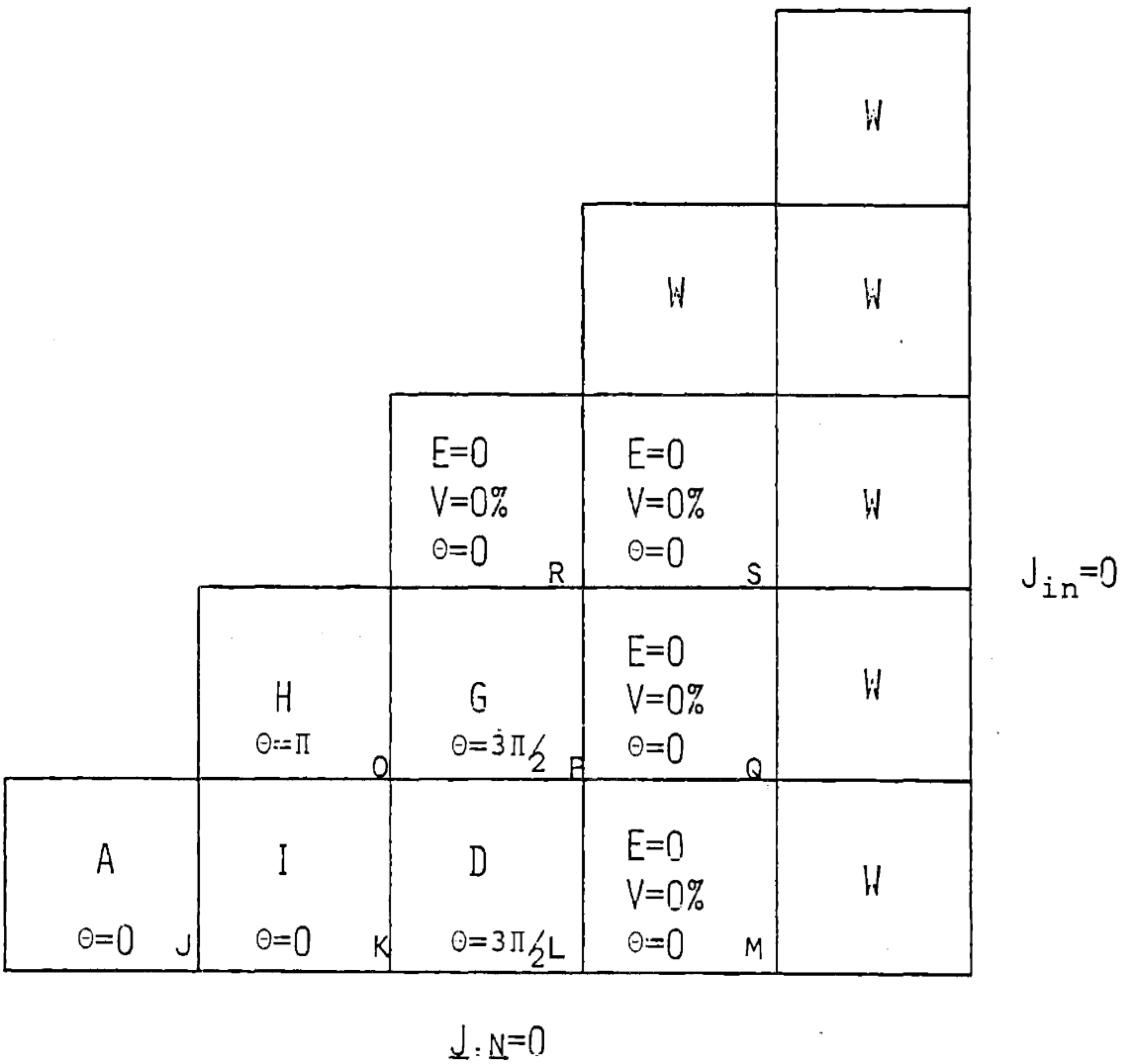

Assemblies described by letters (A, D, G, H, I) have been depleted in the first cycle.

Total Power = 0.197606 MW/cm height.

Depletion Time = 10,000 hours.

Fig. A2.2.2 Core layout for the second cycle of the DEP2 BWR Benchmark.

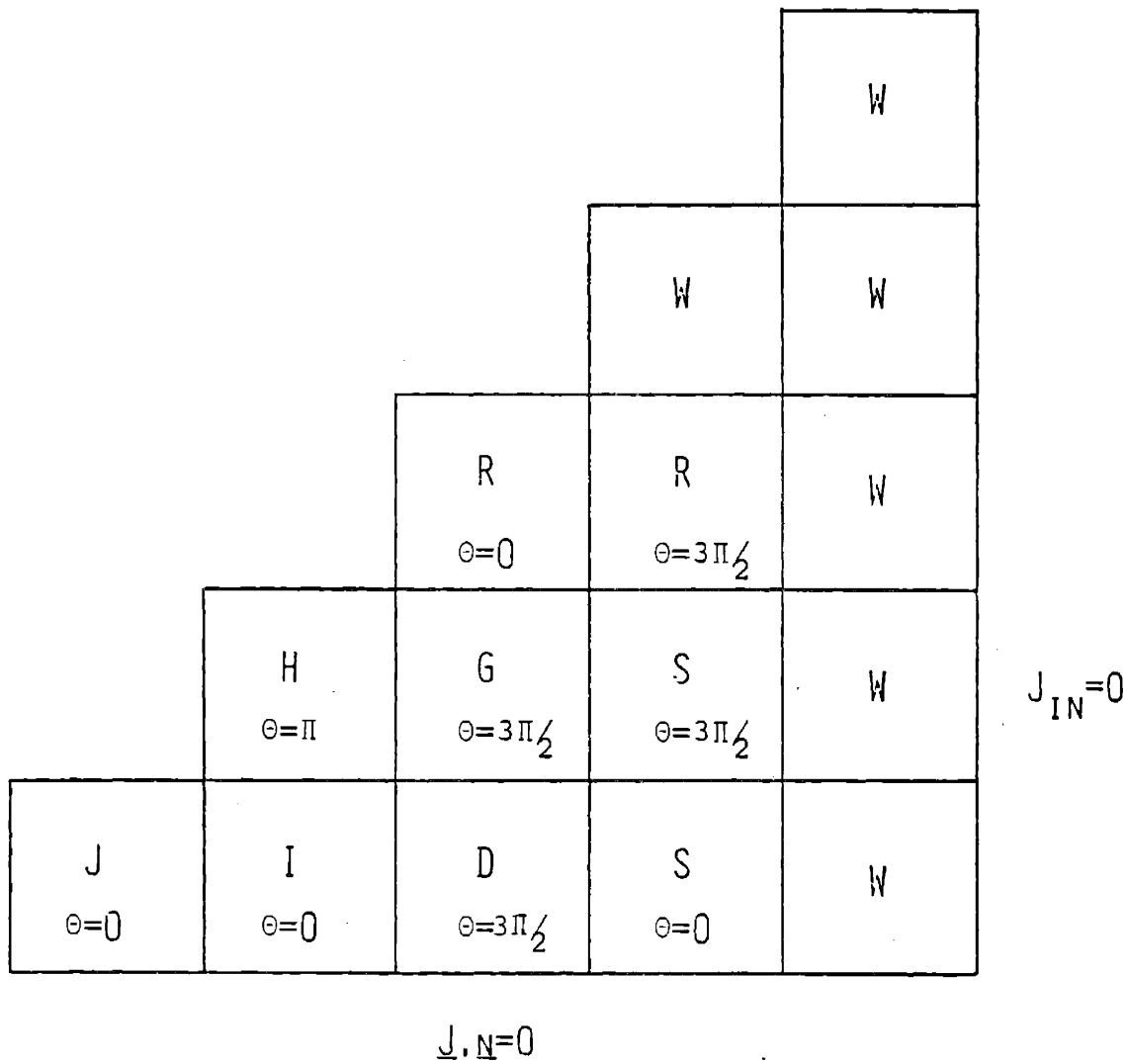

All assemblies come either from the end of the first cycle (D, G, H, I) or from the end of the second cycle (J, R, S).

Fig. A2.2.3 Core layout for the third cycle of the DEP2 BWR Benchmark.

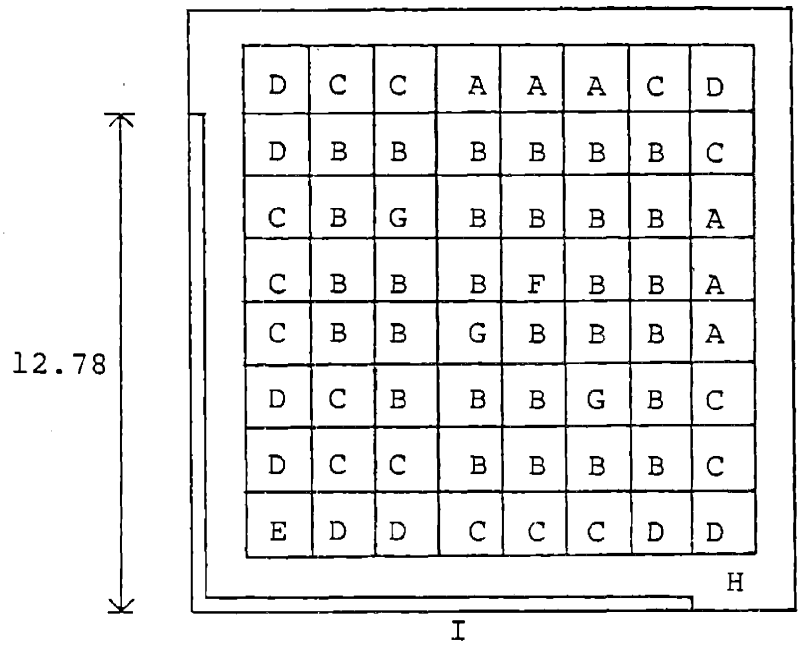

Note: Except for the dimension indicated, all properties are the same as for the assemblies of the LSH BWR Benchmark.

Fig. A2.2.4 Assembly description for the DEP2 Benchmark.

	ASSEMBLY				
	E=10	E=10	E=0	E=0	REFLECTOR
ZONE	V=40% (controlled)	V=70%	V=40%	V=0%	
A	1	10	18	27	26
B	2	11	19	28	26
C	3	12	20	29	26
D	4	13	21	30	26
E	5	14	22	31	26
F	6	15	23	32	26
G	7	16	24	33	26
H	8	17	25	34	26
I	9	17	25	34	26

Table A2.2.1 Material positions for assemblies of the DEP2 Benchmark.

Table A2.2.2 Heterogeneous cross sections for the DEP2 BWR Benchmark at burnup = 0.

COMPOSITION	GROUP	DIFFUSION COEFFICIENT	ABSORPTION CROSS-SECTION	REMOVAL CROSS-SECTION	NU-FISSION CROSS-SECTION	FISSION CROSS-SECTION
1	1	1.69650E+00	1.00330E-02	9.68360E-03	5.53826E-03	2.09078E-03
	2	5.09440E-01	8.58602E-02	0.0	1.27471E-01	4.89434E-02
2	1	1.69210E+00	9.29696E-03	8.93505E-03	5.52626E-03	2.09415E-03
	2	5.21717E-01	8.52809E-02	0.0	1.28286E-01	4.94623E-02
3	1	1.66796E+00	9.51737E-03	9.15521E-03	4.64103E-03	1.73274E-03
	2	5.24600E-01	7.31272E-02	0.0	1.03122E-01	3.90269E-02
4	1	1.64590E+00	9.70867E-03	9.44093E-03	4.10598E-03	1.51600E-03
	2	5.28302E-01	6.50874E-02	0.0	8.69670E-02	3.24070E-02
5	1	1.61159E+00	9.81442E-03	8.90403E-03	3.53208E-03	1.28983E-03
	2	5.46608E-01	5.68254E-02	0.0	7.14367E-02	2.61436E-02
6	1	1.97258E+00	3.89766E-04	1.87512E-02	0.0	0.0
	2	3.98052E-01	6.74359E-03	0.0	0.0	0.0
7	1	1.70827E+00	9.79361E-03	8.74182E-03	5.47473E-03	2.09207E-03
	2	5.23160E-01	9.52183E-02	0.0	1.30173E-01	5.05322E-02
8	1	1.61264E+00	5.67930E-04	2.21935E-02	0.0	0.0
	2	3.44296E-01	7.98029E-03	0.0	0.0	0.0
9	1	1.16838E+00	7.85783E-02	4.55109E-04	0.0	0.0
	2	2.01085E-01	9.79095E-01	0.0	0.0	0.0
10	1	1.98800E+00	9.23400E-03	4.81900E-03	5.19600E-03	1.96500E-03
	2	7.36800E-01	8.29600E-02	0.0	1.25400E-01	4.80900E-02

Table A2.2.2 (continued)

COMPOSITION	GROUP	DIFFUSION COEFFICIENT	ABSORPTION CROSS-SECTION	REMOVAL CROSS-SECTION	NU-FISSION CROSS-SECTION	FISSION CROSS-SECTION
11	1	2.01300E+00	8.30100E-03	4.53700E-03	5.23500E-03	1.98400E-03
	2	7.42100E-01	8.27200E-02	0.0	1.26300E-01	4.86900E-02
12	1	1.99400E+00	8.86200E-03	5.04900E-03	4.52500E-03	1.68900E-03
	2	7.45000E-01	7.11200E-02	0.0	1.01900E-01	3.85900E-02
13	1	1.97500E+00	9.23500E-03	5.42300E-03	4.07300E-03	1.50400E-03
	2	7.50000E-01	6.34200E-02	0.0	8.62400E-02	3.21700E-02
14	1	1.95800E+00	9.78600E-03	5.90700E-03	3.68700E-03	1.34500E-03
	2	7.53500E-01	5.64100E-02	0.0	7.18400E-02	2.63800E-02
15	1	2.43000E+00	3.30000E-04	1.33300E-02	0.0	0.0
	2	5.18500E-01	5.20500E-03	0.0	0.0	0.0
16	1	2.04600E+00	8.69300E-03	4.39800E-03	5.18400E-03	1.97900E-03
	2	7.38100E-01	9.28700E-02	0.0	1.29000E-01	5.00700E-02
17	1	1.67000E+00	5.20000E-04	2.47100E-02	0.0	0.0
	2	3.34800E-01	8.11600E-03	0.0	0.0	0.0
18	1	1.68800E+00	9.12900E-03	1.00000E-02	6.34000E-03	2.48000E-03
	2	5.26200E-01	7.61800E-02	0.0	1.22100E-01	5.04100E-02
19	1	1.69600E+00	8.56200E-03	9.56500E-03	6.21400E-03	2.42700E-03
	2	5.37400E-01	7.39200E-02	0.0	1.18500E-01	4.88900E-02
20	1	1.68800E+00	8.61000E-03	1.03500E-02	5.46600E-03	2.12000E-03
	2	5.30500E-01	6.35800E-02	0.0	9.63600E-02	3.97700E-02

Table A2.2.2 (continued)

COMPOSITION	GROUP	DIFFUSION COEFFICIENT	ABSORPTION CROSS-SECTION	REMOVAL CROSS-SECTION	NU-FISSION CROSS-SECTION	FISSION CROSS-SECTION
21	1	1.67400E+00	8.62300E-03	1.09700E-02	4.85600E-03	1.87200E-03
	2	5.31700E-01	5.47500E-02	0.0	7.81700E-02	3.22600E-02
22	1	1.66000E+00	8.74000E-03	1.17000E-02	4.38700E-03	1.68100E-03
	2	5.31200E-01	4.78100E-02	0.0	6.37800E-02	2.63200E-02
23	1	1.97100E+00	3.88600E-04	1.94300E-02	0.0	0.0
	2	4.07500E-01	6.60200E-03	0.0	0.0	0.0
24	1	1.69500E+00	1.29400E-02	9.34500E-03	5.60700E-03	2.19300E-03
	2	3.56900E-01	4.43000E-01	0.0	2.73900E-02	1.13100E-02
25	1	1.60700E+00	5.44200E-04	2.77900E-02	0.0	0.0
	2	3.15600E-01	8.57700E-03	0.0	0.0	0.0
26	1	2.01000E+00	5.27000E-04	3.51600E-02	0.0	0.0
	2	3.25900E-01	9.96300E-03	0.0	0.0	0.0
27	1	1.41500E+00	9.58000E-03	1.68200E-02	6.62400E-03	2.58500E-03
	2	3.67600E-01	8.03700E-02	0.0	1.25700E-01	5.18600E-02
28	1	1.41600E+00	9.20000E-03	1.62400E-02	6.52000E-03	2.54200E-03
	2	3.75900E-01	7.82700E-02	0.0	1.22300E-01	5.04900E-02
29	1	1.41300E+00	9.06000E-03	1.72500E-02	5.70200E-03	2.20600E-03
	2	3.70400E-01	6.71100E-02	0.0	9.86900E-02	4.07300E-02
30	1	1.40000E+00	9.00000E-03	1.81500E-02	5.07400E-03	1.95000E-03
	2	3.70700E-01	5.78800E-02	0.0	7.97600E-02	3.29100E-02

Table A2.2.2 (continued)

COMPOSITION	GROUP	DIFFUSION COEFFICIENT	ABSORPTION CROSS-SECTION	REMOVAL CROSS-SECTION	NU-FISSION CROSS-SECTION	FISSION CROSS-SECTION
31	1	1.38900E+00	9.03000E-03	1.91700E-02	4.58500E-03	1.75200E-03
	2	3.70400E-01	5.06100E-02	0.0	6.48100E-02	2.67400E-02
32	1	1.58100E+00	4.60000E-04	2.74500E-02	0.0	0.0
	2	3.08300E-01	8.67800E-03	0.0	0.0	0.0
33	1	1.40600E+00	1.38600E-02	1.60700E-02	5.86400E-03	2.29300E-03
	2	2.65000E-01	4.53000E-01	0.0	2.59900E-02	1.07200E-02
34	1	1.52800E+00	5.70000E-04	3.08200E-02	0.0	0.0
	2	2.93300E-01	9.19000E-03	0.0	0.0	0.0

$\chi_1 = 1.0$

$\chi_2 = 0.0$

Table A2.2.3 Heterogeneous cross sections for the DEP2 BWR Benchmark at burnup = 10,000 MWD/MT.

COMPOSITION	GROUP	DIFFUSION COEFFICIENT	ABSORPTION CROSS-SECTION	REMOVAL CROSS-SECTION	NU-FISSION CROSS-SECTION	FISSION CROSS-SECTION
1	1	1.69949E+00	1.04481E-02	9.55512E-03	5.08483E-03	1.88382E-03
	2	5.07565E-01	8.47012E-02	0.0	1.19754E-01	4.47393E-02
2	1	1.69682E+00	9.74520E-03	8.71517E-03	4.97773E-03	1.84322E-03
	2	5.17614E-01	8.49371E-02	0.0	1.20531E-01	4.49302E-02
3	1	1.67165E+00	1.01467E-02	8.98217E-03	4.10233E-03	1.48697E-03
	2	5.22065E-01	7.19403E-02	0.0	9.30803E-02	3.37377E-02
4	1	1.64958E+00	1.04903E-02	9.28885E-03	3.66426E-03	1.31159E-03
	2	5.26098E-01	6.46132E-02	0.0	7.81461E-02	2.77985E-02
5	1	1.62018E+00	1.10246E-02	8.73378E-03	3.14495E-03	1.11032E-03
	2	5.44411E-01	5.72176E-02	0.0	6.19040E-02	2.15358E-02
6	1	1.97258E+00	3.89766E-04	1.87512E-02	0.0	0.0
	2	3.98052E-01	6.74359E-03	0.0	0.0	0.0
7	1	1.71390E+00	1.02729E-02	8.47611E-03	4.86108E-03	1.81197E-03
	2	5.19663E-01	9.04753E-02	0.0	1.23939E-01	4.64516E-02
8	1	1.61264E+00	5.67930E-04	2.21935E-02	0.0	0.0
	2	3.44296E-01	7.98029E-03	0.0	0.0	0.0
9	1	1.16838E+00	7.85783E-02	4.55109E-04	0.0	0.0
	2	2.01085E-01	9.79095E-01	0.0	0.0	0.0
10	1	1.99092E+00	9.69238E-03	4.70194E-03	4.59540E-03	1.69408E-03
	2	7.33908E-01	8.15497E-02	0.0	1.15339E-01	4.26184E-02

Table A2.2.3 (continued)

COMPOSITION	GROUP	DIFFUSION COEFFICIENT	ABSORPTION CROSS-SECTION	REMOVAL CROSS-SECTION	NU-FISSION CROSS-SECTION	FISSION CROSS-SECTION
11	1	2.01709E+00	8.68922E-03	4.37525E-03	4.66420E-03	1.72517E-03
	2	7.36451E-01	8.20693E-02	0.0	1.17477E-01	4.36775E-02
12	1	1.99495E+00	9.39273E-03	4.94200E-03	4.05144E-03	1.47423E-03
	2	7.43105E-01	6.97220E-02	0.0	9.24223E-02	3.36680E-02
13	1	1.97595E+00	9.86924E-03	5.34061E-03	3.70210E-03	1.33323E-03
	2	7.48314E-01	6.27581E-02	0.0	7.85777E-02	2.81922E-02
14	1	1.95787E+00	1.04852E-02	5.85314E-03	3.41224E-03	1.21854E-03
	2	7.52636E-01	5.61833E-02	0.0	6.56986E-02	2.32702E-02
15	1	2.43000E+00	3.30000E-04	1.33300E-02	0.0	0.0
	2	5.18500E-01	5.20500E-03	0.0	0.0	0.0
16	1	2.05033E+00	9.08979E-03	4.20849E-03	4.58488E-03	1.70756E-03
	2	7.34126E-01	8.83240E-02	0.0	1.22702E-01	4.59460E-02
17	1	1.67000E+00	5.20000E-04	2.47100E-02	0.0	0.0
	2	3.34800E-01	8.11600E-03	0.0	0.0	0.0
18	1	1.69351E+00	9.90140E-03	9.60953E-03	5.58031E-03	2.11355E-03
	2	5.10948E-01	8.53239E-02	0.0	1.27449E-01	4.92230E-02
19	1	1.71128E+00	9.20755E-03	9.01493E-03	5.55297E-03	2.09940E-03
	2	5.15017E-01	8.58361E-02	0.0	1.28605E-01	4.95716E-02
20	1	1.69673E+00	9.53519E-03	9.86440E-03	4.82517E-03	1.80153E-03
	2	5.14256E-01	7.32276E-02	0.0	1.03081E-01	3.91827E-02

Table A2.2.3 (continued)

COMPOSITION	GROUP	DIFFUSION COEFFICIENT	ABSORPTION CROSS-SECTION	REMOVAL CROSS-SECTION	NU-FISSION CROSS-SECTION	FISSION CROSS-SECTION
21	1	1.68180E+00	9.80384E-03	1.04832E-02	4.33423E-03	1.59907E-03
	2	5.15502E-01	6.52413E-02	0.0	8.67764E-02	3.24978E-02
22	1	1.66669E+00	1.01806E-02	1.16043E-02	3.92731E-03	1.43491E-03
	2	5.16430E-01	5.78591E-02	0.0	7.19649E-02	2.65962E-02
23	1	1.97100E+00	3.88600E-04	1.94300E-02	0.0	0.0
	2	4.07500E-01	6.60200E-03	0.0	0.0	0.0
24	1	1.74258E+00	9.07270E-03	8.60264E-03	5.33857E-03	2.01554E-03
	2	5.44237E-01	2.98247E-02	0.0	1.49558E-01	5.76363E-02
25	1	1.60700E+00	5.44200E-04	2.77900E-02	0.0	0.0
	2	3.15600E-01	8.57700E-03	0.0	0.0	0.0
26	1	2.01000E+00	5.27000E-04	3.51600E-02	0.0	0.0
	2	3.25900E-01	9.96300E-03	0.0	0.0	0.0
27	1	1.41750E+00	1.04190E-02	1.63910E-02	5.89930E-03	2.23390E-03
	2	3.59580E-01	8.81870E-02	0.0	1.29130E-01	5.00950E-02
28	1	1.42920E+00	9.92510E-03	1.54890E-02	5.84130E-03	2.20600E-03
	2	3.62920E-01	8.90370E-02	0.0	1.30370E-01	5.03330E-02
29	1	1.41880E+00	1.00980E-02	1.66520E-02	5.06700E-03	1.88840E-03
	2	3.61510E-01	7.58910E-02	0.0	1.03860E-01	3.95570E-02
30	1	1.40690E+00	1.03160E-02	1.75280E-02	4.53730E-03	1.67010E-03
	2	3.61610E-01	6.78210E-02	0.0	8.71440E-02	3.26220E-02

Table A2.2.3 (continued)

COMPOSITION	GROUP	DIFFUSION COEFFICIENT	ABSORPTION CROSS-SECTION	REMOVAL CROSS-SECTION	NU-FISSION CROSS-SECTION	FISSION CROSS-SECTION
31	1	1.39390E+00	1.06510E-02	1.85870E-02	4.09780E-03	1.49150E-03
	2	3.61800E-01	6.04450E-02	0.0	7.21090E-02	2.65620E-02
32	1	1.58100E+00	4.60000E-04	2.74500E-02	0.0	0.0
	2	3.08300E-01	8.67800E-03	0.0	0.0	0.0
33	1	1.43930E+00	1.12530E-02	1.50320E-02	5.34490E-03	2.01250E-03
	2	3.47160E-01	1.49380E-01	0.0	1.13030E-01	4.28730E-02
34	1	1.52800E+00	5.70000E-04	3.08200E-02	0.0	0.0
	2	2.93300E-01	9.19000E-03	0.0	0.0	0.0

$\chi_1 = 1.0$

$\chi_2 = 0.0$

Table A2.2.4 Heterogeneous cross sections for the DEP2 BWR Benchmark at burnup = 20,000 MWD/MT.

COMPOSITION	GROUP	DIFFUSION COEFFICIENT	ABSORPTION CROSS-SECTION	REMOVAL CROSS-SECTION	NU-FISSION CROSS-SECTION	FISSION CROSS-SECTION
1	1	1.70252E+00	1.07784E-02	9.46851E-03	4.71144E-03	1.71661E-03
	2	5.07116E-01	8.27686E-02	0.0	1.11421E-01	4.06817E-02
2	1	1.70140E+00	1.00720E-02	8.58094E-03	4.54601E-03	1.65132E-03
	2	5.16783E-01	8.24584E-02	0.0	1.10129E-01	4.00101E-02
3	1	1.67668E+00	1.05815E-02	8.89501E-03	3.78714E-03	1.34890E-03
	2	5.22525E-01	6.95262E-02	0.0	8.31529E-02	2.93917E-02
4	1	1.65592E+00	1.09994E-02	9.21999E-03	3.49453E-03	1.23769E-03
	2	5.26439E-01	6.35380E-02	0.0	7.14607E-02	2.50253E-02
5	1	1.63901E+00	1.14231E-02	8.75427E-03	3.58886E-03	1.32253E-03
	2	5.46867E-01	5.82378E-02	0.0	6.45179E-02	2.42002E-02
6	1	1.97258E+00	3.89766E-04	1.87512E-02	0.0	0.0
	2	3.98052E-01	6.74359E-03	0.0	0.0	0.0
7	1	1.71882E+00	1.05957E-02	8.32704E-03	4.38393E-03	1.60080E-03
	2	5.18560E-01	8.78680E-02	0.0	1.12072E-01	4.09142E-02
8	1	1.61264E+00	5.67930E-04	2.21935E-02	0.0	0.0
	2	3.44296E-01	7.98029E-03	0.0	0.0	0.0
9	1	1.16838E+00	7.85783E-02	4.55109E-04	0.0	0.0
	2	2.01085E-01	9.79095E-01	0.0	0.0	0.0
10	1	1.99482E+00	1.00196E-02	4.64125E-03	4.15526E-03	1.50110E-03
	2	7.35918E-01	7.84680E-02	0.0	1.03698E-01	3.73184E-02

Table A2.2.4 (continued)

COMPOSITION	GROUP	DIFFUSION COEFFICIENT	ABSORPTION CROSS-SECTION	REMOVAL CROSS-SECTION	NU-FISSION CROSS-SECTION	FISSION CROSS-SECTION
11	1	2.02129E+00	8.98103E-03	4.27951E-03	4.21934E-03	1.52953E-03
	2	7.37597E-01	7.88336E-02	0.0	1.05246E-01	3.80633E-02
12	1	1.99785E+00	9.79555E-03	4.88229E-03	3.74039E-03	1.33756E-03
	2	7.44486E-01	6.76590E-02	0.0	8.35089E-02	2.96418E-02
13	1	1.97883E+00	1.03522E-02	5.29140E-03	3.49439E-03	1.24030E-03
	2	7.48827E-01	6.19490E-02	0.0	7.26134E-02	2.54802E-02
14	1	1.96122E+00	1.10246E-02	5.81927E-03	3.28600E-03	1.16070E-03
	2	7.52466E-01	5.62953E-02	0.0	6.21022E-02	2.16109E-02
15	1	2.43000E+00	3.30000E-04	1.33300E-02	0.0	0.0
	2	5.18500E-01	5.20500E-03	0.0	0.0	0.0
16	1	2.05452E+00	9.35275E-03	4.10584E-03	4.12709E-03	1.50533E-03
	2	7.33872E-01	8.58650E-02	0.0	1.10423E-01	4.02326E-02
17	1	1.67000E+00	5.20000E-04	2.47100E-02	0.0	0.0
	2	3.34800E-01	8.11600E-03	0.0	0.0	0.0
18	1	1.69747E+00	1.04643E-02	9.43834E-03	4.97779E-03	1.83740E-03
	2	5.07110E-01	8.48585E-02	0.0	1.18877E-01	4.41612E-02
19	1	1.71491E+00	9.69907E-03	8.81220E-03	4.97301E-03	1.83581E-03
	2	5.11567E-01	8.42988E-02	0.0	1.18234E-01	4.39889E-02
20	1	1.69907E+00	1.01762E-02	9.71672E-03	4.33162E-03	1.57431E-03
	2	5.11584E-01	7.22041E-02	0.0	9.39180E-02	3.42777E-02

Table A2.2.4 (continued)

COMPOSITION	GROUP	DIFFUSION COEFFICIENT	ABSORPTION CROSS-SECTION	REMOVAL CROSS-SECTION	NU-FISSION CROSS-SECTION	FISSION CROSS-SECTION
21	1	1.68312E+00	1.05602E-02	1.03657E-02	3.95041E-03	1.42023E-03
	2	5.13216E-01	6.49547E-02	0.0	7.94880E-02	2.85452E-02
22	1	1.66816E+00	1.10485E-02	2.66833E-03	3.63186E-03	1.29505E-03
	2	5.14259E-01	5.84524E-02	0.0	6.67402E-02	2.36335E-02
23	1	1.97100E+00	3.88600E-04	1.94300E-02	0.0	0.0
	2	4.07500E-01	6.60200E-03	0.0	0.0	0.0
24	1	1.72149E+00	1.23692E-02	8.63485E-03	4.47236E-03	1.65535E-03
	2	4.19885E-01	2.81513E-01	0.0	6.09828E-02	2.10378E-02
25	1	1.60700E+00	5.44200E-04	2.77900E-02	0.0	0.0
	2	3.15600E-01	8.57700E-03	0.0	0.0	0.0
26	1	2.01000E+00	5.27000E-04	3.51600E-02	0.0	0.0
	2	3.25900E-01	9.96300E-03	0.0	0.0	0.0
27	1	1.42020E+00	1.10580E-02	1.62080E-02	5.29510E-03	1.95500E-03
	2	3.56900E-01	8.79390E-02	0.0	1.20880E-01	4.51000E-02
28	1	1.43300E+00	1.05080E-02	1.52610E-02	5.25320E-03	1.93680E-03
	2	3.60600E-01	8.72800E-02	0.0	1.19510E-01	4.45460E-02
29	1	1.42100E+00	1.08210E-02	1.65040E-02	4.56220E-03	1.65600E-03
	2	3.59670E-01	7.46480E-02	0.0	9.41830E-02	3.44050E-02
30	1	1.40900E+00	1.11430E-02	1.74480E-02	4.14950E-03	1.48950E-03
	2	3.60370E-01	6.70200E-02	0.0	7.88420E-02	2.83110E-02

Table A2.2.4 (continued)

COMPOSITION	GROUP	DIFFUSION COEFFICIENT	ABSORPTION CROSS-SECTION	REMOVAL CROSS-SECTION	NU-FISSION CROSS-SECTION	FISSION CROSS-SECTION
31	1	1.39600E+00	1.15790E-02	1.85690E-03	3.80250E-03	1.35320E-03
	2	3.60890E-01	6.01530E-02	0.0	6.52550E-02	2.30830E-02
32	1	1.58100E+00	4.60000E-04	2.74500E-02	0.0	0.0
	2	3.08300E-01	8.67800E-03	0.0	0.0	0.0
33	1	1.45080E+00	1.09260E-02	1.46610E-02	4.83080E-03	1.77090E-03
	2	3.66970E-01	7.07750E-02	0.0	1.25060E-01	4.63480E-02
34	1	1.52800E+00	5.70000E-04	3.08200E-02	0.0	0.0
	2	2.93300E-01	9.19000E-03	0.0	0.0	0.0

APPENDIX 3

CURRENT AND FLUX SHAPES IN THE LSH BWR AND MVY BWR BENCHMARKS

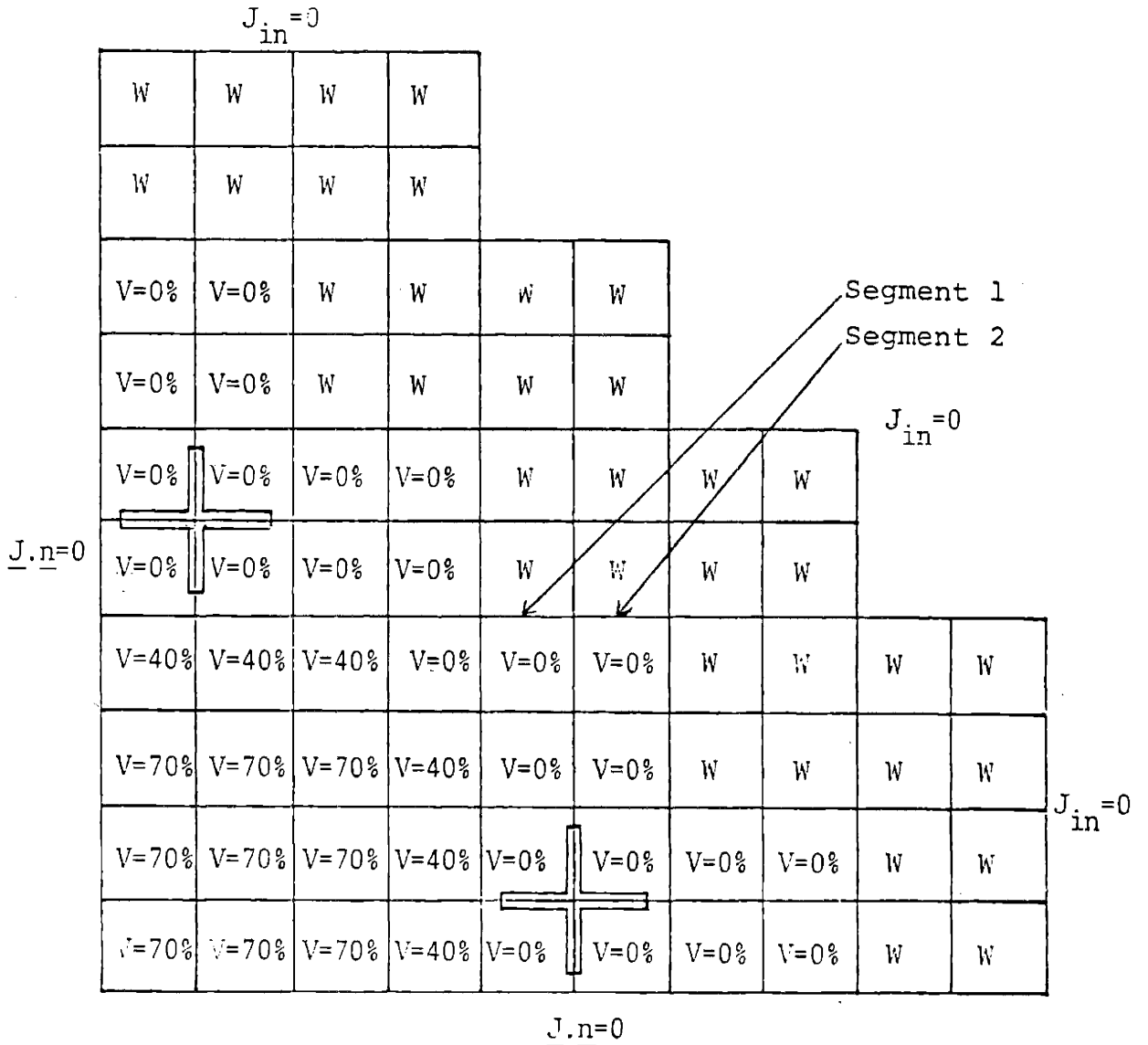

Fig. A3.1 Location of Figures A3.2 to A3.9 in the LSH BWR Benchmark.

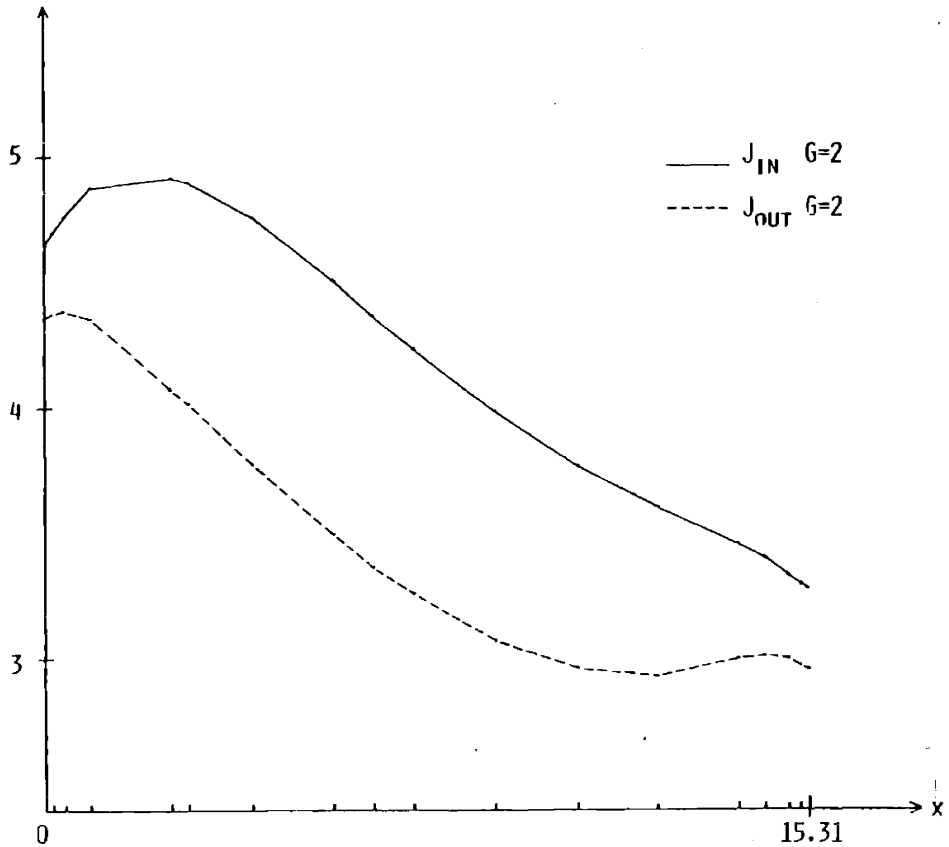

Fig. A3-2 Partial currents along Segment 1.

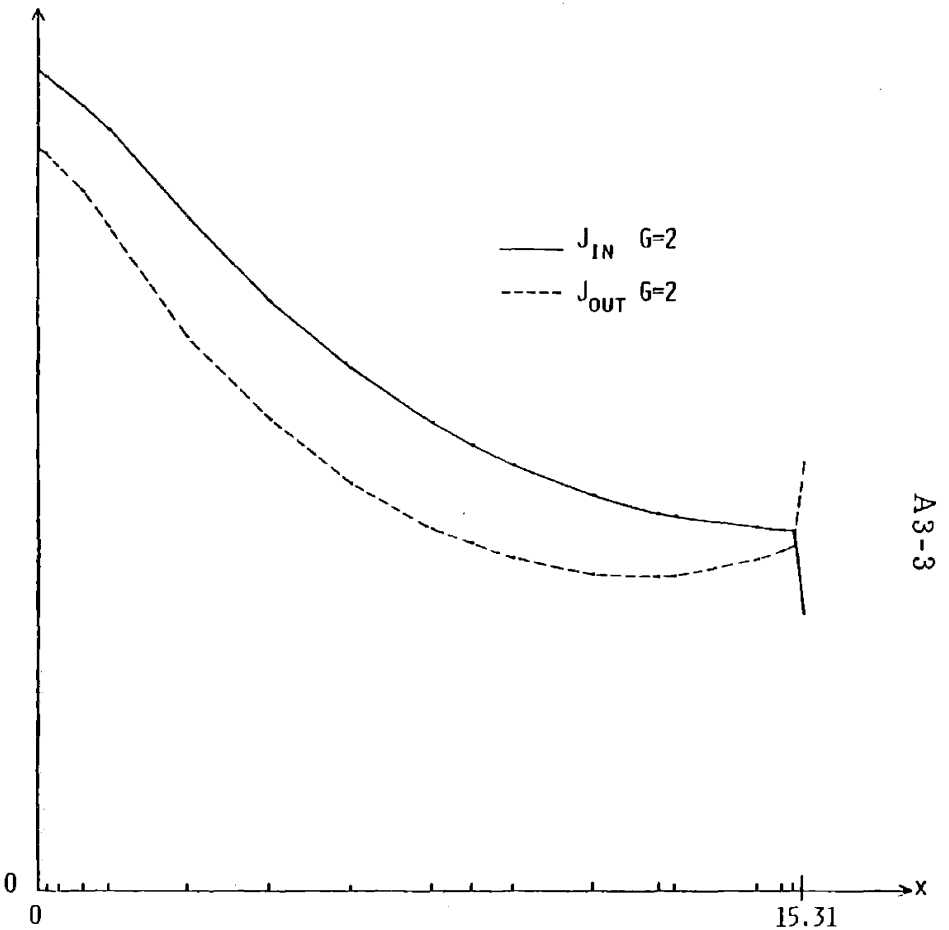

Fig. A3.3 Partial currents along Segment 2.

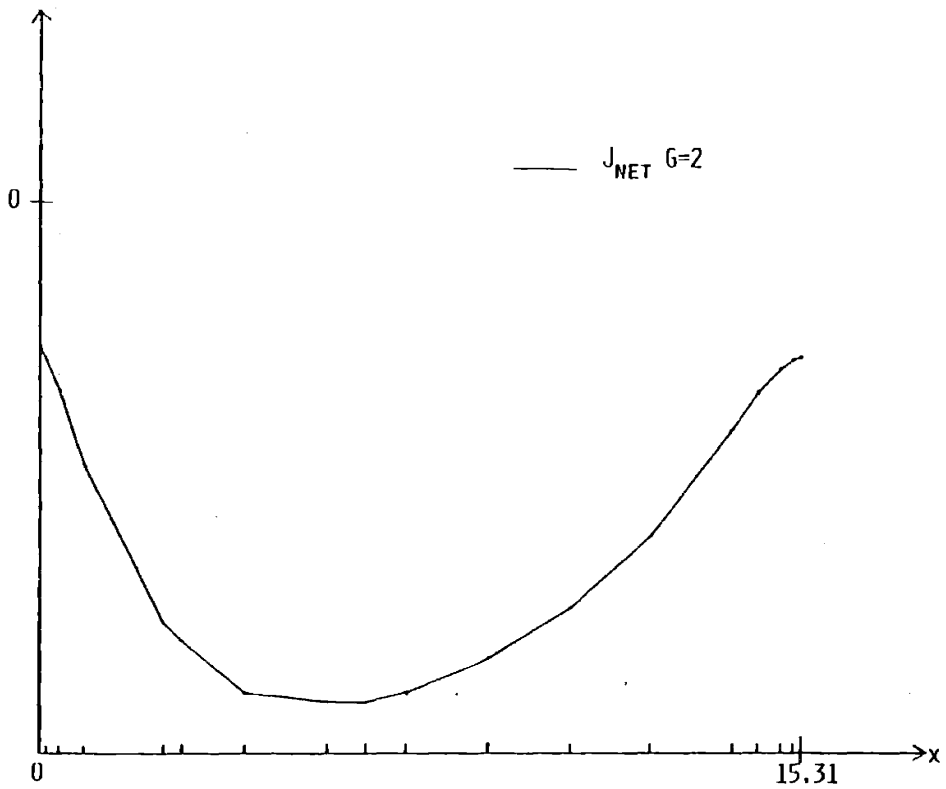

Fig. A3.4 Net transverse current along Segment 1.

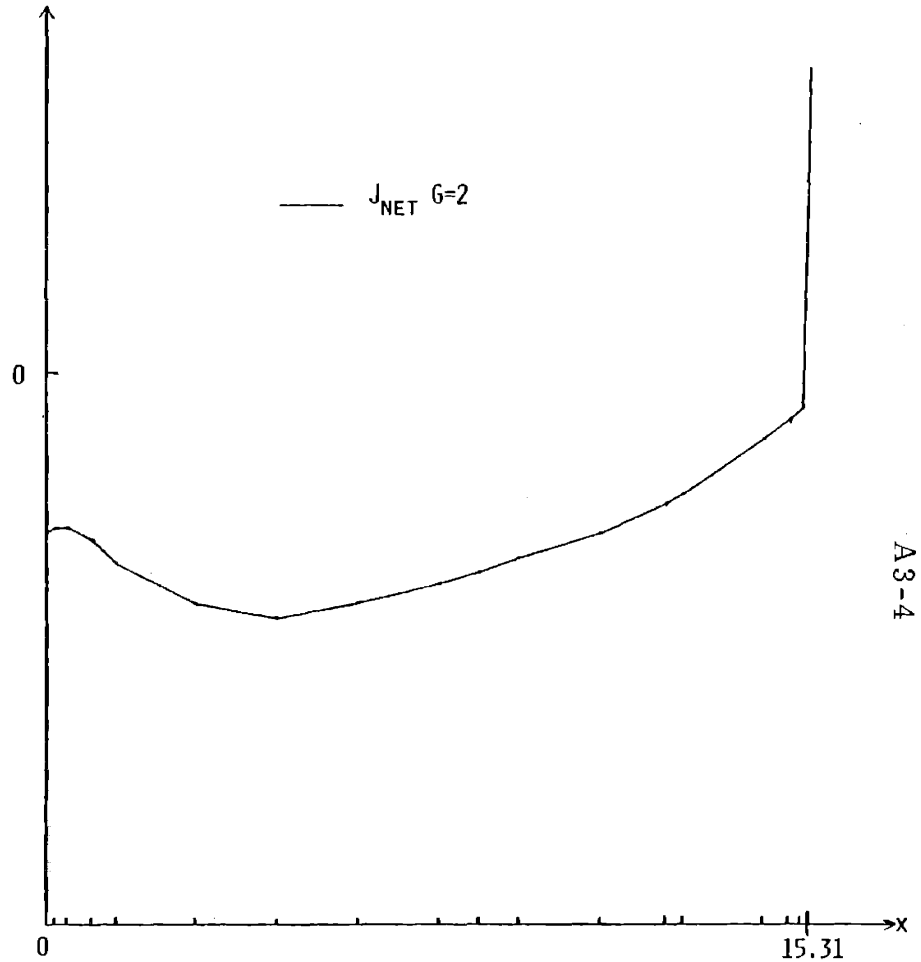

Fig. A3.5 Net transverse current along Segment 2.

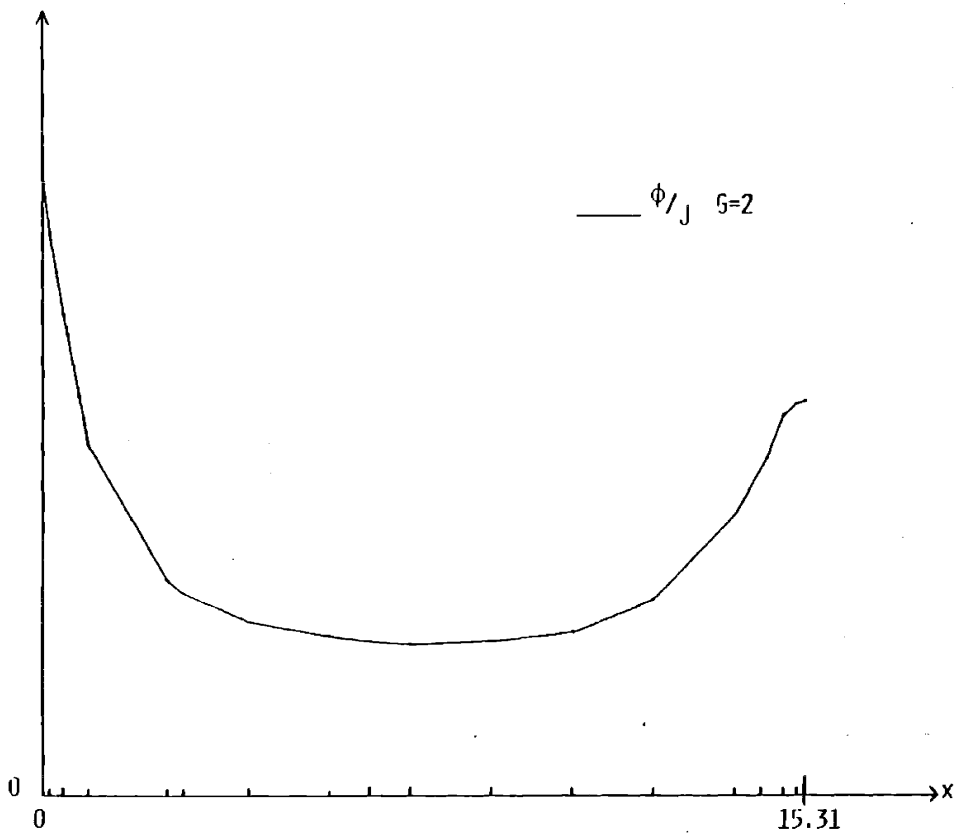

Fig. A3.6 Albedo along Segment 1.

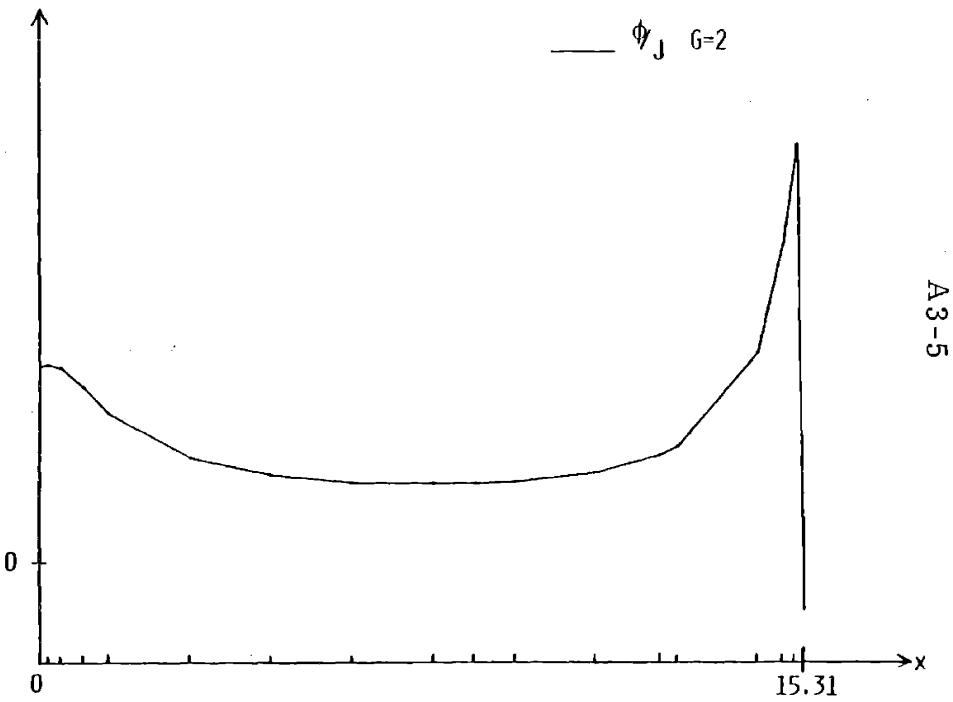

Fig. A3.7 Albedo along Segment 2.

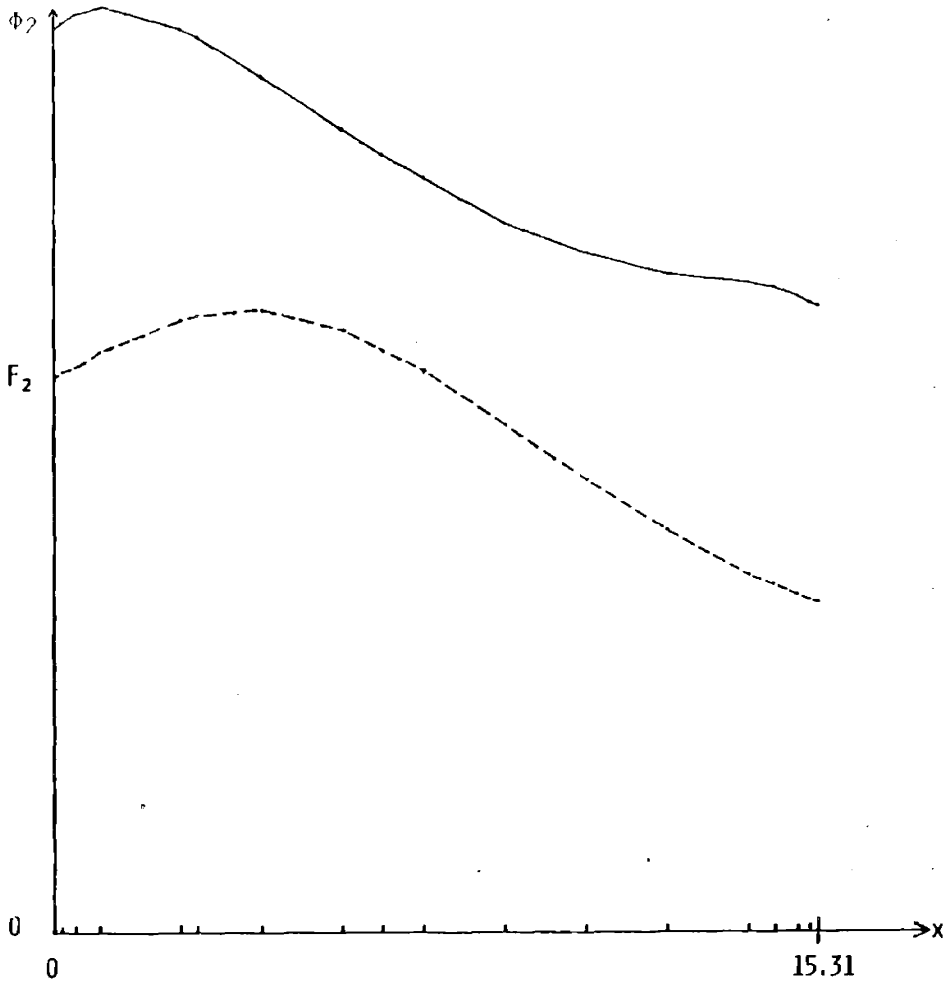

Fig. A3.8 Flux and form function along Segment 1.

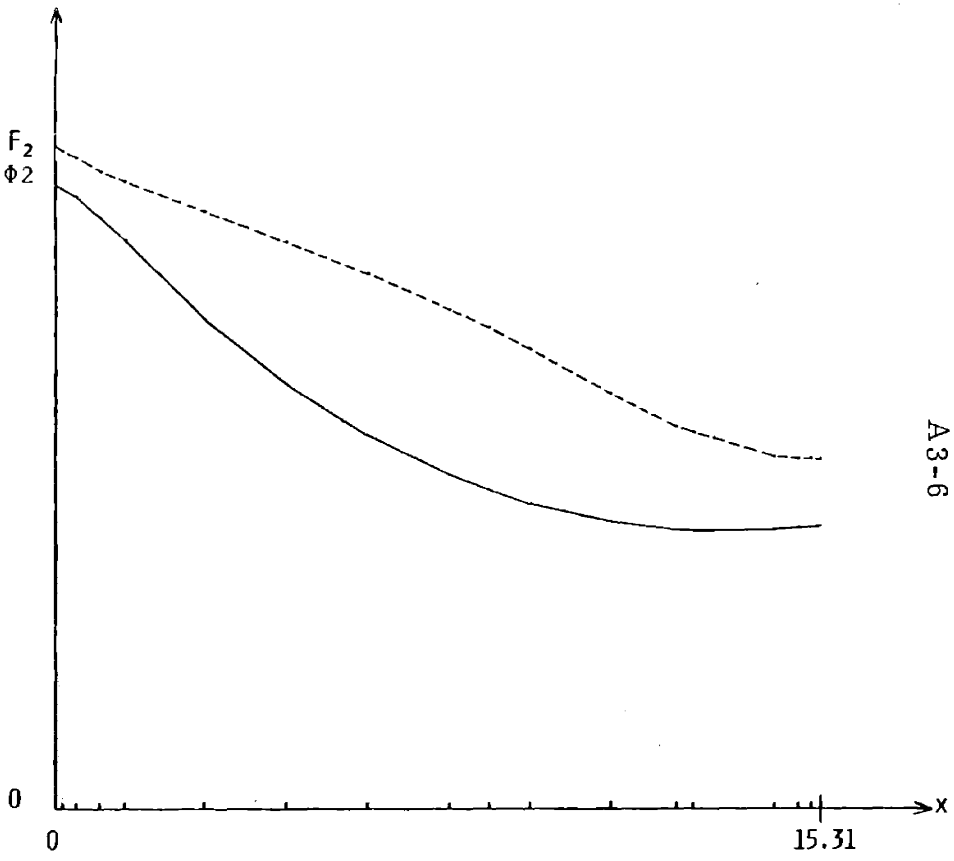

Fig. A3.9 Flux and form function along Segment 2.

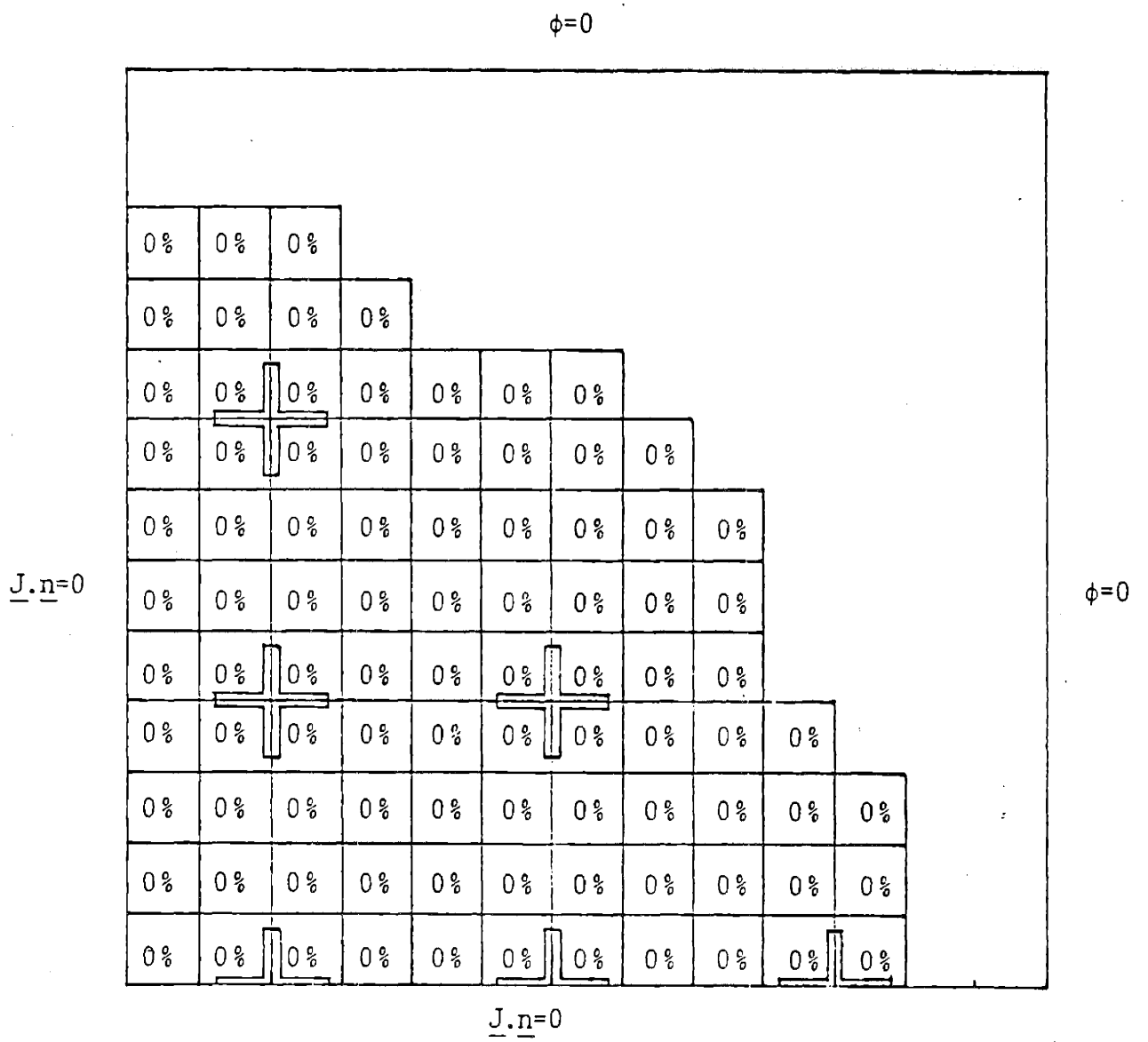

Fig. A3.10 Location of Figures A3-11 to A3-22 in the MVY BWR Benchmark.

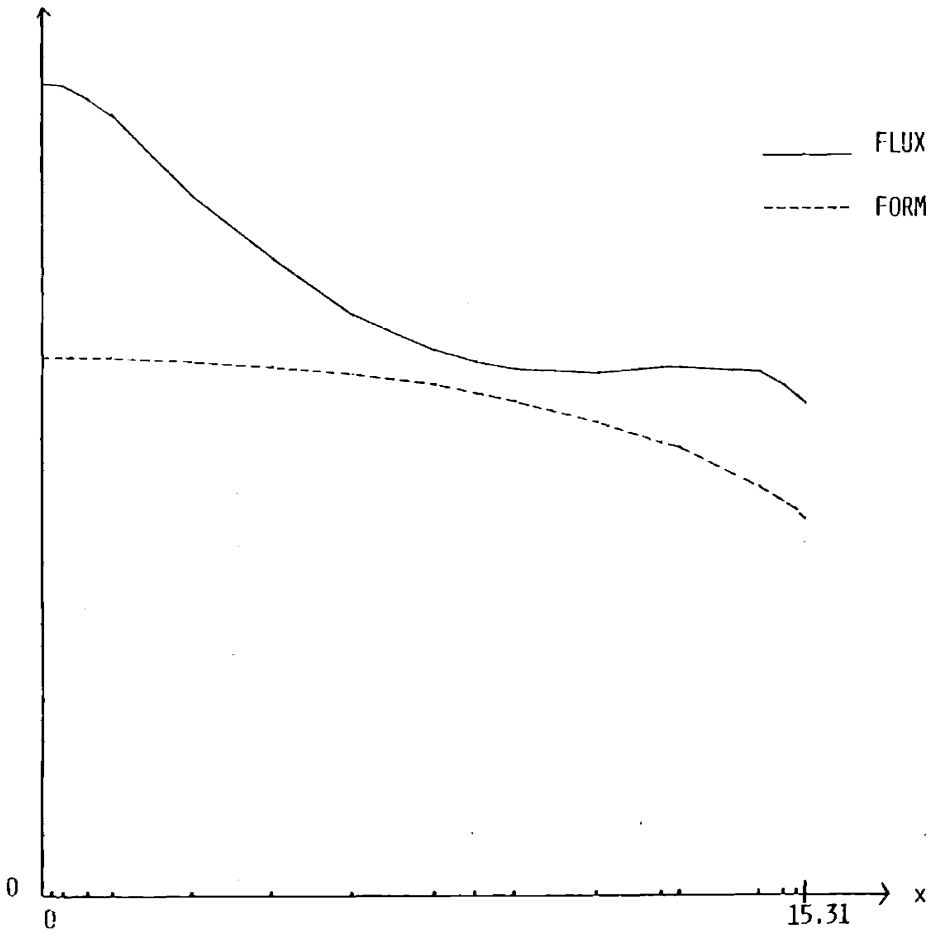

Fig. A3.11 Flux and form function along Segment 1.

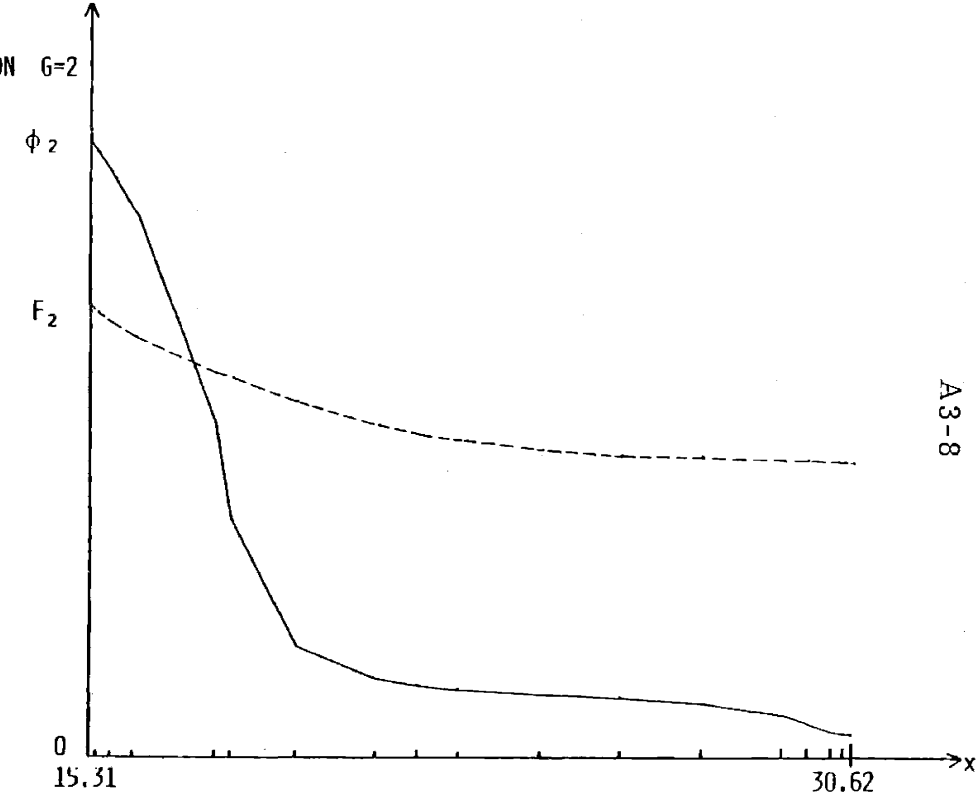

Fig. A3.12 Flux and form function along Segment 2.

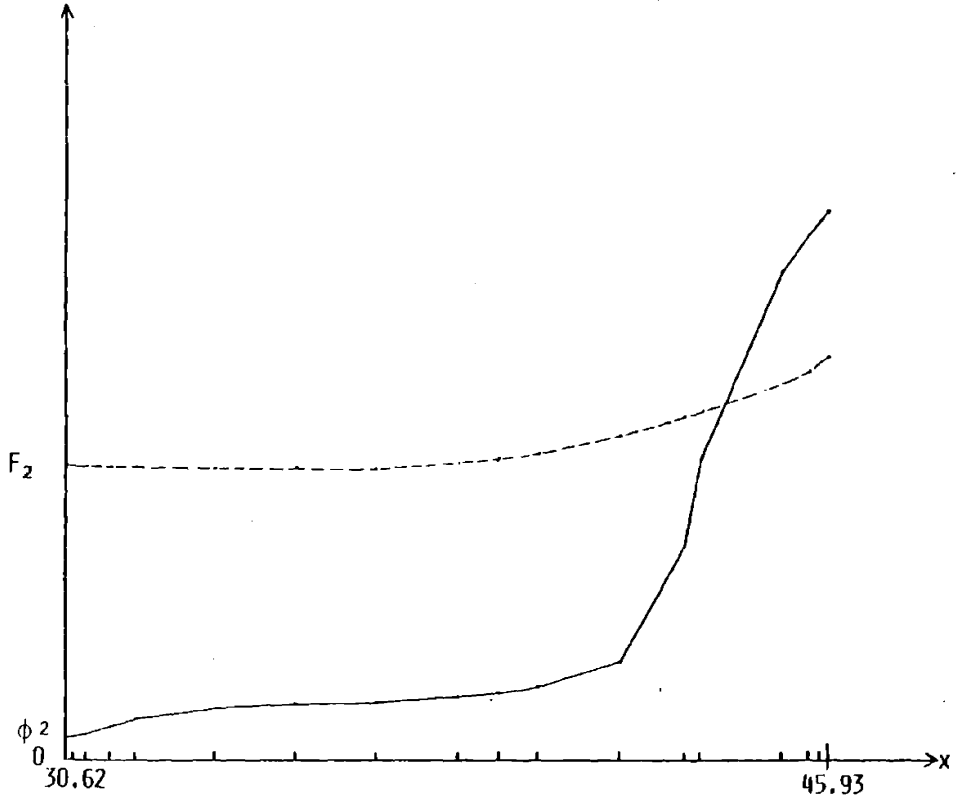

Fig. A3.13 Flux and form function along Segment 3.

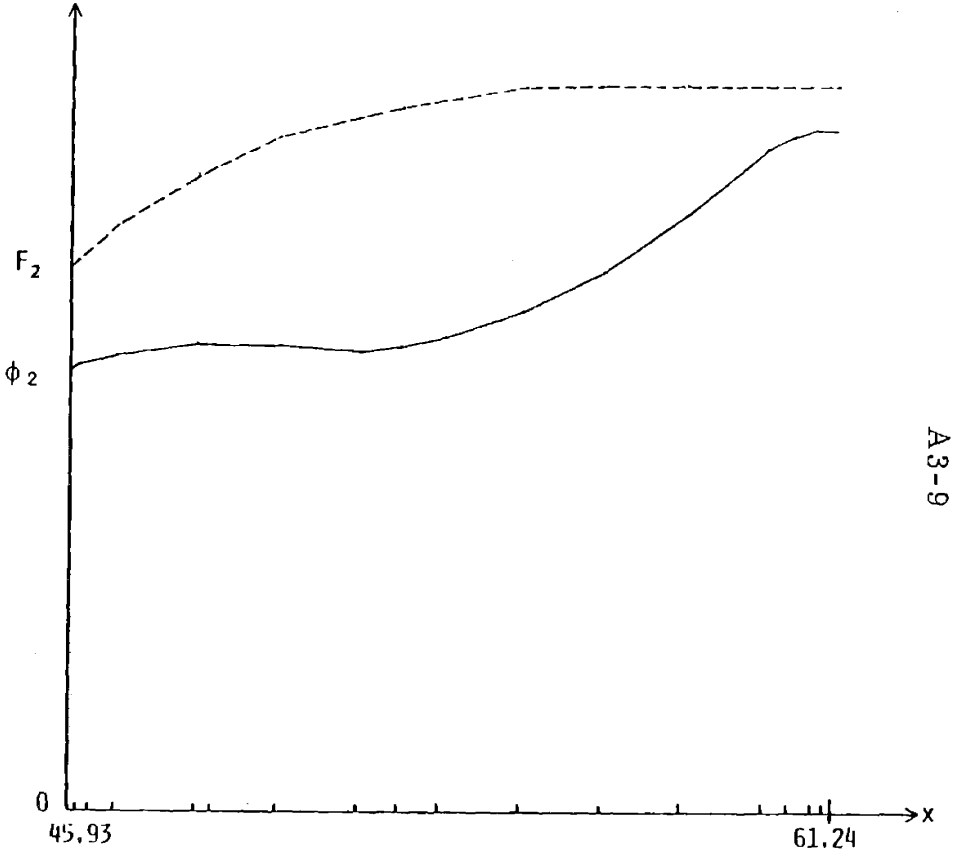

Fig. A3.14 Flux and form function along Segment 4.

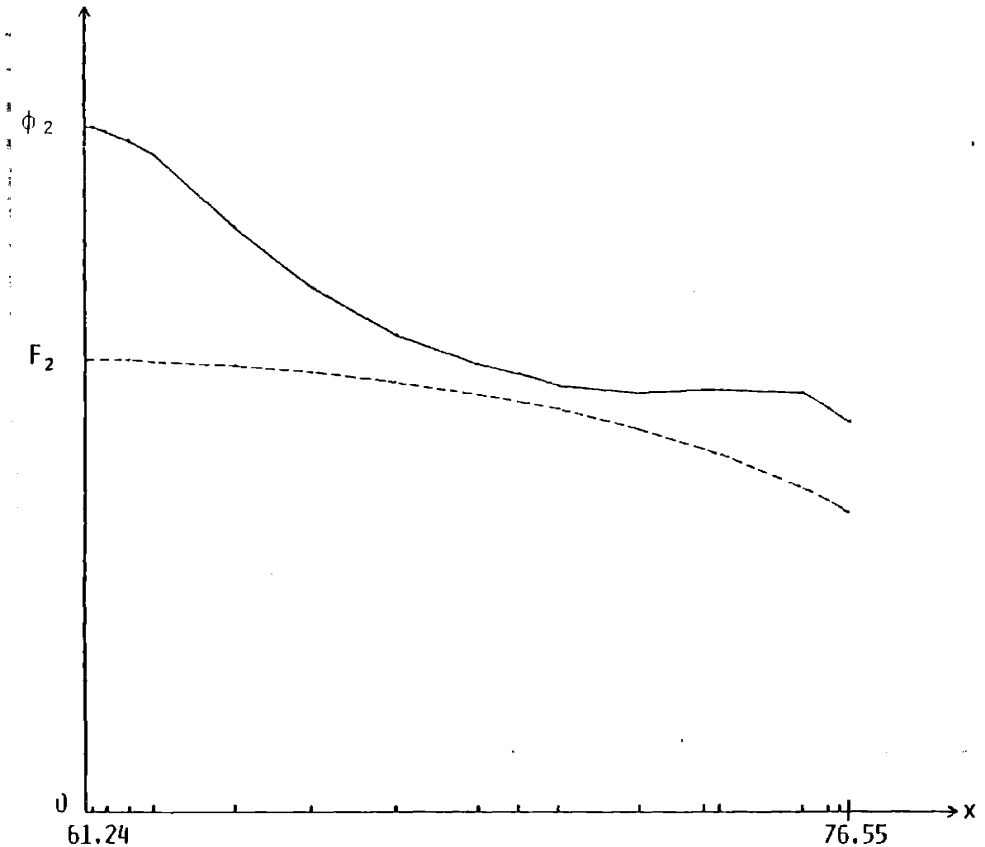

Fig. A3.15 Flux and form function along Segment 5.

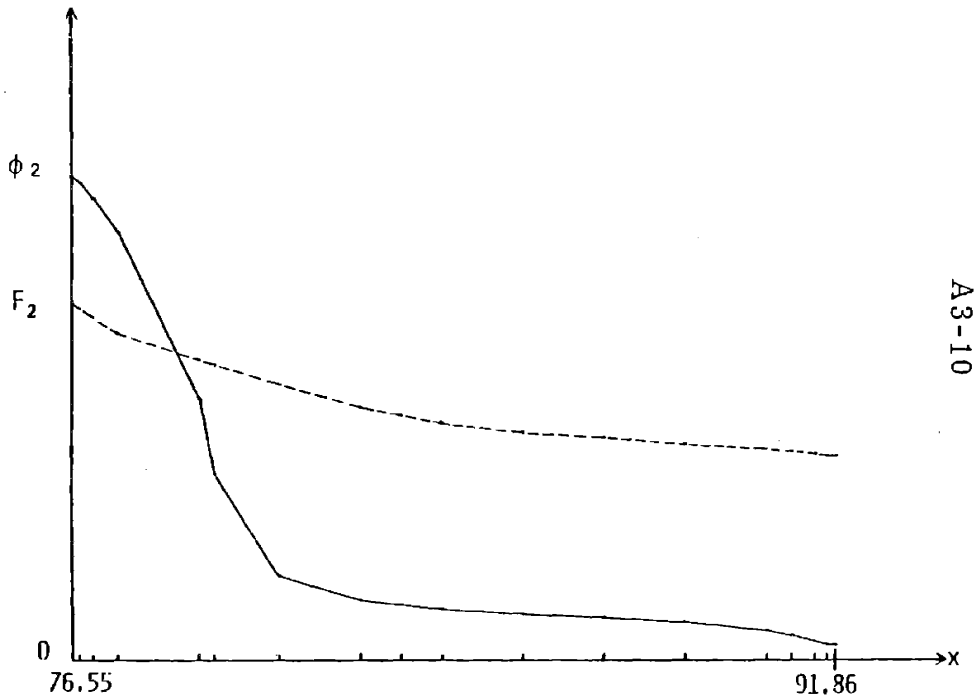

Fig. A3.16 Flux and form function along Segment 6.

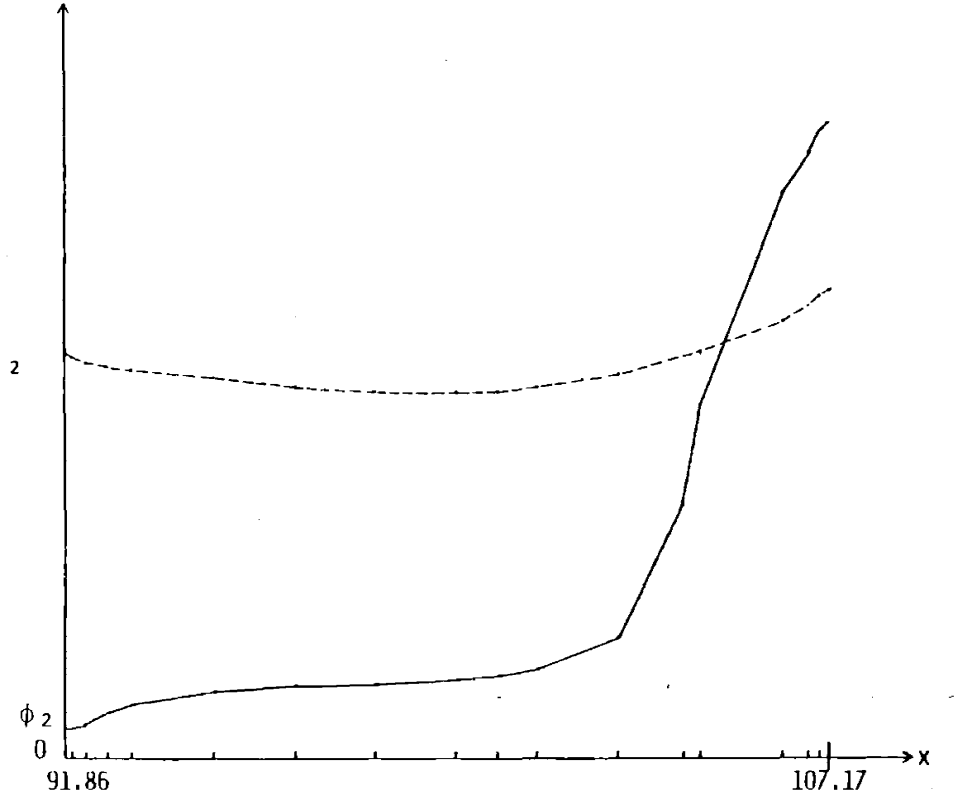

Fig. A3.17 Flux and form function along Segment 7.

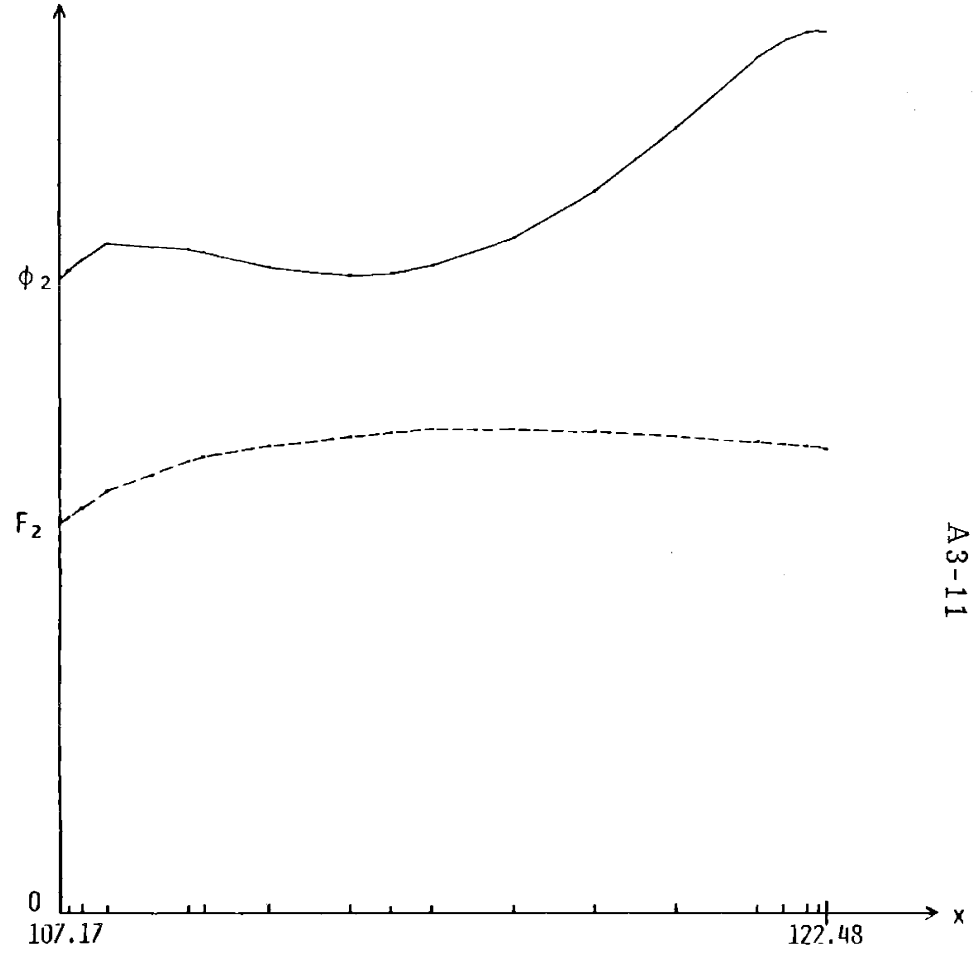

Fig. A3.18 Flux and form function along Segment 8.

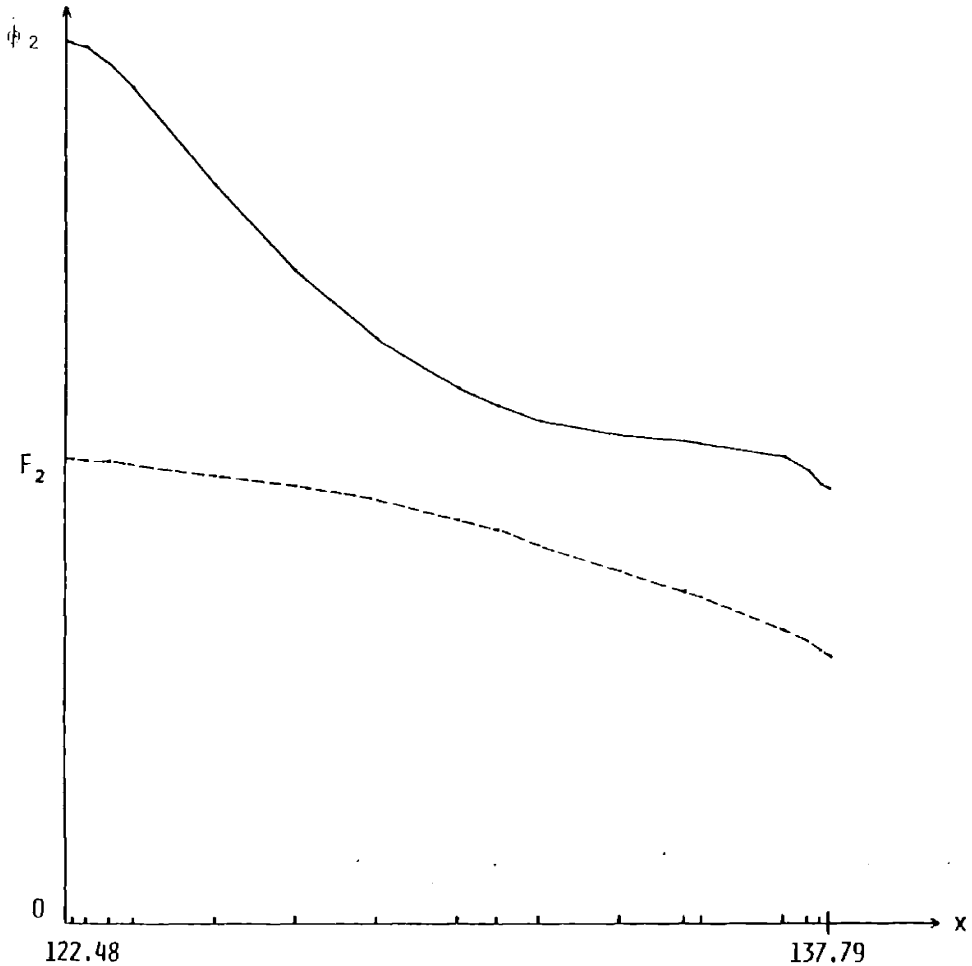

Fig. A3.19 Flux and form function along Segment 9.

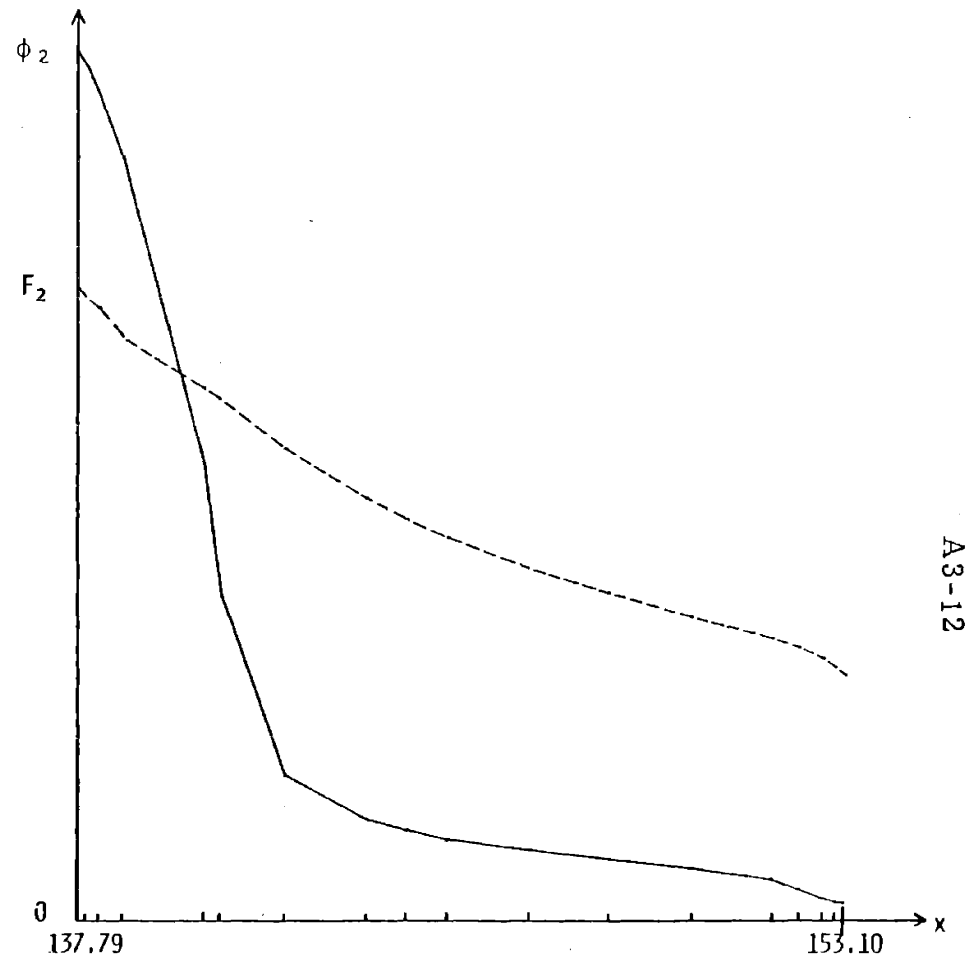

Fig. A3.20 Flux and form function along Segment 10.

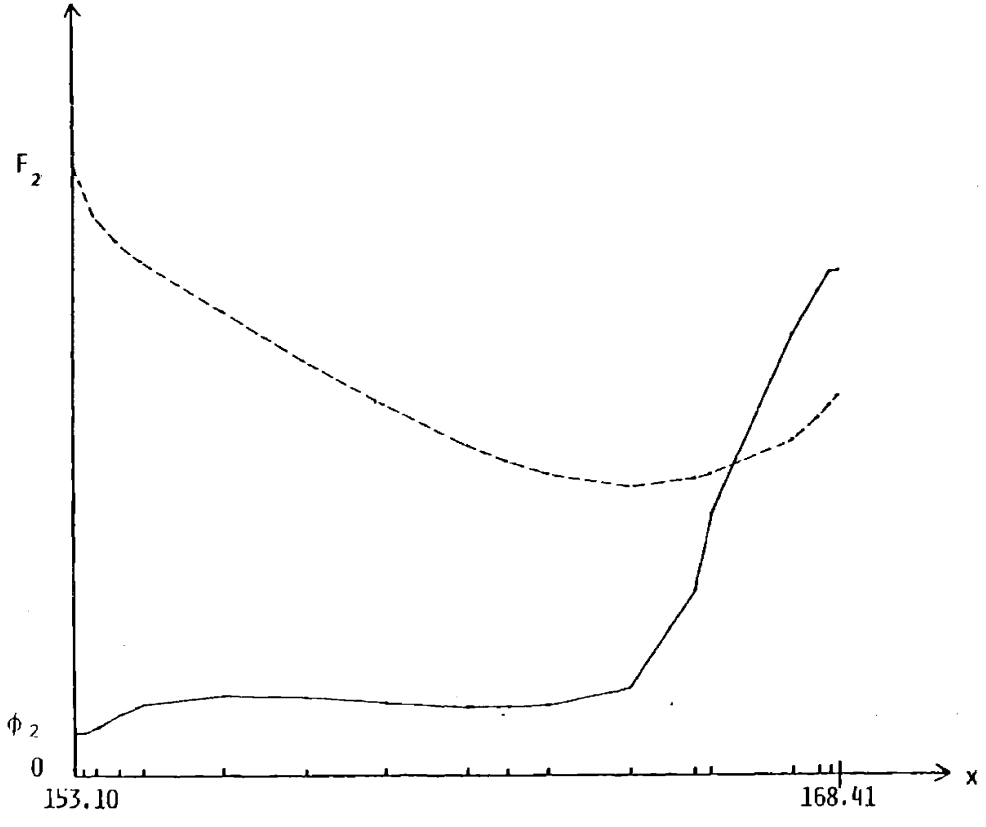

Fig. A3.21 Flux and form function along Segment 11.

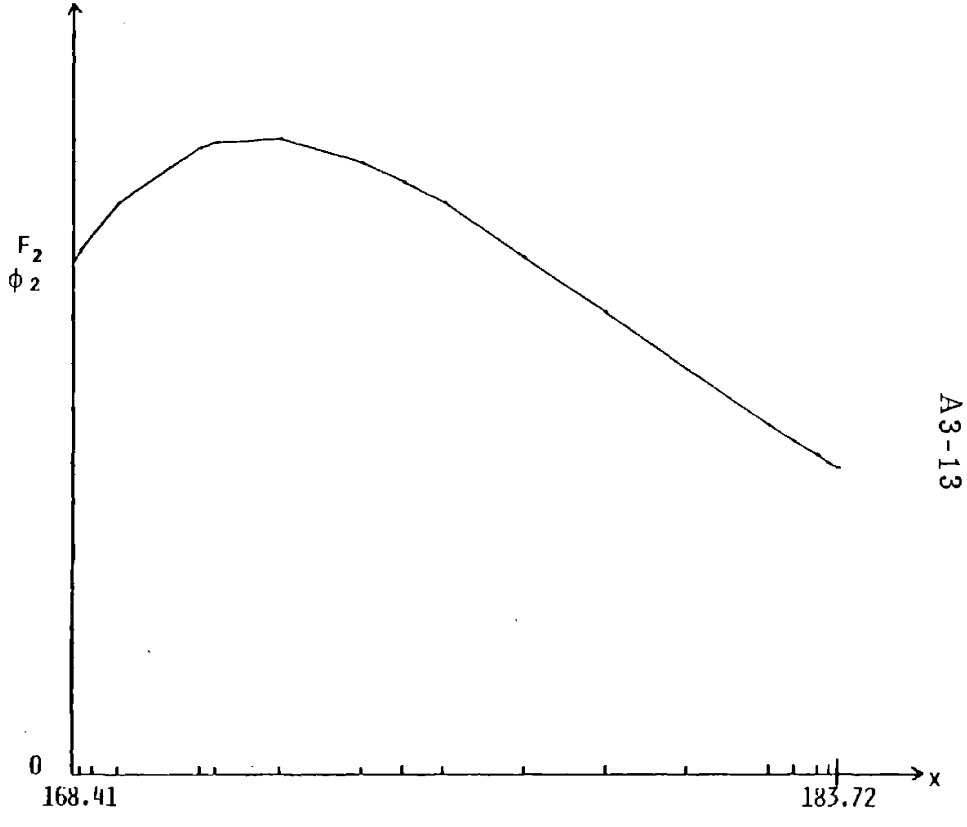

Fig. A3.22 Flux and form function along Segment 12.

APPENDIX 4

EQUATIONS FOR CORNERPOINT FLUXES INTERPOLATION

A4.1 Introduction

The purpose of this appendix is to derive the linear equation which relates, in each energy group, a cornerpoint flux to its four neighbors, when the quadradratic form function approximation is made. The resulting linear system, relating all cornerpoint fluxes in the core, is easily solved by a classical iterative method (Gauss-Seidel, S.O.R., ...).

A4.2 Problem Description

Figure A4.1 describes the unknown and known quantities entering in the derivation of cornerpoint fluxes:

$\varphi^g_{i,j}$ is the value of the flux in group g at cornerpoint (i, j);

$\bar{\varphi}^g_k$ is the average value of the surface flux, obtained from a nodal calculation, on face k;

A^g_k is the fine-mesh "assembly flux" on face k (defined by Equation (3.2));

ℓ_k is the length of face k;

D^g_n is the diffusion coefficient in quadrant n.

A4.3 Problem Solution

On face k, the heterogeneous flux is approximated by the product of the assembly flux and a quadratic form function:

$$\varphi^g_k(x) = F^g_k(x)\, A^g_k(x)$$

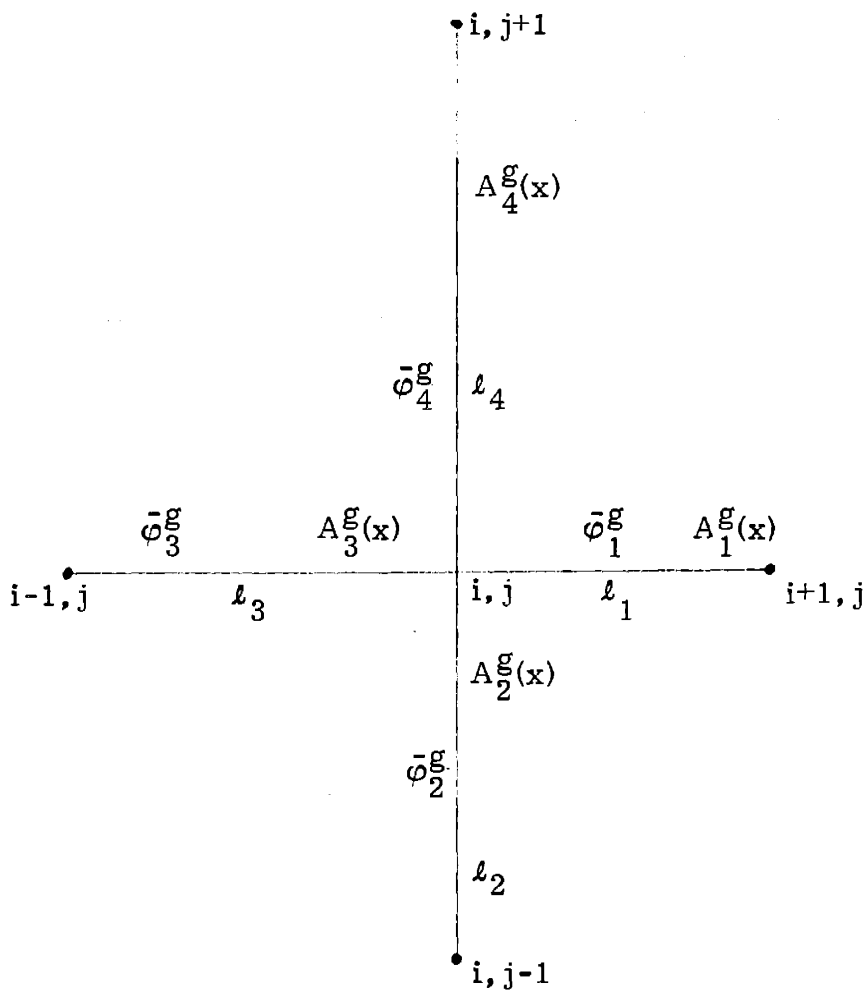

Fig. A4.1 Definition of quantities used in cornerpoint flux interpolation.

where

$$F_k^g(x) = a_k^g x^2 + b_k^g x + c_k^g$$

The coefficients of F_k^g are then chosen so that φ_k^g matches the cornerpoint fluxes φ_L^g and φ_R^g and the average surface flux, $\bar{\varphi}_k^g$, on that face:

$$\begin{cases} \varphi_k^g(x_L) = \varphi_L^g \\ \varphi_k^g(x_R) = \varphi_R^g \\ \int_{x_L}^{x_R} \varphi_k^g(x)\, dx = (x_R - x_L)\, \bar{\varphi}_k^g \end{cases}$$

This linear system of three equations and three unknowns (a_k^g, b_k^g, c_k^g) has a unique solution. If one defines:

$$\alpha_k^g = \int_{x_L}^{x_R} A_k^g(x)\, x^2\, dx$$

$$\beta_k^g = \int_{x_L}^{x_R} A_k^g(x)\, x\, dx$$

$$\gamma_k^g = \int_{x_L}^{x_R} A_k^g(x)\, dx$$

$$\delta_k^g = \frac{\varphi_R^k}{A_k^g(x_R)} - \frac{\varphi_L^k}{A_k^g(x_L)} \Big/ \ell_k$$

then:

$$a_k^g = (\bar{\varphi}_k^g - \gamma_k^g\, c_k^g - \beta_k^g\, \delta_k^g)$$

$$b_k^g = \delta_k^g - a_k^g\, \ell_k$$

$$c_k^g = \omega_L^g / A_k^g(x_L)$$

The derivative of the flux at $x = x_o$ on face k is:

$$\frac{d}{dx} A_k^g F_k^g \Big|_{x = x_o} = A_k^g(x_o) \frac{d}{dx} F_k^g \Big|_{x = x_o} + F_k^g(x_o) \frac{d}{dx} A_k^g \Big|_{x = x_o}$$

Thus, the source-free condition around point $\varphi_{i,j}^g$ leads to the following equation:

$$A_1^g(o) \frac{D_1^g + D_2^g}{2} b_1^g + A_4^g(o) \frac{D_1^g + D_4^g}{2} b_4^g$$

$$- A_3^g(o) \frac{D_3^g + D_4^g}{2} b_3^g - A_2^g(o) \frac{D_2^g + D_3^g}{2} b_2^g$$

$$= \frac{D_3^g + D_4^g}{2} c_3^g \frac{d}{dx} A_3^g \Big|_{x=o}$$

$$+ \frac{D_2^g + D_3^g}{2} c_2^g \frac{d}{dx} A_2^g \Big|_{x=o}$$

$$- \frac{D_1^g + D_2^g}{2} c_1^g \frac{d}{dx} A_1^g \Big|_{x=o}$$

$$- \frac{D_1^g + D_4^g}{2} c_4^g \frac{d}{dx} A_4^g \Big|_{x=o}$$

It should be noted that the right hand side of this equation is zero if the assembly fluxes are obtained from zero-current eigenvalue calculations, or the currents obtained from these assembly calculations are continuous across assembly interfaces.

APPENDIX 5

THE GENERATION OF SURFACE FLUX RESPONSE MATRICES

A5.1 Introduction

The purpose of this appendix is to define the surface flux response matrices based on the quadratic form function assumption, and describe how they are generated in practical cases.

A5.2 Definition of Surface Flux Response Matrices

Equation (3.4) defined the 10 G x 8 G response matrices for each assembly:

$$[N.Q] = [R_\lambda] [\varphi]$$

We shall assume in this section that the following quantities are known:

$a^{IF}_{\lambda_{g'g}}(x,y)$, defined in Chapter 3;

$b^{IC}_{\lambda_{g'g}}(x,y)$, defined in Chapter 3;

$D_g(x,y)$, $\Sigma_{ag}(x,y)$, $\Sigma_{rg}(xy)$, $\nu\Sigma_{fg}(x,y)$, $\Sigma_{fg}(x,y)$, the heterogeneous cross sections in group g, at point (x, y).

We shall derive the matrix elements corresponding to the input of a cornerpoint flux (IC) in group g'. They relate that input to the following outputs in group g:

1. The face averaged net current on face k, in group g:

$$\frac{-\int_{Sk} D_g(x,y) \frac{\partial}{\partial u} b^{IC}_{\lambda_{gg'}}(x,y)\, dv}{\int_{Sk} dx\, dy}$$

where $\{u, v\} \equiv \{x, y\}$.

2. The volume averaged flux in group g:

$$\frac{\int_V b^{IC}_{\lambda_{gg'}}(x, y)\, dx\, dy}{\int_V dx\, dy}$$

3. The integrated reaction rates in group g:

$$\frac{\int_V \Sigma_{\alpha g}(x, y)\, b^{IC}_{\lambda_{gg'}}(x, y)\, dx\, dy}{\int_V dx\, dy}$$

where $\Sigma_\alpha = D, \Sigma_a, \Sigma_r, \nu\Sigma_f, \Sigma_f$.

A5.3 The Generation of Surface Flux Response Matrices Using CITATION

The manner in which fixed-source calculations with surface flux boundary conditions are implemented in CITATION is described by Parsons [12].

For each assembly face (k = 1, ···, 4), and in each energy group, three successive fixed-source calculations are performed, with the following boundary conditions:

1. $\varphi^k_g(x) = A^k_g(x)$

2. $\varphi^k_g(x) = A^k_g(x) \cdot x$

3. $\varphi^k_g(x) = A^k_g(x) \cdot x^2$

where

x is the dimensional variable on face k;

$A_g^k(x)$ is the assembly flux in group g on face k;

$\varphi_g^k(x)$ is the imposed surface flux.

The fluxes on the three other faces are set to 0.

Once the intra-assembly fluxes corresponding to these boundary conditions are calculated, simple algebraic manipulations yield $a^{IF}_{\lambda_{g'g}}(xy)$ (IF = 1, ···, 4), and $b^{IC}_{\lambda_{g'g}}(x, y)$ (IC = 1, ···, 4).

It should be noted that the fact of imposing finite fluxes on one face while fluxes are zero on the other faces can be detrimental to the resulting fluxes within the assembly. In particular, extremely large flux tilts in locations close to the cornerpoints may result in important truncation errors.

A5.4 The Generation of Surface Flux Response Matrices in the PDQ7 Formalism

A small computer code was written to perform fixed source calculations for a given eigenvalue. The mathematical formalism of the finite differences equations is the same as is used in the PDQ7 computer code [17]. Two levels of iterations are performed.

1. The inner (flux) iterations are performed for each energy group by a Gauss-Seidel iterative scheme, accelerated by S.O.R.
2. The outer (source) iterations are not accelerated.

The versatility of that program is such that it can handle cases where fluxes become negative. Thus, the $a^{IF}_{\lambda_{gg'}}$ and $b^{IC}_{\lambda_{gg'}}$ can be calculated directly, by setting the corresponding physical quantity to one, and

all other matrix inputs to zero in a fixed source calculation.

APPENDIX 6

DETAILED NODAL RESULTS

A6.1 THE PRELIMINARY TEST PROBLEM

A6.2 THE CISE BWR BENCHMARK PROBLEM

A6.3 THE CLSH BWR BENCHMARK PROBLEM

A6.4 THE NLSH BWR BENCHMARK PROBLEM

A6.5 THE MVY BWR BENCHMARK PROBLEM

A6.6 THE TRD BWR BENCHMARK PROBLEM

A6.7 THE DEP2 BWR BENCHMARK PROBLEM

A6.1 NODAL RESULTS FOR THE PRELIMINARY TEST PROBLEM

Reference Eigenvalue: $\lambda = 0.63753$

1.4300	0.8367	0.2127	---------- REFERENCE
-2.66%	2.87%	-1.41%	---------- ADF-AXS
3.15%	1.65%	-4.00%	---------- FIRST ITERATION
3.08%	2.12%	-4.51%	---------- CONVERGED SOLUTION
3.08%	2.07%	-4.23%	---------- AVGE OF THIRD & FOURTH ITERATIONS
2.1570	0.6569	0.4556	
-5.80%	9.85%	4.50%	
-0.51%	-1.16%	-0.92%	
-0.42%	-1.70%	-1.01%	
-0.37%	-1.69%	-1.01%	
0.9031	1.6910	0.6576	
4.75%	0.77%	0.09%	
-1.92%	-0.89%	0.78%	
-2.15%	-0.59%	0.14%	
-2.13%	-0.65%	0.14%	

Table A6.1.1 Nodal powers for the preliminary Test Problem.

A6.2 NODAL RESULTS FOR THE CISE BENCHMARK PROBLEM

Reference Eigenvalue: $\lambda = 0.9523989$

Table A6.2.1 Nodal powers for the CISE Benchmark Problem.

	REFERENCE	0.6493
ERRORS FROM:	ADF-AXS (QUADRATIC LEAKAGE)	-1.36%
	RESPONSE MATRICES (FLAT LEAKAGE)	-0.22%
	RESPONSE MATRICES (QUADRATIC LEAKAGE)	-0.58%

				0.6846	0.7850	0.6271	
				-0.13%	-0.03%	-0.60%	
				-0.37%	-0.10%	0.41%	
				-0.47%	-0.35%	-0.35%	
			0.8821	0.7304	0.8842	0.8655	
			-3.06%	-2.40%	0.12%	-0.29%	
			0.15%	-0.05%	0.07%	-0.25%	
			0.11%	-0.09%	-0.05%	-0.53%	
		0.9109	1.0830	1.2820	1.1200	1.0640	0.7516
		-1.66%	1.12%	0.99%	-0.07%	-0.24%	-0.72%
		0.24%	0.92%	0.27%	-0.40%	-0.85%	-0.71%
		0.19%	0.92%	0.23%	-0.31%	-0.75%	0.59%
	0.8888	0.8102	1.2570	1.2200	1.4170	1.1010	0.8753
	-0.84%	-1.29%	1.72%	0.90%	0.04%	-0.28%	-0.56%
	0.71%	0.51%	0.72%	0.33%	-0.85%	-0.86%	-0.83%
	0.64%	0.45%	0.72%	0.33%	-0.74%	-0.64%	-0.53%
0.8814	1.0360	1.2090	0.8404	1.0290	1.2580	1.3360	0.9722
-0.50%	2.12%	2.32%	-0.64%	-2.19%	0.43%	-0.02%	-0.50%
0.84%	1.83%	1.41%	0.26%	-0.44%	-0.44%	-1.05%	-0.86%
0.69%	1.74%	1.28%	0.23%	-0.39%	-0.40%	-0.86%	-0.64%

A6.3 NODAL RESULTS FOR THE CLSH BENCHMARK PROBLEM

Reference Eigenvalue: $\lambda = 0.9766051$

Table A6.3.1 Nodal powers for the CLSH Benchmark Problem.

REFERENCE ----------			1.4395	1.0378	0.5283		
ADF-AXS (QUADRATIC LEAKAGE) ------			1.92%	-0.64%	2.03%		
RESPONSE MATRICES (FLAT LEAKAGE) -			-0.10%	-0.17%	0.23%		
RESPONSE MATRICES (QUAD LEAKAGE) -			-0.10%	-0.08%	0.30%		
		1.4255	1.4424	1.2212	0.6741		
		-0.83%	-0.57%	-0.66%	2.86%		
		-0.25%	0.11%	0.47%	0.40%		
		-0.28%	0.08%	0.47%	0.47%		
	1.6944	1.5376	1.4774	0.9563	0.4499	0.3884	0.1945
	0.27%	-0.23%	0.18%	-8.85%	8.05%	3.09%	5.81%
	-0.61%	-0.17%	0.51%	0.79%	0.17%	-0.88%	-0.15%
	-0.67%	-0.23%	0.48%	0.81%	0.22%	-0.82%	-0.08%
1.8779	1.7798	1.5992	1.5012	0.9178	0.4275	0.4123	0.2399
0.47%	0.38%	-0.13%	0.17%	-9.07%	9.61%	4.83%	6.34%
-1.01%	-0.78%	-0.26%	0.59%	0.95%	-0.36%	-1.12%	0.00%
-1.03%	-0.80%	-0.29%	0.59%	0.96%	-0.33%	-1.06%	0.06%

A6.4 NODAL RESULTS FOR THE NLSH BENCHMARK PROBLEM

Reference Eigenvalue: $\lambda = 0.964283$

Table A6.4.1 Interpolated cornerpoint fluxes in the fast group for the fueled region of the NLSH Benchmark.

			REFERENCE ----------		2.16460	0.88745	0.29913	
			ERRORS FROM: UDF-AXS ----------		-1.24%	5.70%	6.75%	
			ADF-AXS ----------		0.20%	-0.71%	2.92%	
			RESPONSE MATRICES ----------		-0.28%	-0.26%	1.36%	
				4.25530	3.34470	1.85170	0.63696	
				6.10%	2.98%	11.50%	8.15%	
				0.56%	0.67%	2.74%	1.38%	
				-0.15%	-0.16%	1.16%	0.51%	
		6.14060	5.04840	4.02270	1.98480	0.97648	0.34937	0.10923
		-1.68%	1.08%	-6.11%	8.22%	1.94%	12.60%	13.80%
		-0.15%	-0.24%	-0.23%	-0.15%	3.86%	1.99%	6.52%
		0.32%	0.30%	0.64%	0.13%	-1.72%	-2.76%	-0.38%
	6.59390	6.29800	5.09990	3.57850	1.24400	0.98621	0.63003	0.21088
	6.65%	2.36%	4.84%	1.07%	37.90%	22.30%	21.50%	2.13%
	0.45%	0.12%	1.22%	-2.57%	-12.70%	8.73%	8.55%	7.44%
	0.21%	0.20%	0.98%	-0.27%	-4.51%	-2.27%	0.68%	1.62%
7.59850	7.03940	6.76900	5.41030	4.04220	1.68510	1.20670	0.74017	0.25858
-0.58%	3.07%	-1.37%	0.47%	-9.21%	12.80%	0.62%	14.30%	13.10%
0.19%	0.34%	0.09%	-0.14%	-0.19%	-1.66%	6.03%	5.55%	8.10%
0.19%	0.22%	0.39%	0.50%	1.48%	-0.22%	-3.97%	-1.78%	0.71%

Table A6.4.2 Interpolated cornerpoint fluxes in the thermal group for the fueled region of the NLSH Benchmark.

			REFERENCE ----------		1.80260	1.24560	0.56369	
			ERRORS FROM: UDF-AXS ----------		-14.30%	-9.64%	-2.70%	
			ADF-AXS ----------		4.21%	5.43%	3.57%	
			RESPONSE MATRICES ----------		2.13%	4.85%	-0.55%	
				2.94490	2.20320	1.61090	0.85319	
				-44.70%	-29.30%	-45.50%	-7.64%	
				0.40%	-1.09%	1.72%	4.37%	
				-0.06%	-1.52%	-1.37%	2.43%	
		2.35760	2.55710	2.01430	1.18160	0.81031	0.51452	0.20861
		-22.20%	-32.60%	-33.90%	0.75%	-28.70%	0.51%	3.24%
		-0.35%	-1.86%	1.28%	-1.61%	7.86%	9.74%	7.58%
		0.01%	-1.04%	0.72%	0.78%	-0.16%	5.53%	-2.07%
	3.93380	3.00560	3.21170	1.85190	0.04588	0.57830	0.54824	0.27694
	-47.70%	-34.40%	-48.30%	-7.93%	238.00%	24.50%	-45.40%	-1.88%
	0.20%	-0.49%	2.39%	-7.45%	-43.50%	10.60%	6.85%	7.35%
	0.53%	0.24%	1.78%	-0.45%	-10.90%	-5.66%	-2.43%	-0.39%
2.91600	3.35880	2.59820	2.73760	1.96930	0.81644	0.68462	0.52376	0.30643
-20.70%	-34.10%	-21.80%	-31.80%	-46.40%	43.30%	-55.30%	-15.10%	-0.59%
0.12%	0.11%	-0.01%	-1.41%	1.46%	2.77%	5.79%	3.93%	9.57%
0.24%	0.37%	0.24%	-0.16%	2.23%	2.95%	-3.71%	-2.96%	0.28%

Table A6.4.3 Nodal powers for the NLSH Benchmark.

REFERENCE			1.4237	1.0239	0.5192	
UDF-AXS			-0.33%	0.21%	6.86%	
ADF-AXS			1.99%	-1.06%	1.44%	
RESPONSE MATRICES (ALL ASSEMBLIES)			-0.47%	-0.77%	-0.39%	
RESPONSE MATRICES (EXTENDED ASSEMBLIES)			-0.61%	-0.97%	-0.52%	
RESPONSE MATRICES (RODDED ASSEMBLIES)			2.09%	-1.16%	0.76%	
		1.4433	1.4402	1.2033	0.6578	
		-1.34%	-3.62%	-4.01%	2.40%	
		-0.85%	-0.43%	-0.61%	2.86%	
		-0.09%	-0.29%	-0.11%	-0.38%	
		-0.02%	-0.22%	-0.19%	-0.72%	
		-0.89%	-0.05%	-0.18%	0.96%	
	1.7350	1.5654	1.4814	0.9410	0.4326	0.3741	0.1864
	-1.04%	-1.43%	-5.46%	1.62%	24.60%	5.72%	15.29%
	0.12%	-0.28%	0.48%	-8.75%	8.83%	3.07%	5.69%
	0.35%	0.36%	0.48%	0.43%	-1.02%	-2.09%	-1.39%
	0.46%	0.49%	0.55%	0.44%	-1.28%	-2.47%	-1.64%
	-0.43%	-0.41%	1.22%	1.38%	-0.39%	-4.21%	-2.39%
1.9341	1.8277	1.6330	1.5106	0.9054	0.4092	0.3926	0.2277
-0.52%	-0.80%	-1.53%	-6.33%	-0.92%	23.90%	5.37%	13.22%
0.20%	0.18%	-0.24%	0.42%	-8.94%	10.83%	5.50%	6.72%
0.25%	0.29%	0.49%	0.75%	0.88%	-1.59%	-2.50%	-1.50%
0.41%	0.45%	0.61%	0.89%	0.91%	-1.77%	-2.88%	-2.13%
-0.65%	-0.50%	-0.40%	1.52%	1.92%	-1.22%	-3.76%	-2.42%

A6.5 NODAL RESULTS FOR THE MVY BENCHMARK

Reference Eigenvalue: $\lambda = 0.996161$

Table A6.5.1 Nodal powers for the MVY Benchmark.

2.06870	1.33790	1.24880	1.80140	1.68200	1.00500	0.77199	0.98610	0.80289	0.39779	0.14911
-5.64%	3.60%	5.38%	-4.96%	-4.58%	3.38%	10.43%	-2.08%	-1.04%	2.21%	31.31%
1.56%	-4.93%	-3.77%	1.37%	1.61%	-6.59%	-1.66%	0.99%	1.52%	-11.26%	7.71%
2.20990	1.98640	1.88450	1.93370	1.78620	1.45970	1.19000	1.05960	0.83338	0.53881	0.25523
-4.43%	-5.61%	-4.96%	-3.76%	-3.15%	-4.43%	-2.10%	-0.72%	1.05%	-1.45%	6.88%
0.77%	1.29%	1.67%	0.64%	0.77%	0.84%	2.10%	0.23%	0.64%	-1.62%	-0.72%
2.13230	1.92550	1.82770	1.86630	1.72170	1.40980	1.14220	1.00090	0.77799	0.50738	0.25361
-4.14%	-5.38%	-4.74%	-3.39%	-2.77%	-4.10%	-1.51%	0.31%	3.27%	3.10%	9.74%
0.88%	1.38%	1.71%	0.68%	0.83%	0.72%	2.17%	0.31%	0.94%	-1.22%	-0.08%
1.84460	1.21260	1.13330	1.60780	1.49740	0.90395	0.67562	0.81622	0.64086	0.40816	
-5.40%	2.75%	4.65%	-4.34%	-3.77%	2.96%	10.76%	-0.10%	4.70%	8.41%	
1.11%	-6.23%	-5.06%	0.88%	1.04%	-8.17%	-3.14%	-0.05%	0.41%	-3.67%	
1.64740	1.04640	0.97738	1.43800	1.34330	0.78146	0.55828	0.67237	0.50170		
-4.15%	6.65%	8.96%	-2.64%	-1.96%	7.57%	18.02%	2.92%	8.87%		
1.92%	-3.57%	-2.29%	1.67%	1.76%	-5.84%	0.90%	1.00%	0.98%		
1.59730	1.42780	1.35660	1.40690	1.30770	1.05570	0.80418	0.62621	0.38831		
-2.96%	-3.84%	-2.70%	-0.92%	0.48%	0.03%	0.64%	4.39%	10.38%		
0.54%	0.99%	1.36%	0.29%	0.41%	0.03%	1.76%	-0.94%	0.0 %		
1.38750	1.26170	1.19970	1.22590	1.16160	0.99590	0.75792	0.51987	0.28918		
-2.05%	-3.15%	-1.89%	0.66%	2.96%	3.93%	6.78%	7.10%	13.74%		
0.83%	1.37%	1.61%	0.58%	0.64%	-0.03%	1.07%	-0.88%	-0.30%		
1.04260	0.70529	0.65407	0.89963	0.89338	0.77143	0.56536	0.36919			
-3.89%	2.33%	4.97%	-0.57%	3.45%	4.25%	7.44%	10.86%			
0.13%	-9.03%	-8.10%	-0.56%	-0.62%	-1.74%	-0.74%	-4.57%			
0.71316	0.42052	0.36156	0.54535	0.54658	0.44978	0.32272				
0.03%	15.69%	22.33%	5.00%	8.88%	10.39%	13.91%				
3.08%	0.59%	4.30%	2.70%	1.01%	-0.04%	-0.22%				
0.50186	0.41589	0.34259	0.32451							
1.32%	1.06%	4.18%	10.14%							
0.29%	0.24%	1.05%	-2.19%							
0.28061	0.24494	0.19752	---------- REFERENCE NODAL POWER							
8.41%	9.17%	12.14%	---------- ERRORS FROM UDF-AXS							
2.10%	1.94%	1.31%	---------- ERRORS FROM ADF-AXS							

Table A6.5.1 (continued)

2.06870	1.33790	1.24880	1.80140	1.68200	1.00500	0.77199	0.98610	0.80289	0.39779	0.14911
0.88%	0.75%	0.58%	0.70%	0.77%	0.60%	0.13%	0.27%	0.66%	0.76%	-0.34%
2.19%	1.58%	1.26%	1.56%	1.87%	1.00%	-0.02%	-0.25%	0.77%	-0.34%	-1.55%
2.20990	1.98640	1.88450	1.93370	1.78620	1.45970	1.19000	1.05960	0.83338	0.53881	0.25523
-0.09%	0.84%	0.77%	-0.24%	-0.24%	0.57%	0.50%	-0.62%	-0.55%	0.15%	0.65%
1.14%	1.84%	1.91%	0.53%	0.77%	0.77%	1.09%	-1.28%	-0.62%	-1.99%	0.38%
2.13230	1.92550	1.82770	1.86630	1.72170	1.40980	1.14220	1.00090	0.77799	0.50738	0.25361
-0.11%	0.86%	0.78%	-0.28%	-0.33%	0.51%	0.51%	-0.75%	-0.89%	-0.41%	0.15%
1.23%	1.97%	2.01%	0.60%	0.80%	0.83%	1.16%	-1.46%	-1.03%	-3.17%	-2.13%
1.84460	1.21260	1.13330	1.60780	1.49740	0.90395	0.67562	0.81622	0.64086	0.40816	
0.78%	0.69%	0.50%	0.51%	0.51%	0.47%	-0.11%	-0.35%	-0.46%	-0.73%	
1.62%	1.39%	1.03%	0.88%	1.11%	0.57%	-0.67%	-2.03%	-2.15%	-6.16%	
1.64740	1.04640	0.97738	1.43800	1.34330	0.78146	0.55828	0.67237	0.50170		
0.70%	0.34%	0.10%	0.35%	0.28%	-0.16%	-0.93%	-0.65%	-0.52%		
1.83%	0.73%	0.24%	0.83%	0.98%	-0.56%	-2.16%	-2.29%	-2.29%		
1.59730	1.42780	1.35660	1.40690	1.30770	1.05570	0.80418	0.62621	0.38831		
-0.39%	0.43%	0.25%	-0.85%	-1.05%	-0.73%	-0.88%	-1.60%	-1.39%		
0.08%	0.64%	0.51%	-1.09%	-1.20%	-1.82%	-1.65%	-4.79%	-3.82%		
1.38750	1.26170	1.19970	1.22590	1.16160	0.99590	0.75792	0.51987	0.28918		
-0.40%	0.58%	0.36%	-0.97%	-1.52%	-1.36%	-1.28%	-1.73%	-1.79%		
0.58%	1.17%	0.94%	-0.89%	-1.64%	-2.84%	-2.39%	-4.77%	-4.42%		
1.04260	0.70529	0.65407	0.89963	0.89338	0.77143	0.56536	0.36919			
0.42%	0.57%	0.10%	-0.57%	-1.31%	-1.65%	-1.60%	-1.95%			
0.18%	0.38%	-0.47%	-1.97%	-3.26%	-4.88%	-4.37%	-8.37%			
0.71316	0.42052	0.36156	0.54535	0.54658	0.44978	0.32272				
0.64%	-0.05%	-0.65%	-0.34%	-0.91%	-1.37%	-1.52%				
1.21%	-1.11%	-2.34%	-0.78%	-2.16%	-3.53%	-4.00%				
0.50186	0.41589	0.34259	0.32451							
-0.53%	-0.02%	-0.14%	-1.11%							
-2.72%	-3.05%	-3.31%	-6.40%							
0.28061	0.24494	0.19752	---------- REFERENCE NODAL POWER							
-0.29%	0.51%	0.50%	---------- ERRORS FROM REPONSE							
-1.45%	-1.96%	-2.97%	---------- ERRORS FROM REPONSE (RODDED ASSEMBLIES ONLY)							

A6.6 NODAL RESULTS FOR THE TRD BENCHMARK

Reference Eigenvalue: $\lambda = 0.976717$

	REFERENCE:	ERRORS FROM : UDF:	ADF:						
PL1	0.7130	-5.82%	-0.36%	0.4637	3.21%	-4.70%	0.3872	4.34%	-2.32%
PL2	1.1130	-4.04%	1.17%	0.7264	3.88%	-4.61%	0.6090	4.93%	-2.30%
PL3	1.1720	-4.18%	0.51%	0.8839	10.54%	0.92%	0.7984	6.83%	-0.90%
PL4	1.2930	-2.09%	1.31%	1.1040	9.42%	0.72%	1.0070	9.83%	2.98%
PL5	1.3170	1.37%	1.06%	1.4830	4.18%	2.02%	1.4490	4.90%	2.35%
PL6	1.0200	1.08%	-0.69%	1.1600	1.47%	0.60%	1.1600	2.24%	0.69%
PL7	0.7469	1.42%	-0.42%	0.7636	0.88%	-0.90%	0.7637	1.11%	-0.79%
PL8	0.5150	-0.47%	-2.47%	0.5150	-0.33%	-2.39%	0.5147	-0.25%	-2.35%
	0.8179	-4.05%	-0.92%	0.7442	-4.94%	-0.20%	0.6968	-5.17%	0.01%
	1.2680	-2.44%	0.47%	1.1580	-3.37%	1.21%	1.0880	-3.58%	1.47%
	1.3000	-2.85%	-0.46%	1.2110	-3.63%	0.50%	1.1500	-4.00%	0.70%
	1.3900	-1.22%	0.14%	1.3230	-1.81%	1.21%	1.2760	-1.96%	1.49%
	1.3500	0.81%	0.59%	1.3340	1.35%	0.97%	1.3110	1.53%	0.99%
	1.0240	0.39%	-0.88%	1.0270	0.88%	-0.88%	1.0210	1.18%	-0.78%
	0.7491	1.24%	-0.49%	0.7489	1.39%	-0.41%	0.7473	1.54%	-0.36%
	0.5162	-0.56%	-2.52%	0.5157	-0.48%	-2.48%	0.5152	-0.43%	-2.47%
	0.8946	-2.82%	-0.69%	0.8665	-2.90%	-0.54%	0.8412	-2.92%	-0.36%
	1.3780	-1.23%	0.65%	1.3380	-1.27%	0.82%	1.3010	-2.84%	1.08%
	1.3930	-1.79%	-0.36%	1.3570	-1.77%	-0.07%	1.3250	-1.74%	0.08%
	1.4600	-0.48%	0.21%	1.4320	-0.42%	0.35%	1.4070	-0.43%	0.50%
	1.3880	0.79%	0.50%	1.3710	1.02%	0.80%	1.3560	1.11%	0.88%
	1.0360	0.10%	-0.97%	1.0300	0.29%	-0.87%	1.0240	0.39%	-0.78%
	0.7528	1.05%	-0.58%	0.7507	1.15%	-0.55%	0.7486	1.23%	-0.49%
	0.5175	-0.66%	-2.59%	0.5168	-0.62%	-2.55%	0.5161	-0.56%	-2.54%

Note: PLn is the n^{th} 15 cm plane grouping. n = 1 corresponds to the bottom fueled slice of the core.

Table A6.6.1 Nodal powers for the TRD BWR Benchmark.

Table A6.6.2 Nodal powers for two-dimensional slices of the TRD BWR Benchmark.

	REFERENCE	ERRORS FROM: ADF -AXS	UDF -AXS						
SECTION 1 ----------	0.9906	0.58%	-3.02%	0.6301	-5.25%	5.11%	0.5189	-2.79%	6.40%
SECTION 2 (RODDED) ---	0.9849	0.67%	-3.07%	0.7800	-3.55%	7.10%	0.6667	-1.56%	7.68%
SECTION 2 (UNRODDED) -	0.9591	-0.10%	-0.02%	1.1859	0.26%	0.09%	1.2138	0.35%	0.10%
SECTION 3	0.9711	-0.13%	0.29%	1.1474	0.31%	-0.56%	1.1735	0.30%	-0.30%
SECTION 4	1.0000	0.0 %	0.0 %	1.0000	0.0 %	0.0 %	1.0000	0.0 %	0.0 %
	1.1530	0.09%	-0.95%	1.0428	0.88%	-1.90%	0.9708	1.11%	-2.09%
	1.1036	-0.05%	-1.50%	1.0236	0.72%	-2.40%	0.9647	0.86%	-2.67%
	0.9353	-0.13%	-0.04%	0.9565	-0.13%	-0.04%	0.9637	-0.11%	-0.03%
	0.9475	-0.06%	0.07%	0.9670	-0.13%	0.29%	0.9758	-0.11%	0.35%
	1.0000	0.0 %	0.0 %	1.0000	0.0 %	0.0 %	1.0000	0.0 %	0.0 %
	1.2749	0.40%	0.48%	1.2299	0.58%	0.41%	1.1891	0.75%	0.41%
	1.1940	0.25%	-0.25%	1.1576	0.55%	-0.22%	1.1248	0.73%	-0.25%
	0.9259	-0.13%	-0.04%	0.9287	-0.11%	-0.02%	0.9312	-0.12%	-0.03%
	0.9353	-0.10%	0.0 %	0.9394	-0.09%	0.02%	0.9431	-0.08%	0.01%
	1.0000	0.0 %	0.0 %	1.0000	0.0 %	0.0 %	1.0000	0.0 %	0.0 %

A6.7 NODAL RESULTS FOR THE DEP2 BENCHMARK

Reference Eigenvalues:

Beginning of cycle 1: $\lambda = 0.923458$

End of cycle 1: $\lambda = 0.838761$

Beginning of cycle 2: $\lambda = 0.929696$

End of cycle 2: $\lambda = 0.887143$

Beginning of cycle 3: $\lambda = 0.907373$

Table A6.7.1 Nodal powers for the DEP2 Benchmark.

B.O.C. 1 -------	1.0403	-0.32%	0.93%	0.64%	0.7448	-5.19%	0.68%	0.39%				
E.O.C. 1 -------	1.1202	0.34%	-0.46%	-0.46%	0.8671	-2.53%	-0.54%	-1.28%				
B.O.C. 2 -------	1.1876	0.37%	0.28%	-0.14%	0.8003	-4.83%	0.90%	0.11%				
E.O.C. 2 -------	1.0660	0.84%	-0.47%	N.A.	0.7316	4.54%	0.08%	N.A.				
B.O.C. 3 -------	0.9813	1.22%	0.37%	N.A.	0.6236	-3.66%	-0.12%	N.A.				

				1.1544	2.39%	-0.82%	-0.64%	1.0401	0.57%	-0.68%	-0.49%	0.8917	-2.96%	1.11%	0.92%
				1.0590	1.13%	0.09%	0.76%	1.0076	0.24%	-0.06%	0.44%	0.9796	-0.94%	-0.24%	-0.55%
				1.0980	2.64%	-1.18%	-0.46%	1.0603	1.10%	-1.07%	-1.07%	0.9775	-3.20%	1.01%	1.10%
	ERRORS FROM:			1.1845	1.82%	-1.31%	N.A.	1.0962	1.26%	0.81%	N.A.	0.9026	-2.88%	2.01%	N.A.
REFERENCE	ADF -AXS	R. M.	R. M. (EXT. A'S)	1.2486	0.91%	-0.85%	N.A.	1.1139	0.55%	-0.35%	N.A.	0.8624	-2.38%	0.94%	N.A.
0.9707	1.13%	-1.36%	-0.98%	1.1679	3.60%	-0.76%	-0.42%	1.0913	1.80%	-0.40%	-0.40%	0.9817	-2.04%	1.17%	0.93%
0.8784	-0.90%	-0.73%	-0.14%	1.0477	1.85%	0.41%	0.70%	1.0260	0.78%	0.59%	0.68%	1.0436	-0.34%	0.33%	-0.30%
0.6320	0.20%	-0.59%	-0.70%	1.0747	4.31%	0.21%	-0.07%	1.0744	1.92%	-1.15%	-0.60%	1.0542	-2.49%	1.02%	1.21%
0.6889	-2.59%	-0.51%	N.A.	1.1845	3.25%	-0.97%	N.A.	1.1366	1.88%	-0.76%	N.A.	0.9791	-2.30%	0.44%	N.A.
0.7584	-2.00%	-0.92%	N.A.	1.2606	2.33%	-0.76%	N.A.	1.1816	1.22%	-0.22%	N.A.	0.9640	-1.07%	1.72%	N.A.

Note: R.M. means "Response Matrices".

EXT. A'S means "Extended Assemblies".